Appendix B

Supplementary information for Chapter 3. NMR spectra of ligands and complexes, including 2D spectra, ROESY and TOCSY; infrared spectra, HRMS isotopic pattern matching, photophysical spectra, spectroscopic titration and fitting plots and hydrogen-bonding table for X-ray crystal structure.

B.1. NMR spectra of ligands and complexes

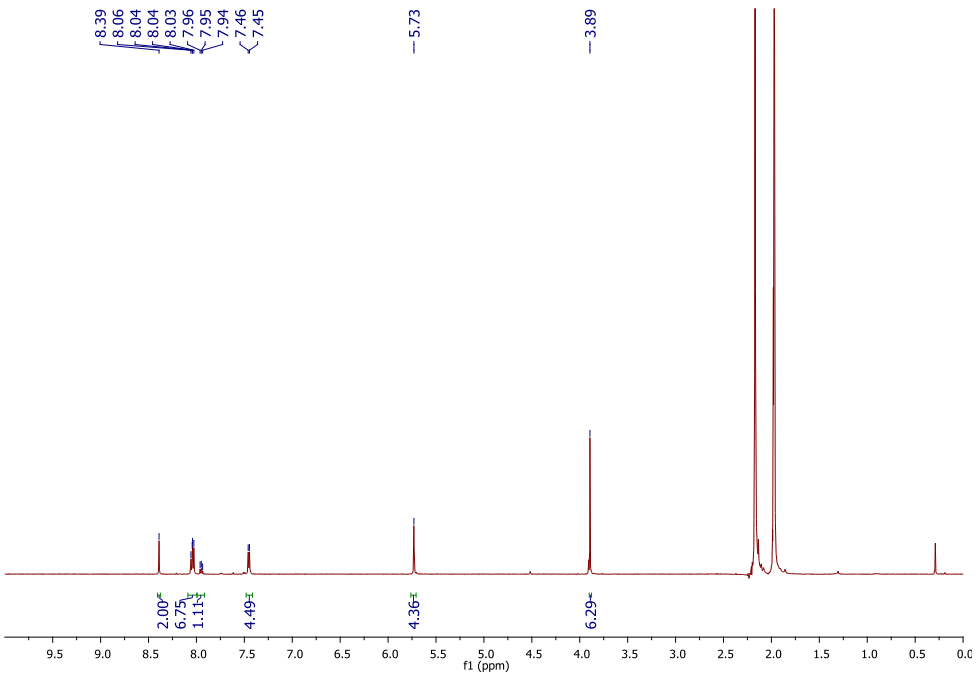

Figure B.1 ^{1}H NMR (600 MHz, CD_3CN) spectrum of ligand **88**.

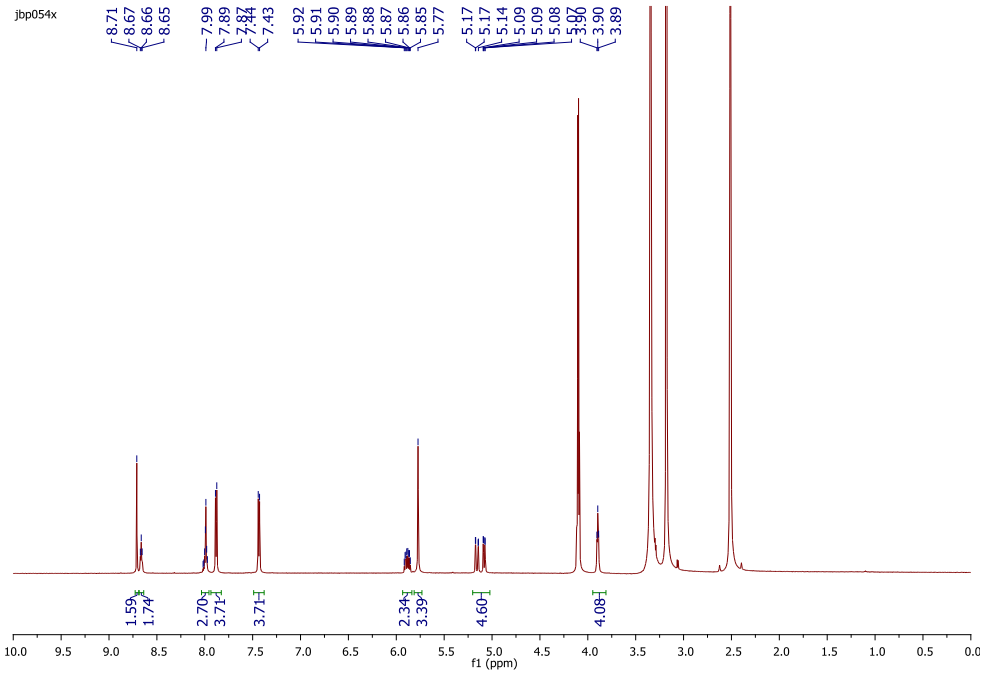

Figure B.2 ^{1}H NMR (600 MHz, DMSO-d_6) spectrum of ligand **90**.

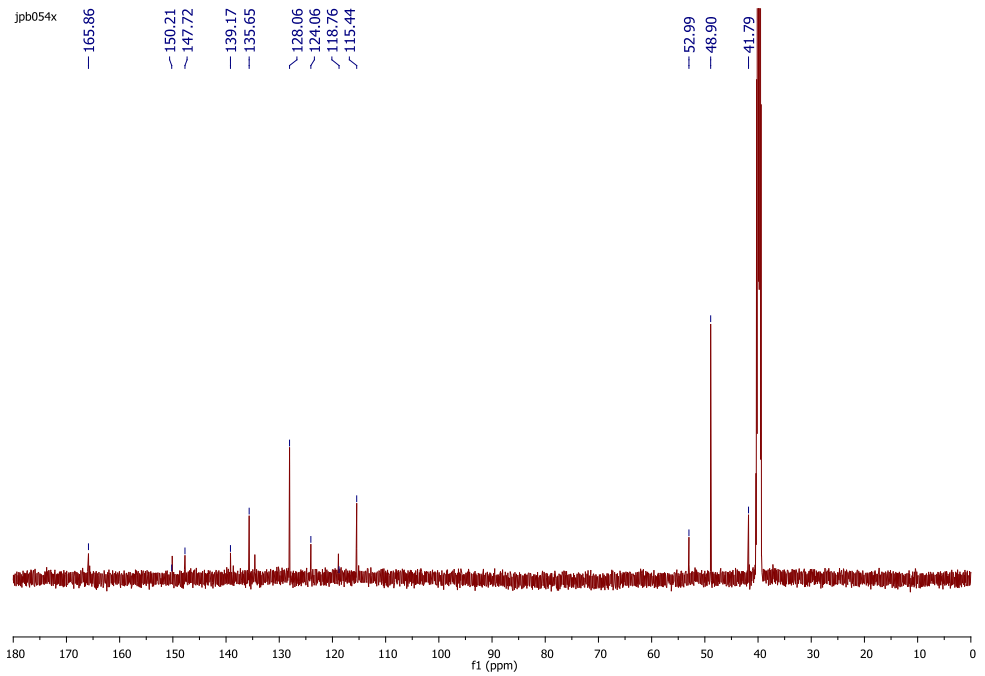

Figure B.3 ^{13}C NMR (150 MHz, DMSO-d_6) spectrum of ligand **90**.

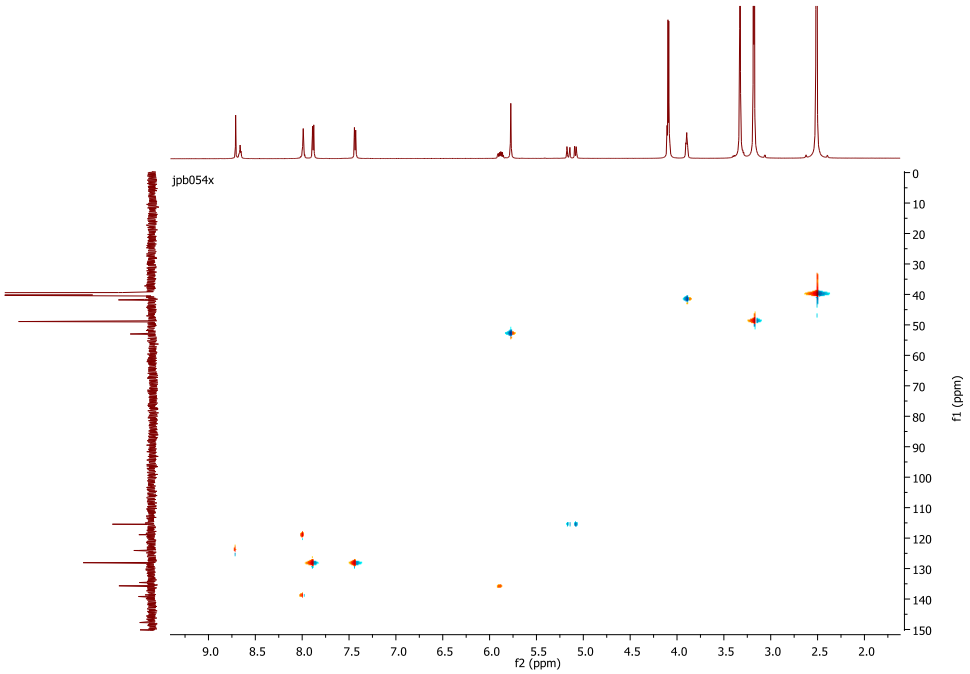

Figure B.4 HSQC of ligand **90**.

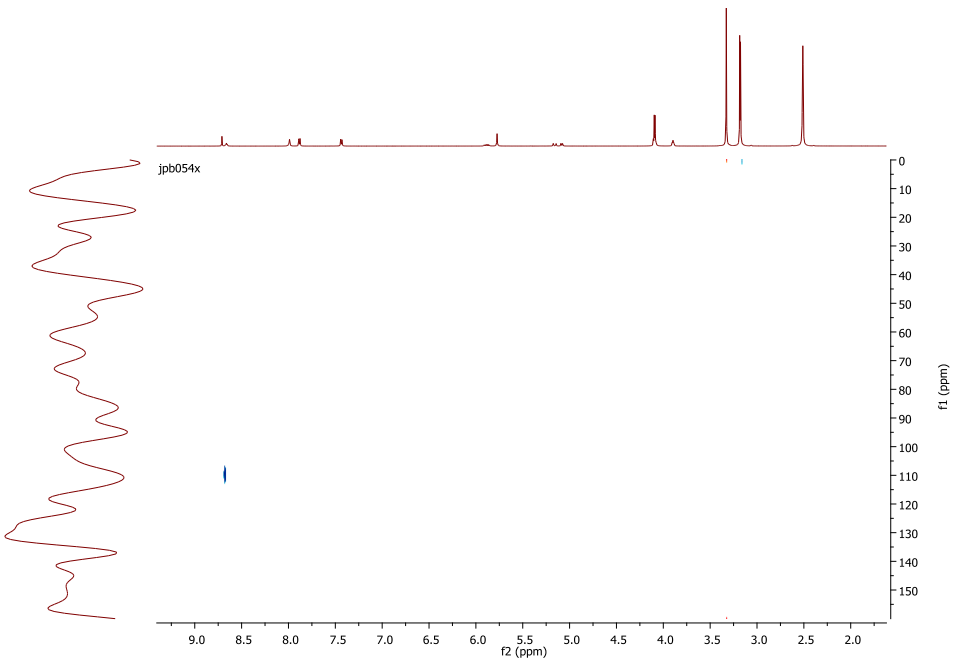

Figure B.5 NH COSY of ligand **90**.

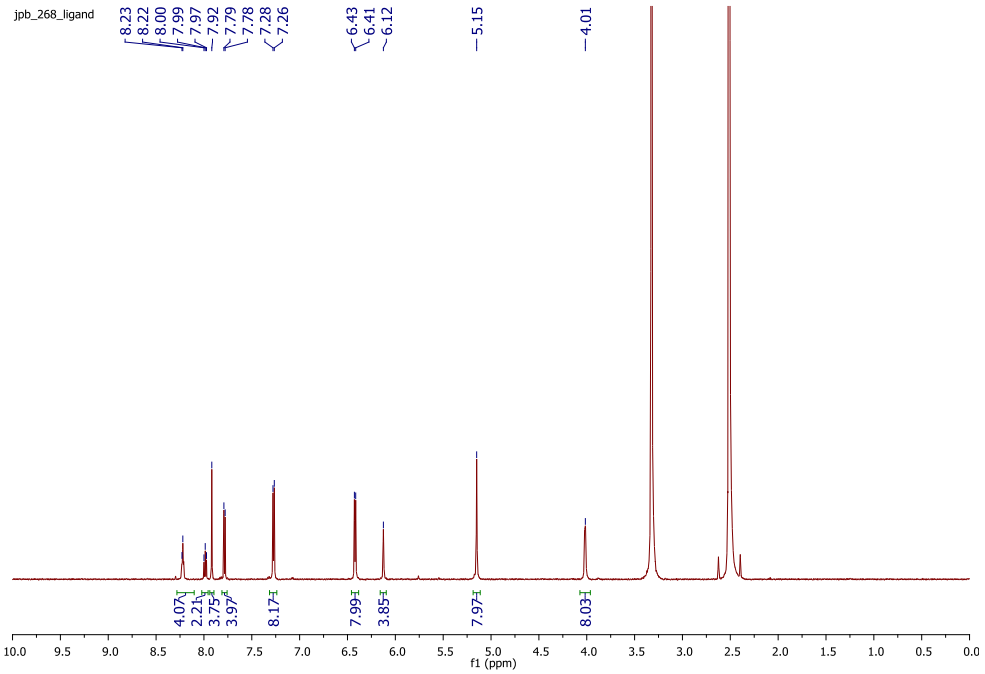

Figure B.6 ^{1}H NMR (600 MHz, DMSO-d_6) spectrum of [n]catenane **95**.

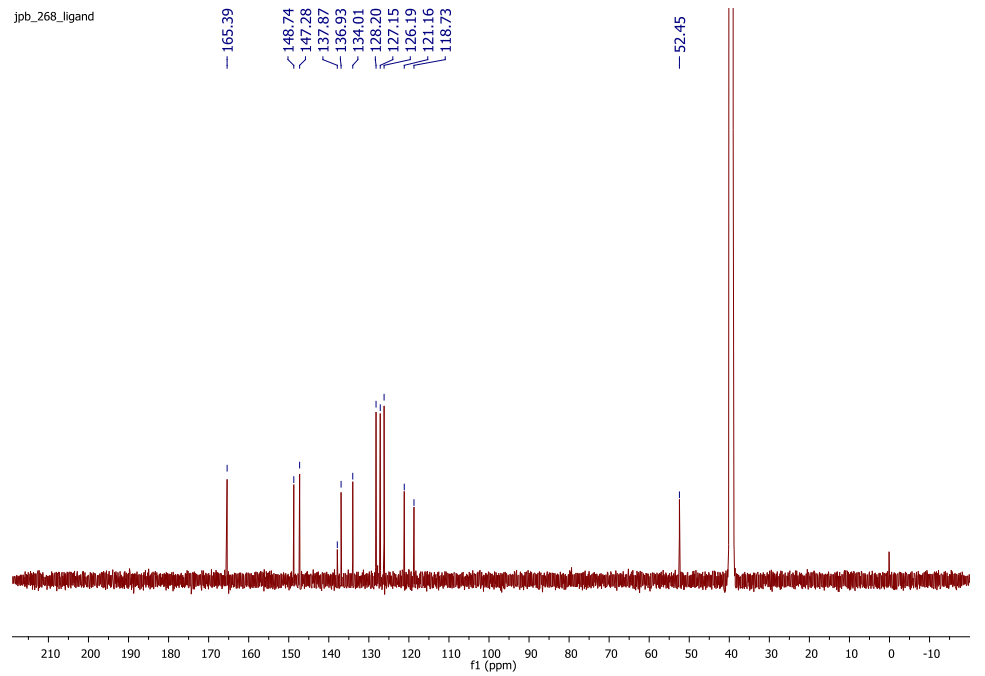

Figure B.7 ^{13}C NMR (150 MHz, DMSO-d_6) spectrum of [n]catenane **95**.

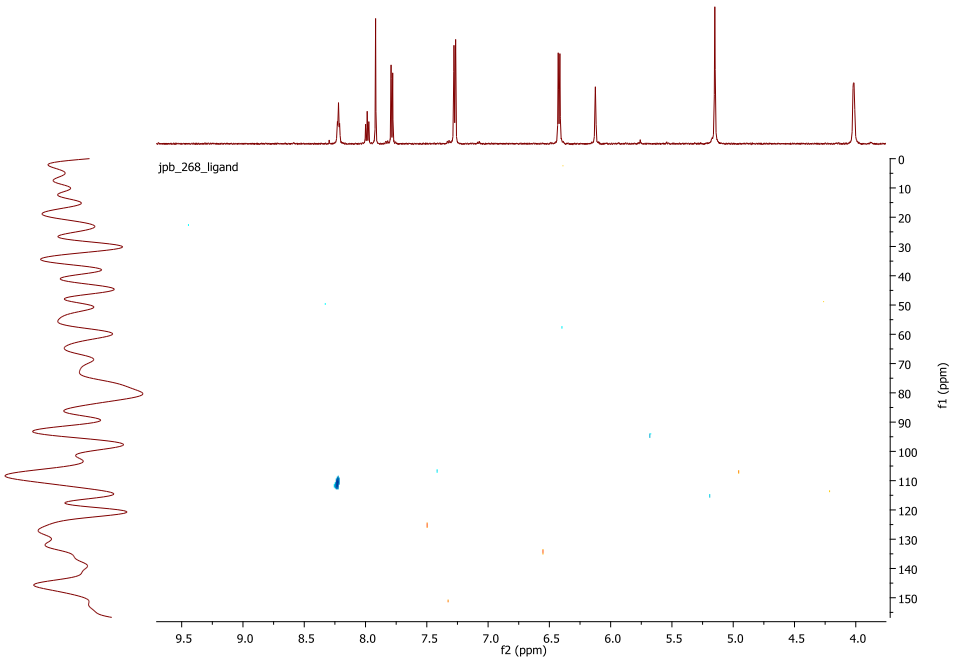

Figure B.8 NH COSY of [n]catenane **95**.

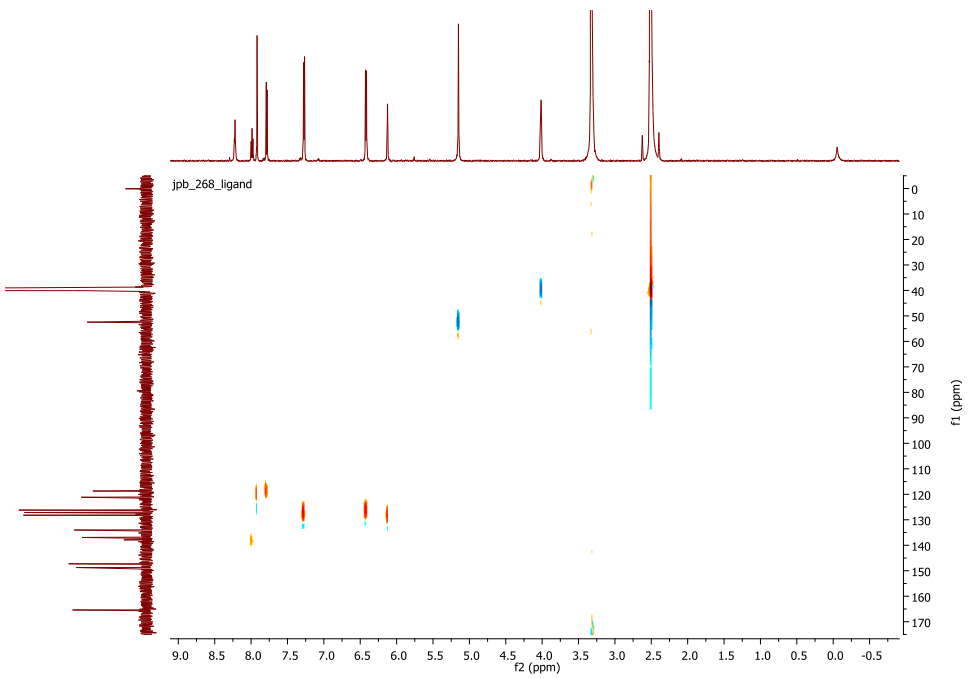

Figure B.9 HSQC of [n]catenane **95**.

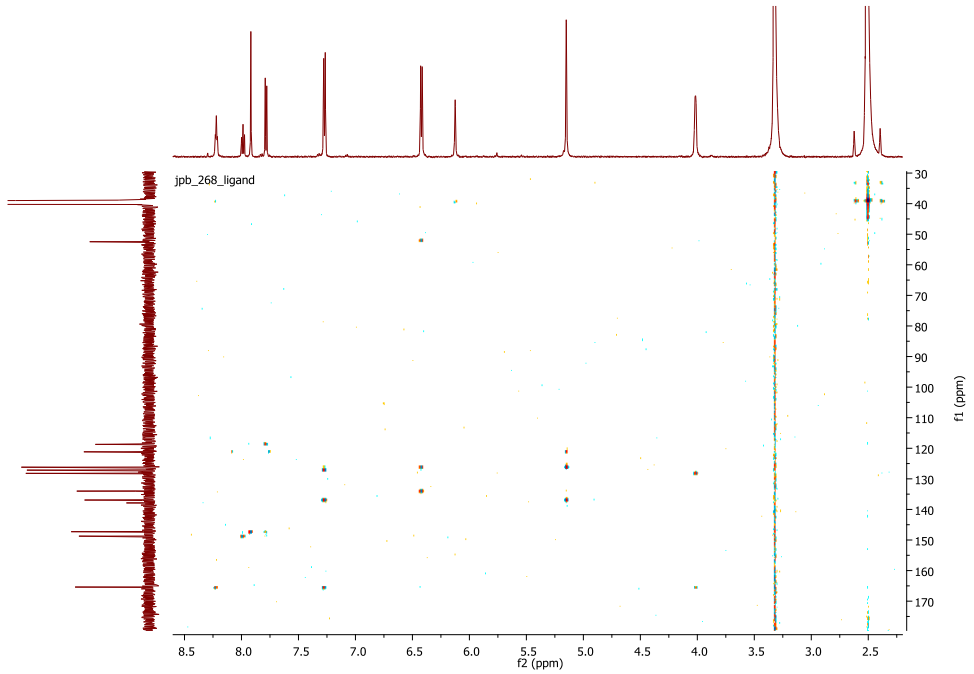

Figure B.10 HMBC of [n]catenane **95**.

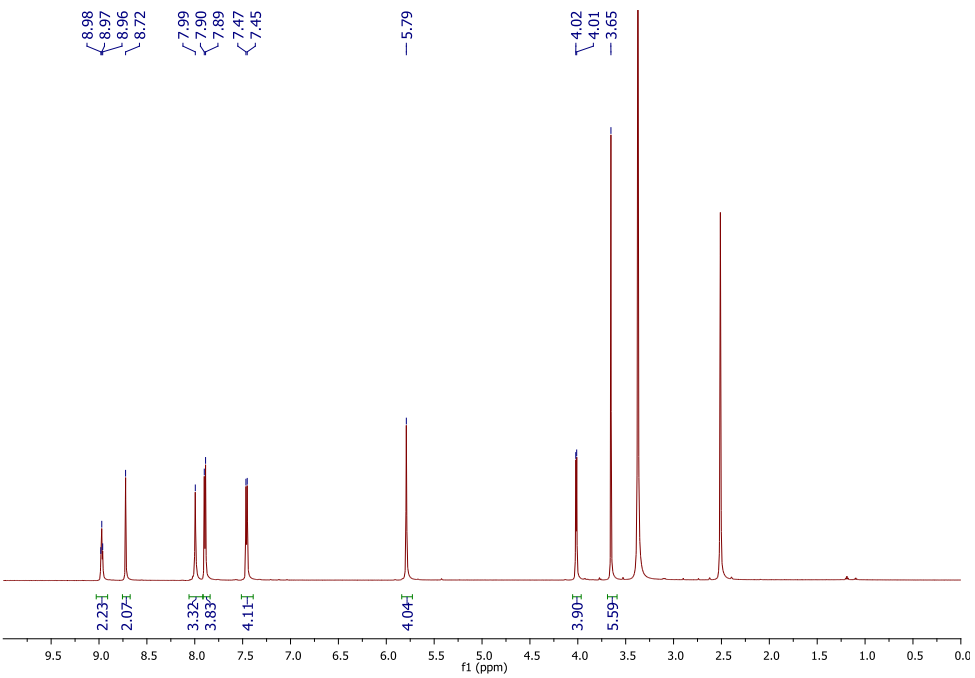

Figure B.11 ^{1}H NMR (600 MHz, DMSO-d_6) spectrum of ligand **91-Gly**.

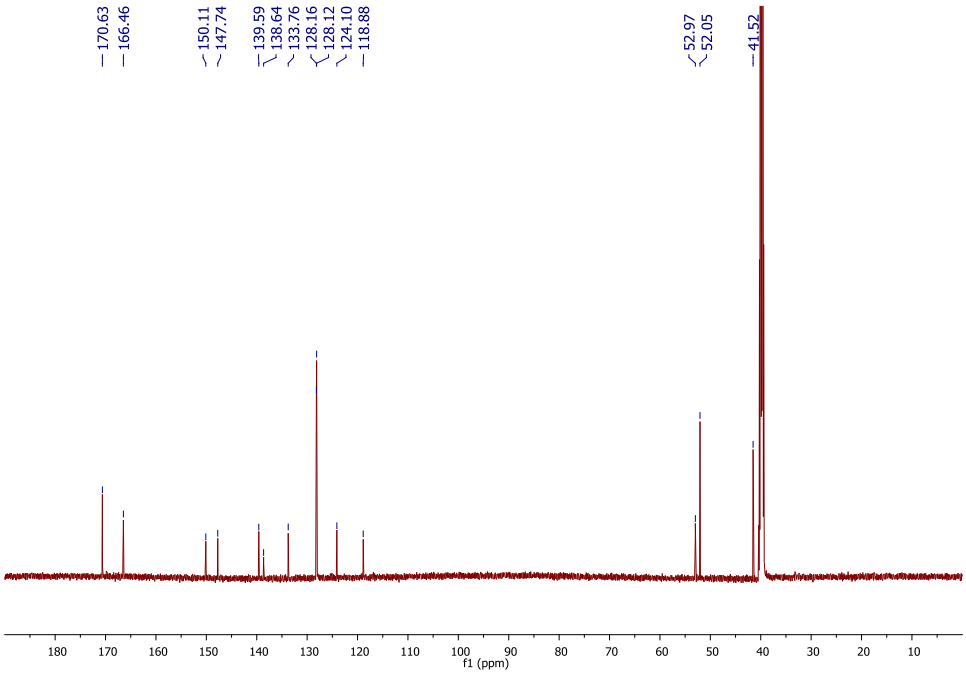

Figure B.12 ^{13}C NMR (150 MHz, DMSO-d_6) spectrum of ligand **91-Gly**.

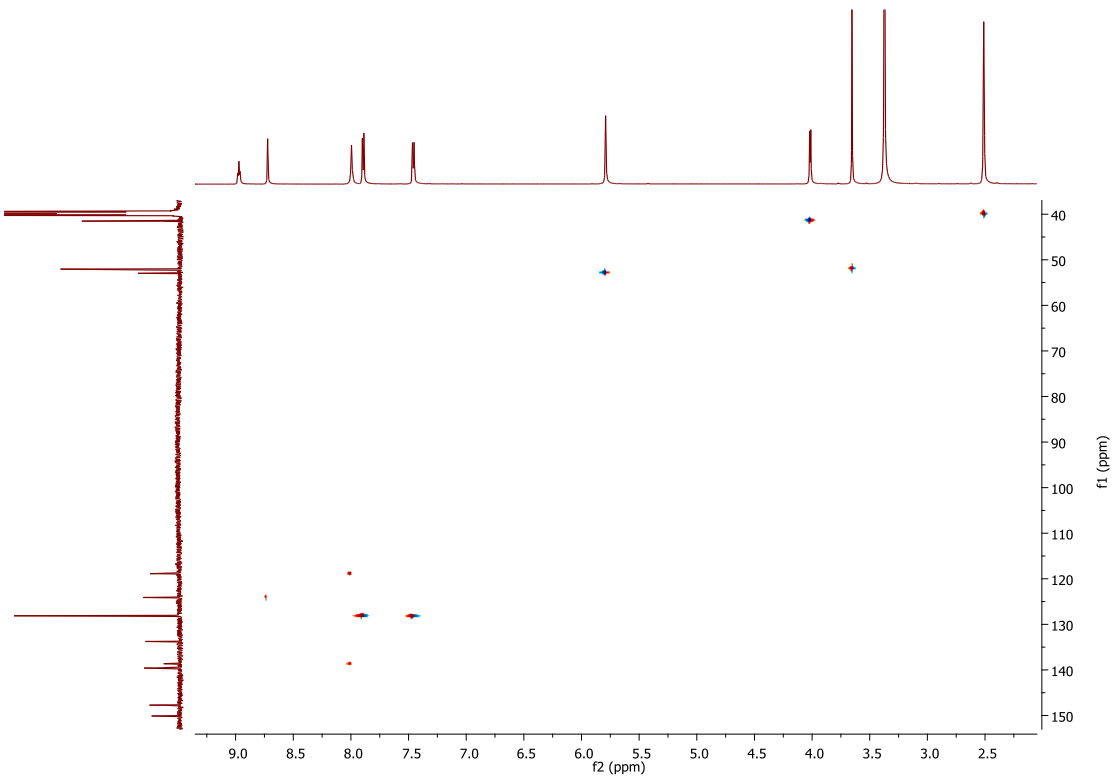

Figure B.13 HSQC (600 MHz, DMSO-d_6) of **91-Gly**.

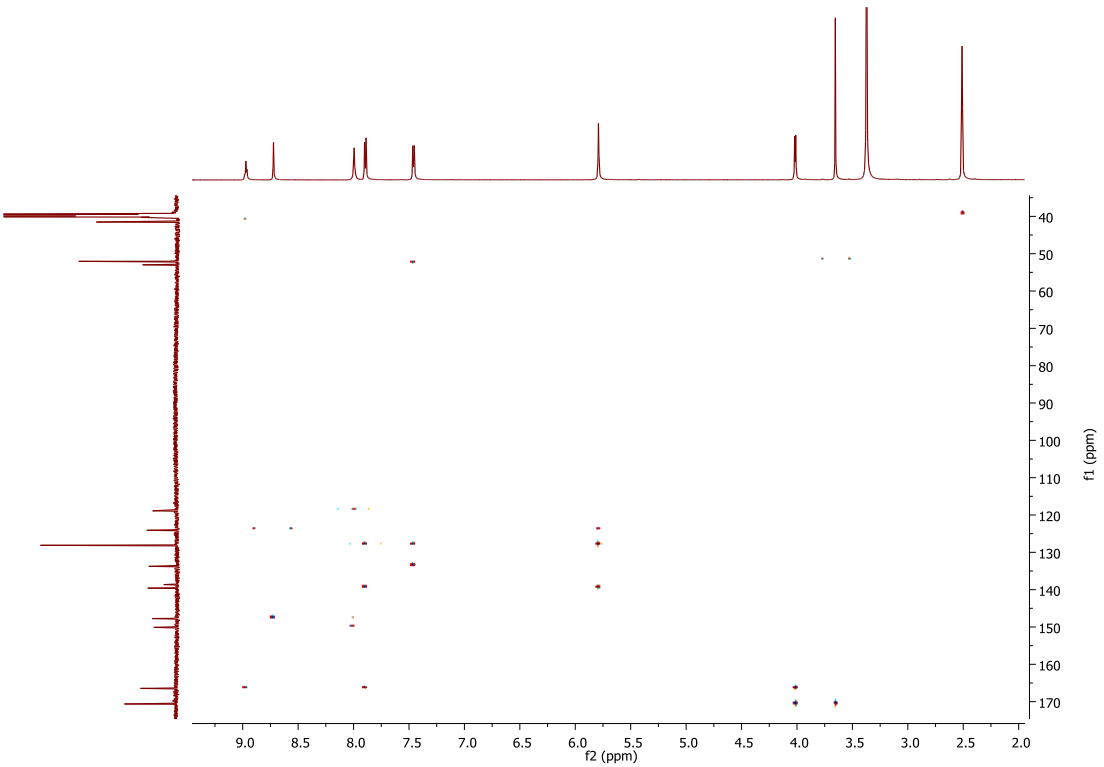

Figure B.14 HMBC (600 MHz, DMSO-d_6) of **91-Gly**.

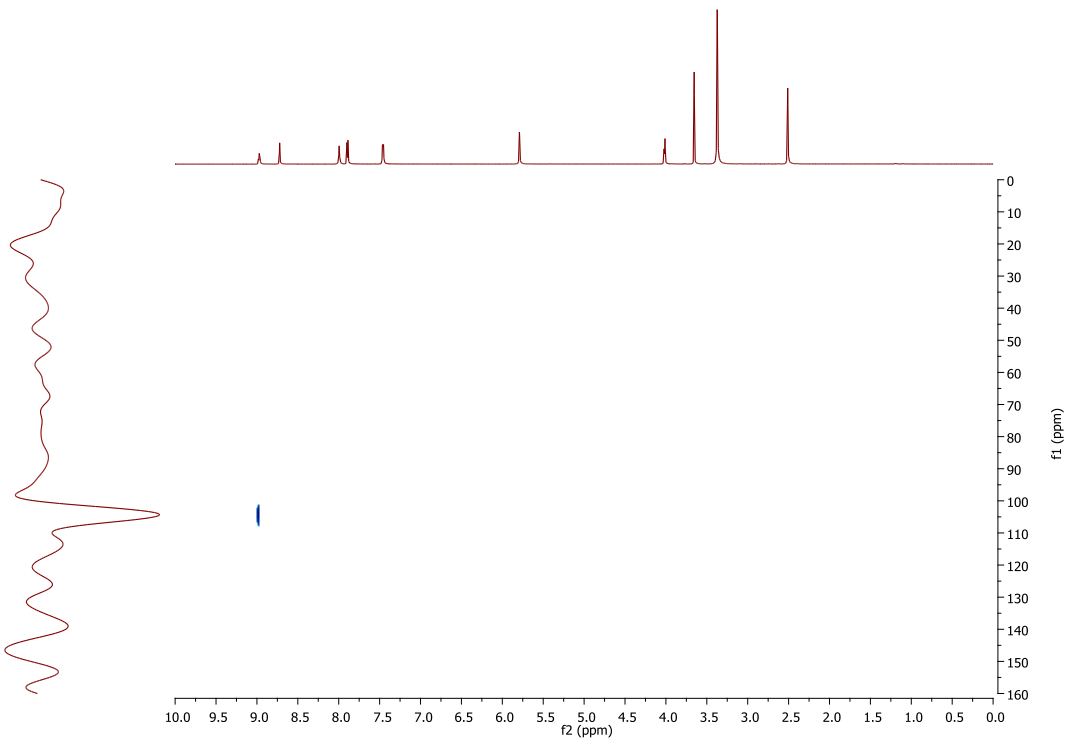

Figure B.15 NH COSY (600 MHz, DMSO-d_6) of **91-Gly**).

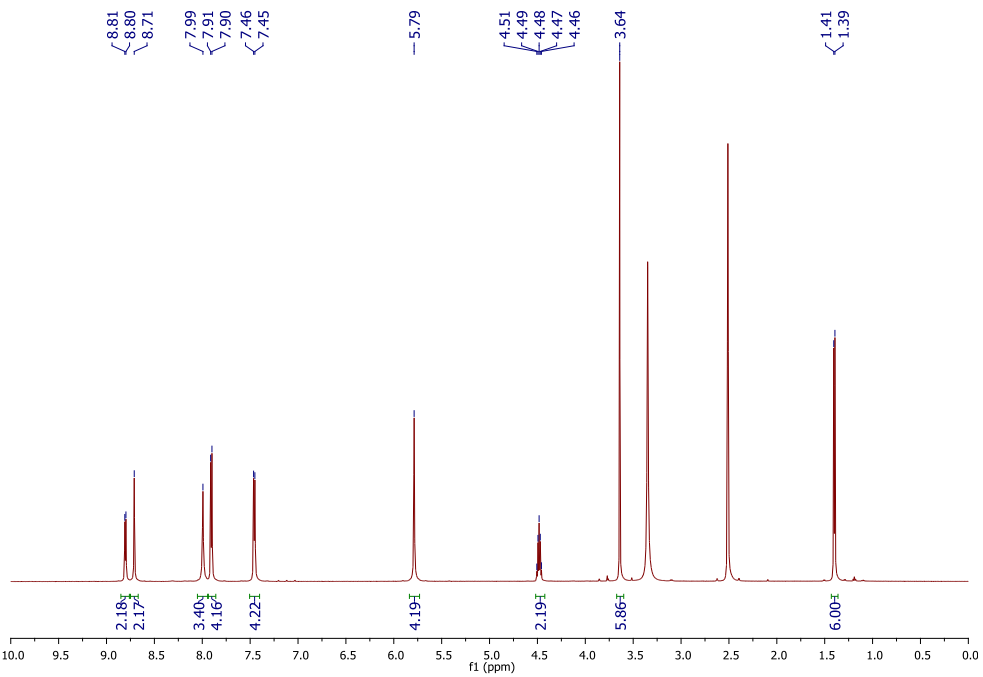

Figure B.16 ^{1}H NMR (600 Mhz, DMSO-d_6) spectrum of ligand **91-*L*-Ala**.

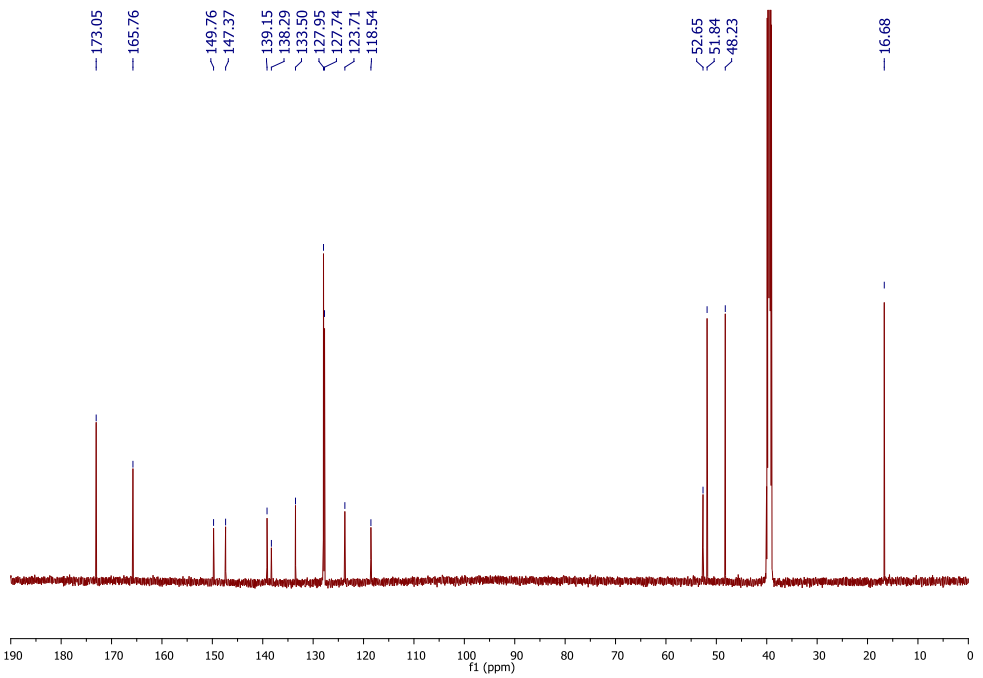

Figure B.17 ^{13}C NMR (150 MHz, DMSO-d_6) spectrum of ligand **91-*L*Ala**.

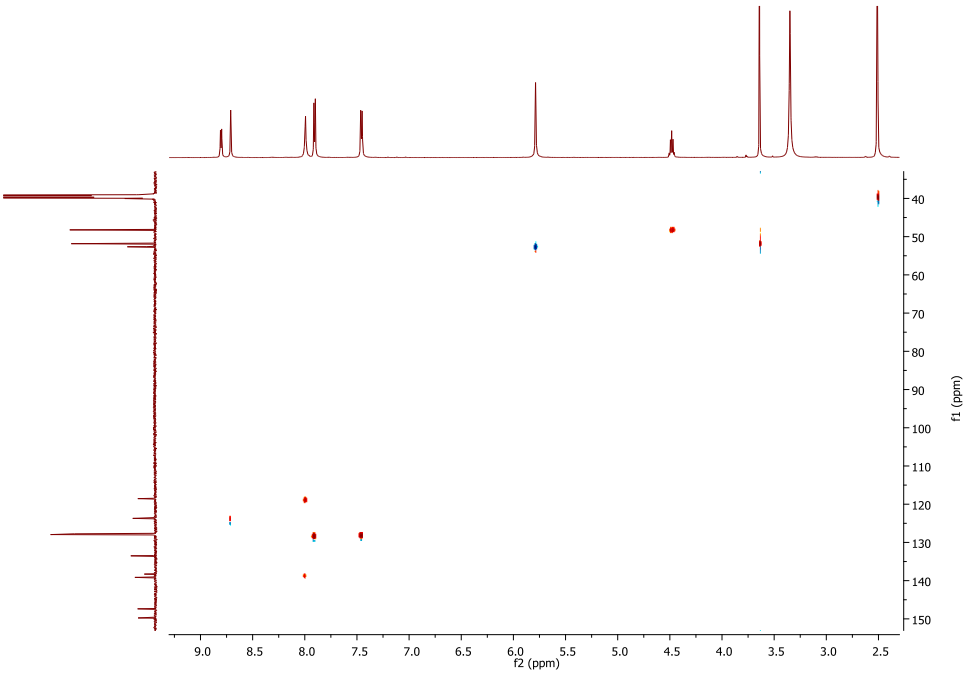

Figure B.18 HSQC (600 MHz, DMSO-d_6) of **91-*L*-Ala**.

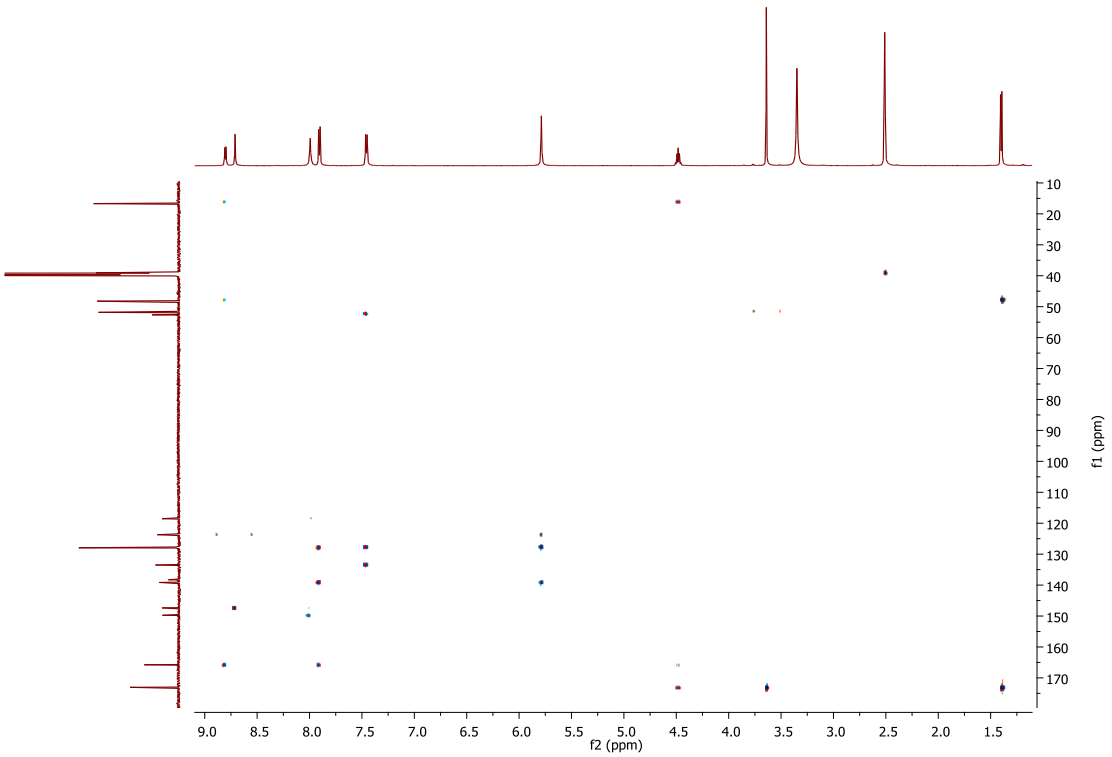

Figure B.19 HMBC (600 MHz, DMSO-d_6) of **91-*L*-Ala**.

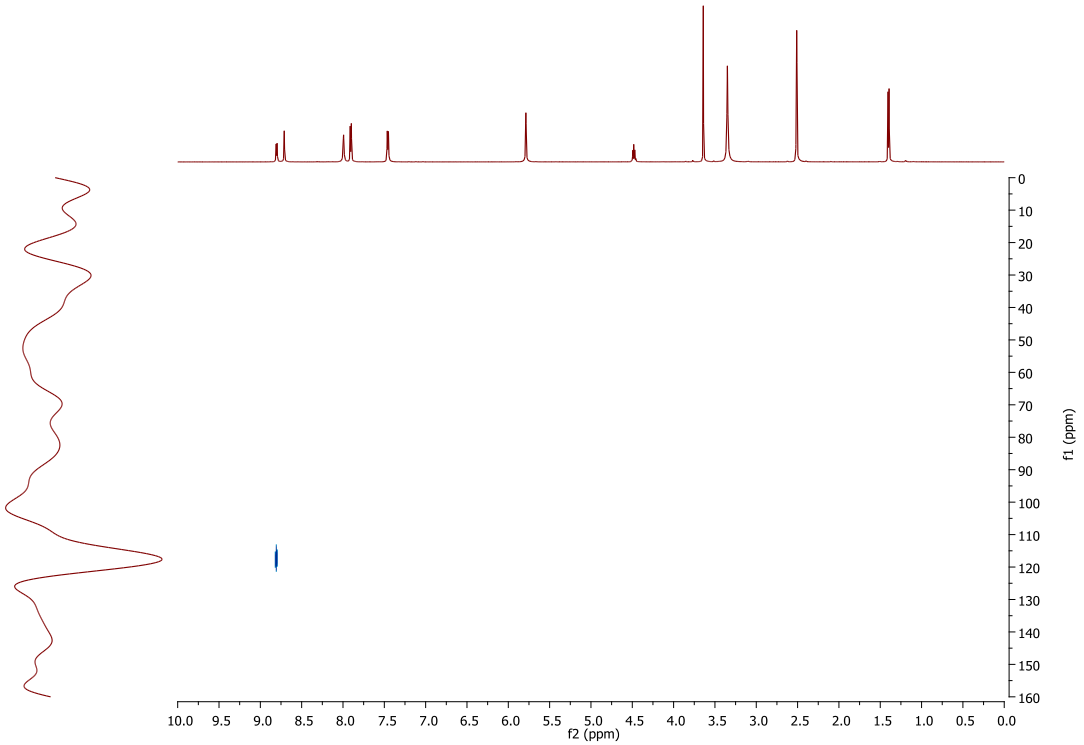

Figure B.20 NH COSY (600 MHz, DMSO-d_6) of **91-*L*-Ala**.

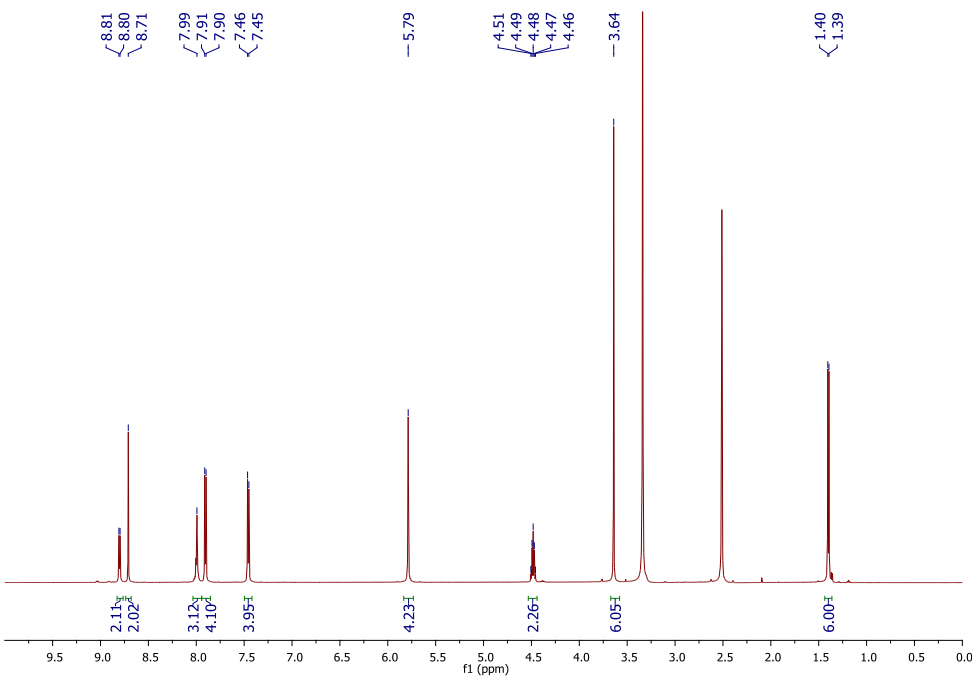

Figure B.21 ^{1}H NMR (600 MHz, DMSO-d_6) spectrum of **91-*D*-Ala**.

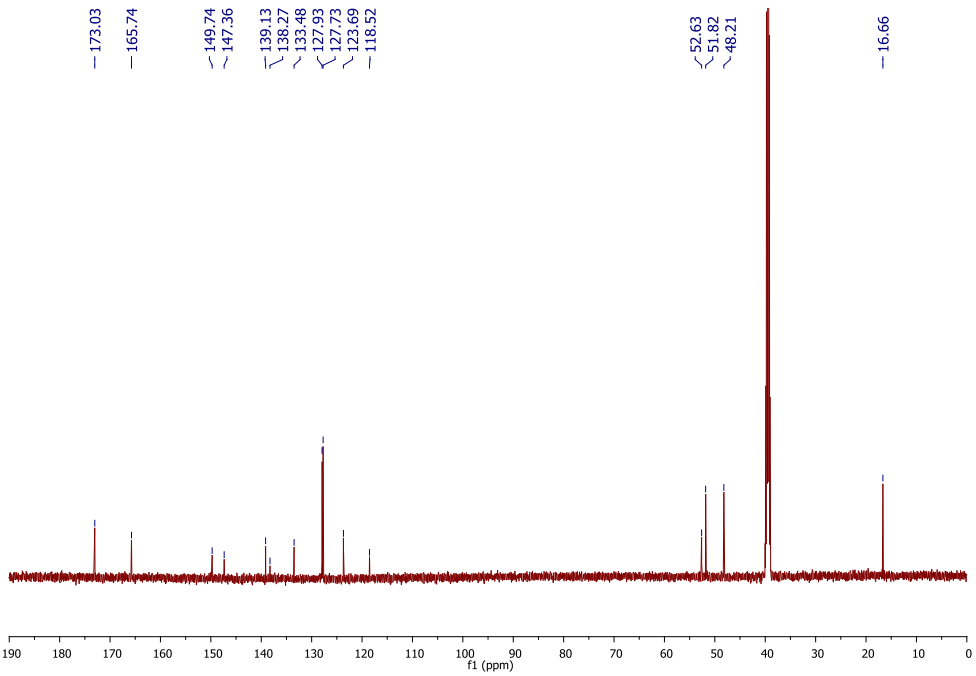

Figure B.22 ^{13}C NMR (150 MHz, DMSO-d_6) spectrum of ligand **91-*D*-Ala**.

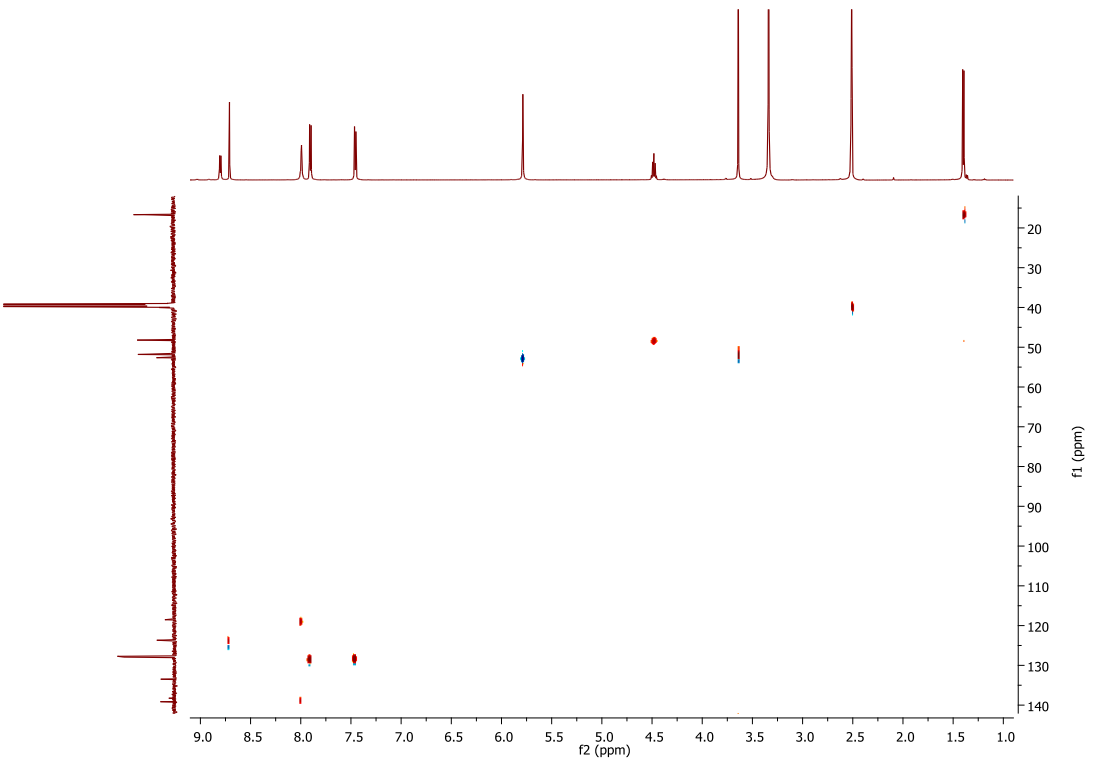

Figure B.23 HSQC (600 MHz, DMSO-d_6) of **91-*D*-Ala**.

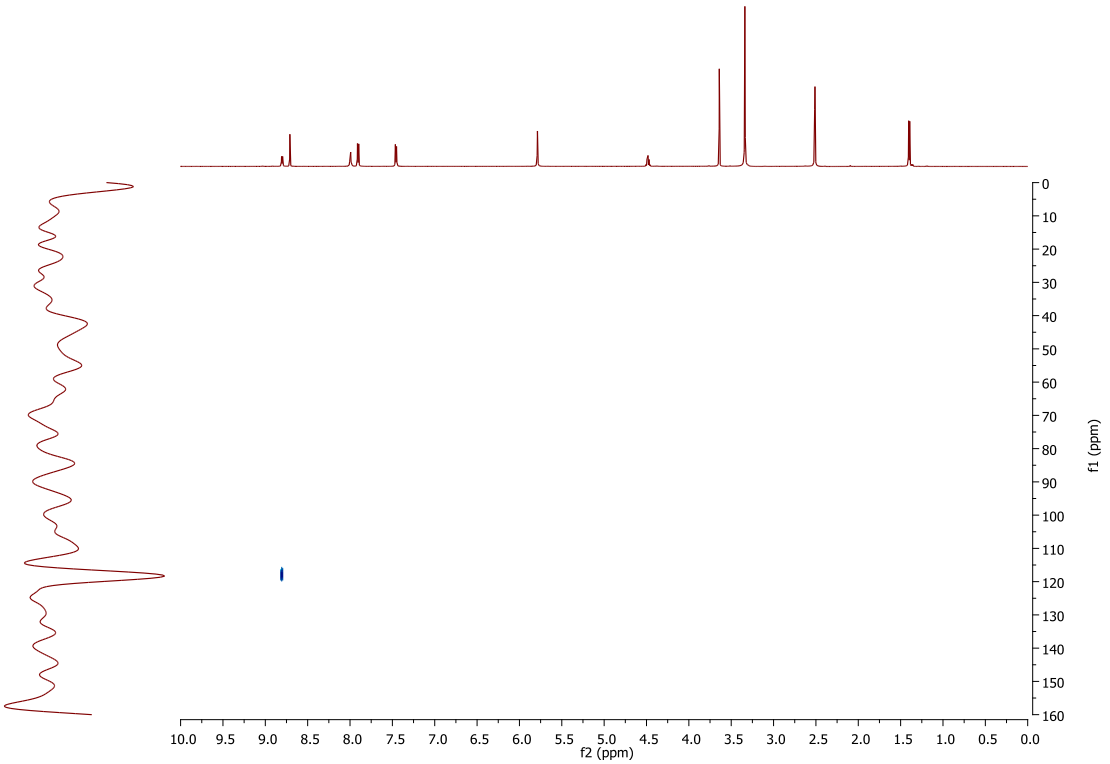

Figure B.24 NH COSY (600 MHz, DMSO-d_6) of **91-*D*-Ala**.

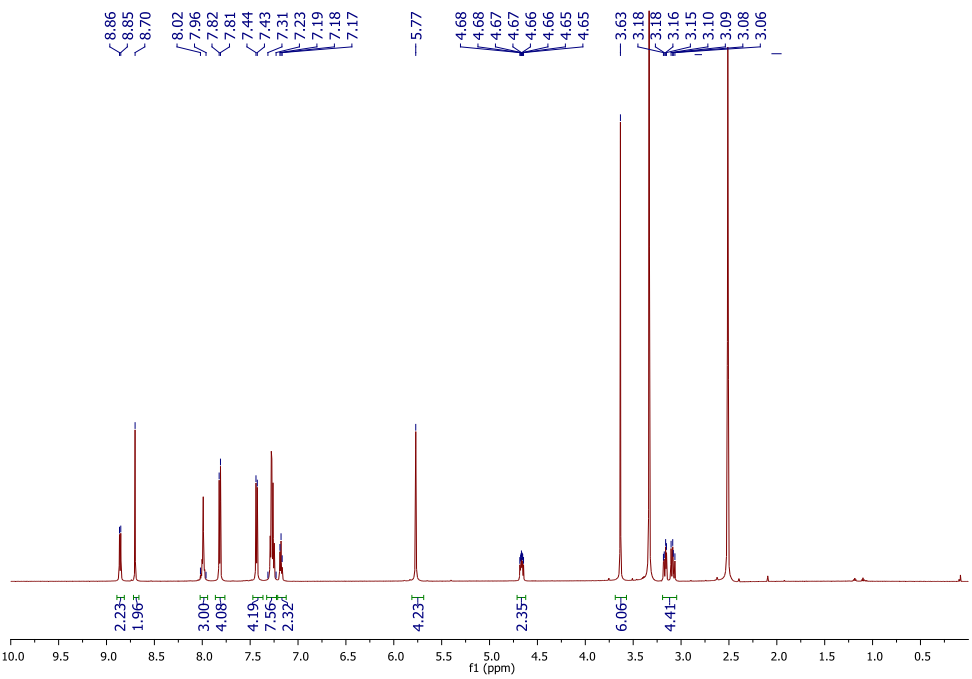

Figure B.25 ^{1}H NMR (600 MHz, DMSO-d_6) spectrum of ligand **91-*L*-Phe**.

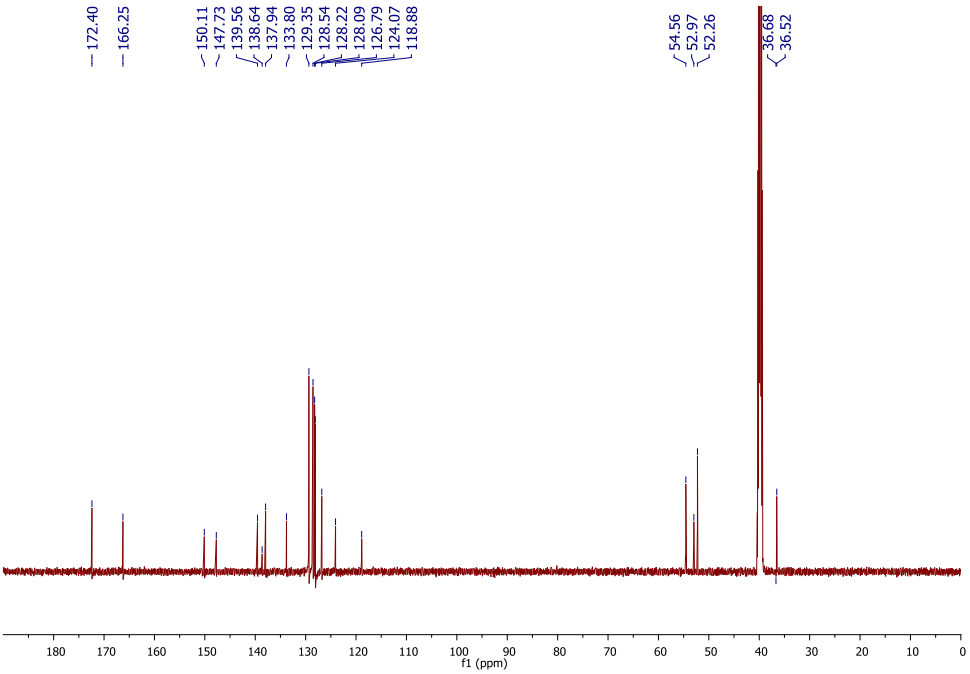

Figure B.26 ^{13}C NMR (150 MHz, DMSO-d_6) spectrum of ligand **91-*L*-Phe**.

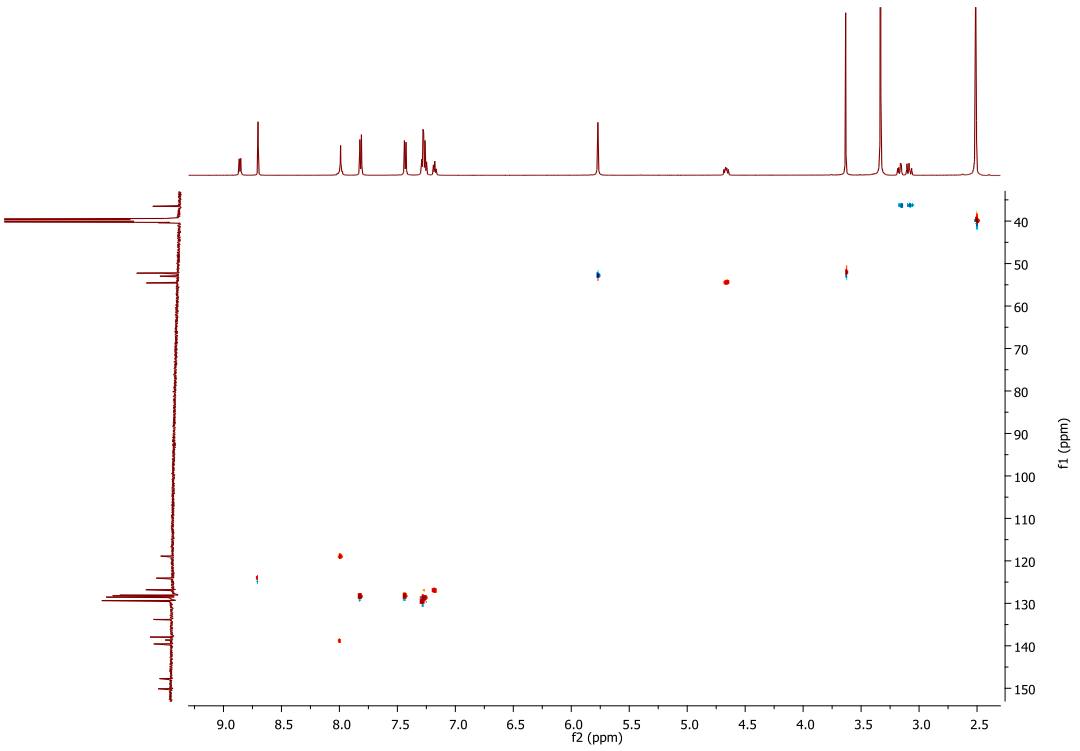

Figure B.27 HSQC (600 MHz, DMSO-d_6) of **91-*L*-Phe**.

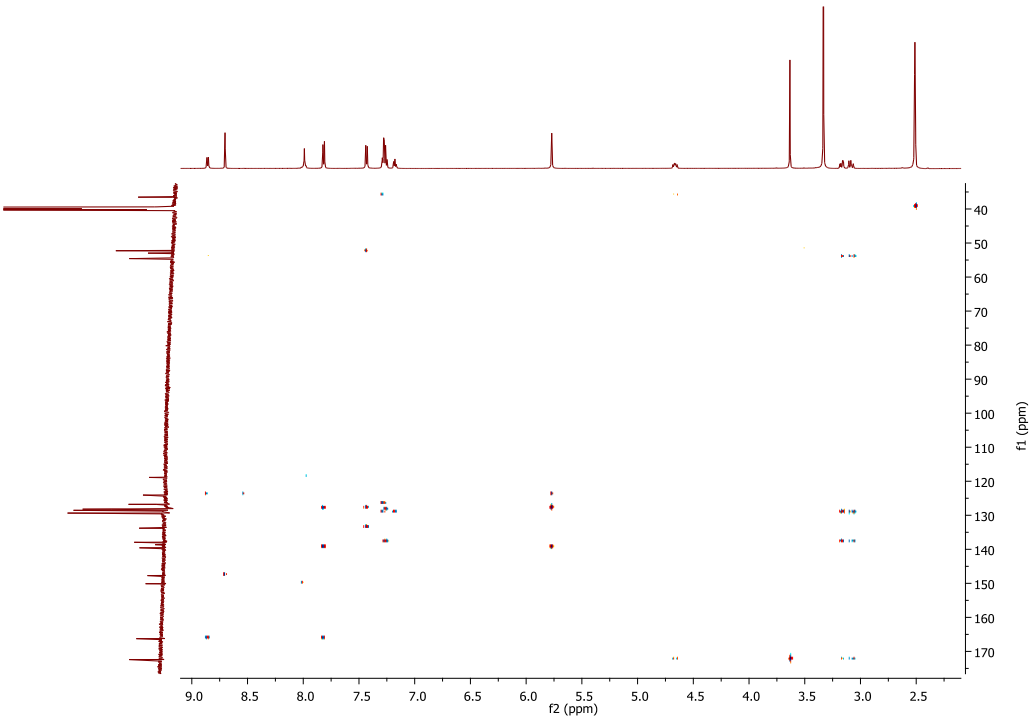

Figure B.28 HMBC (600 MHz, DMSO-d_6) of **91-*L*-Phe**.

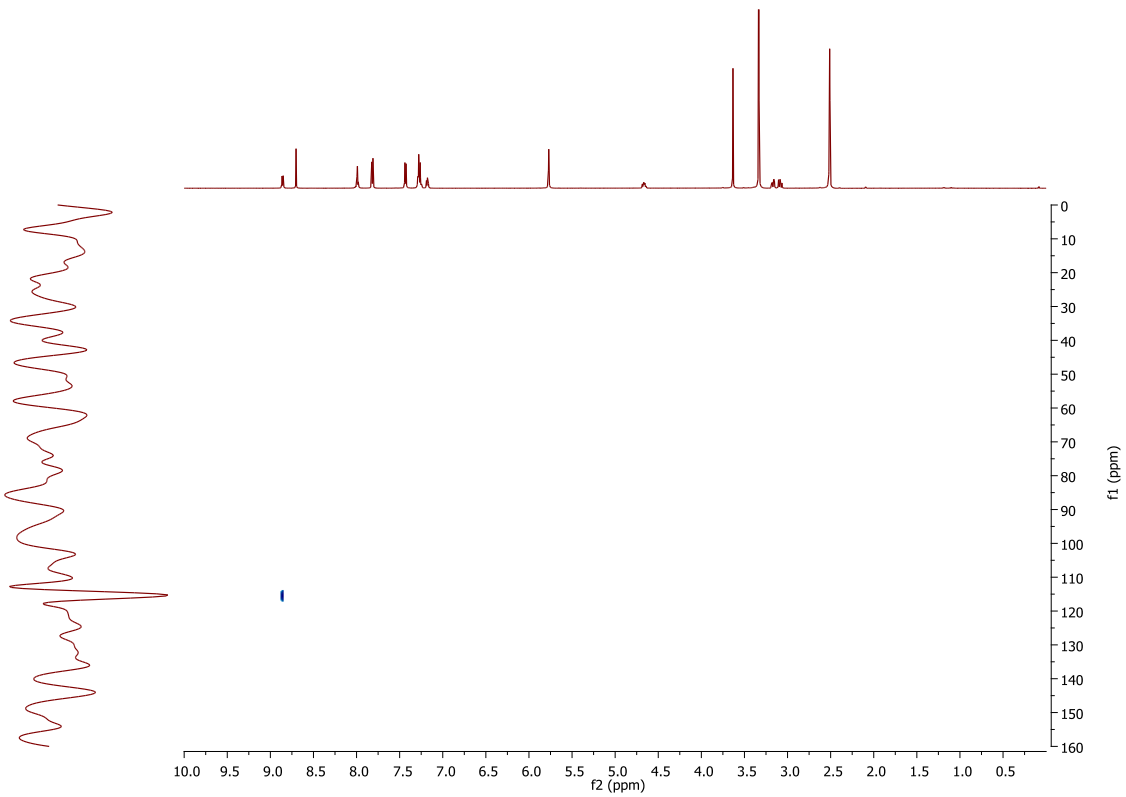

Figure B.29 NH COSY (600 MHz, DMSO-d_6) of **91-*L*-Phe**.

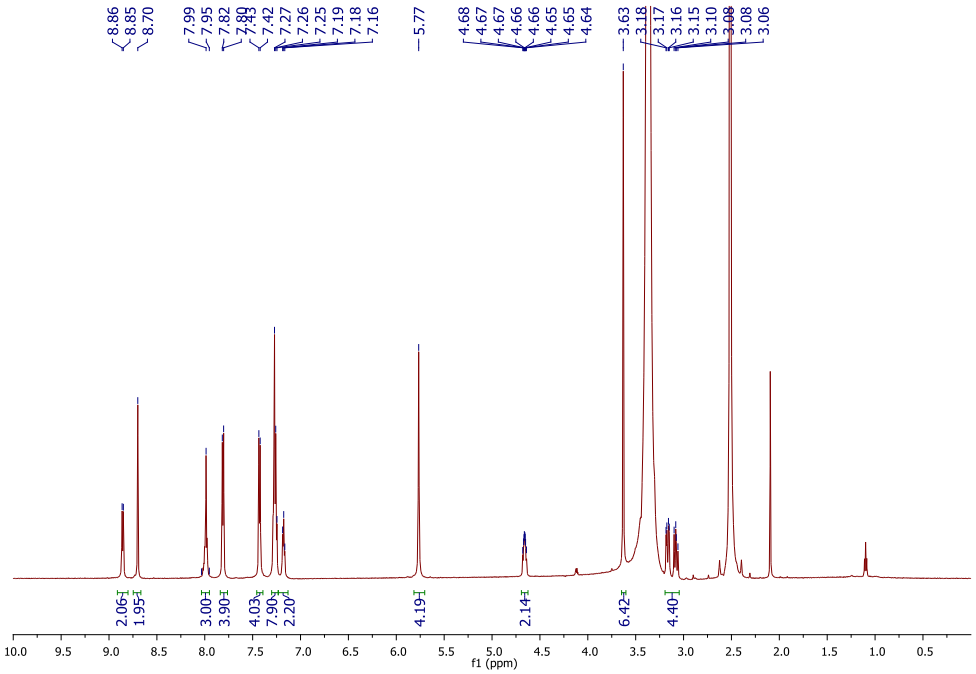

Figure B.30 ^{1}H NMR (600 MHz, DMSO-d_6) spectrum of **91-*D*-Phe**.

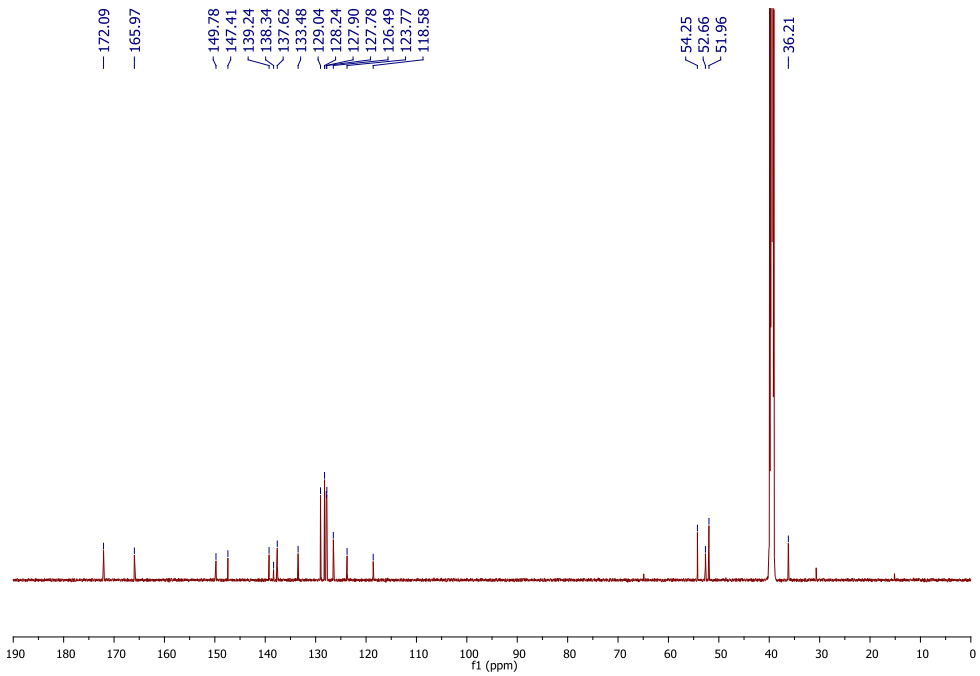

Figure B.31 ^{13}C NMR (150 MHz, DMSO-d_6) spectrum of ligand **91-*D*-Phe**.

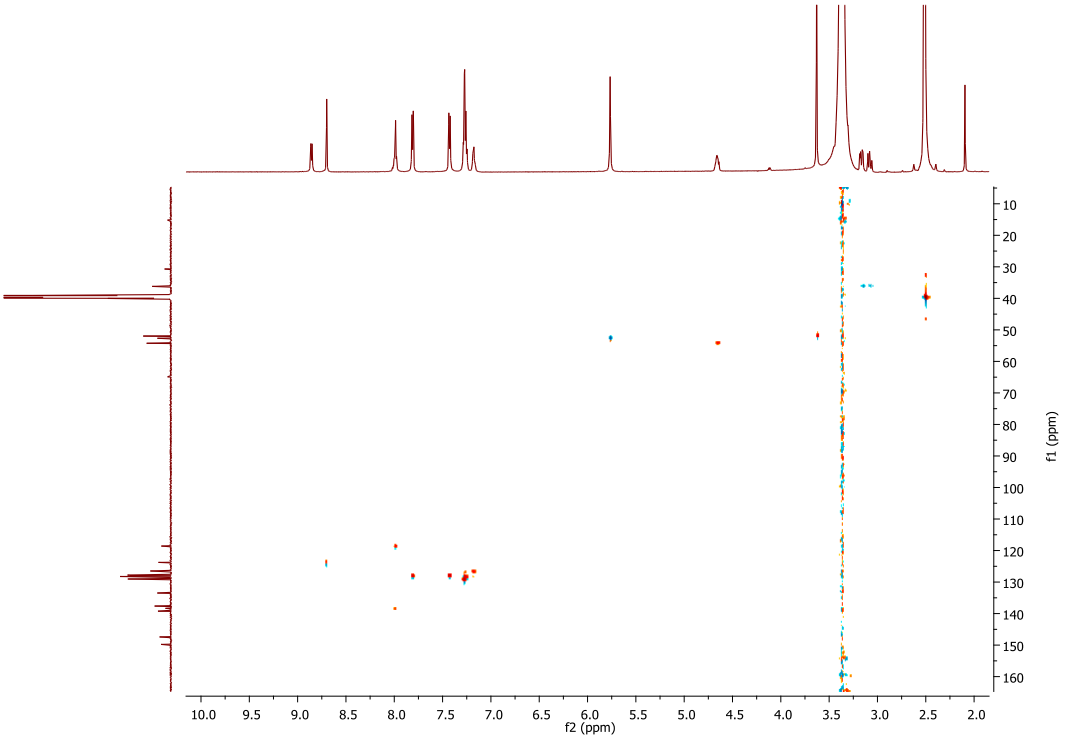

Figure B.32 HSQC (600 MHz, DMSO-d_6) of **91-*D*-Phe**.

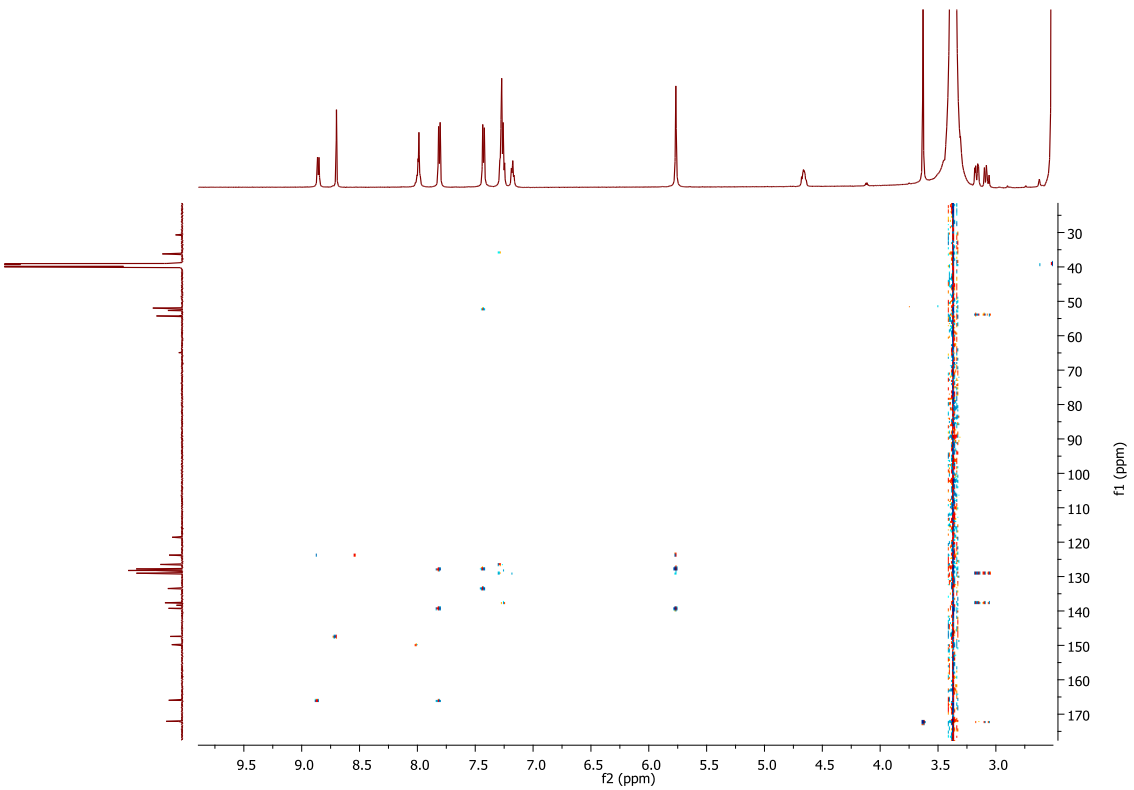

Figure B.33 HMBC (600 MHz, DMSO-d_6) of **91-*D*-Phe**.

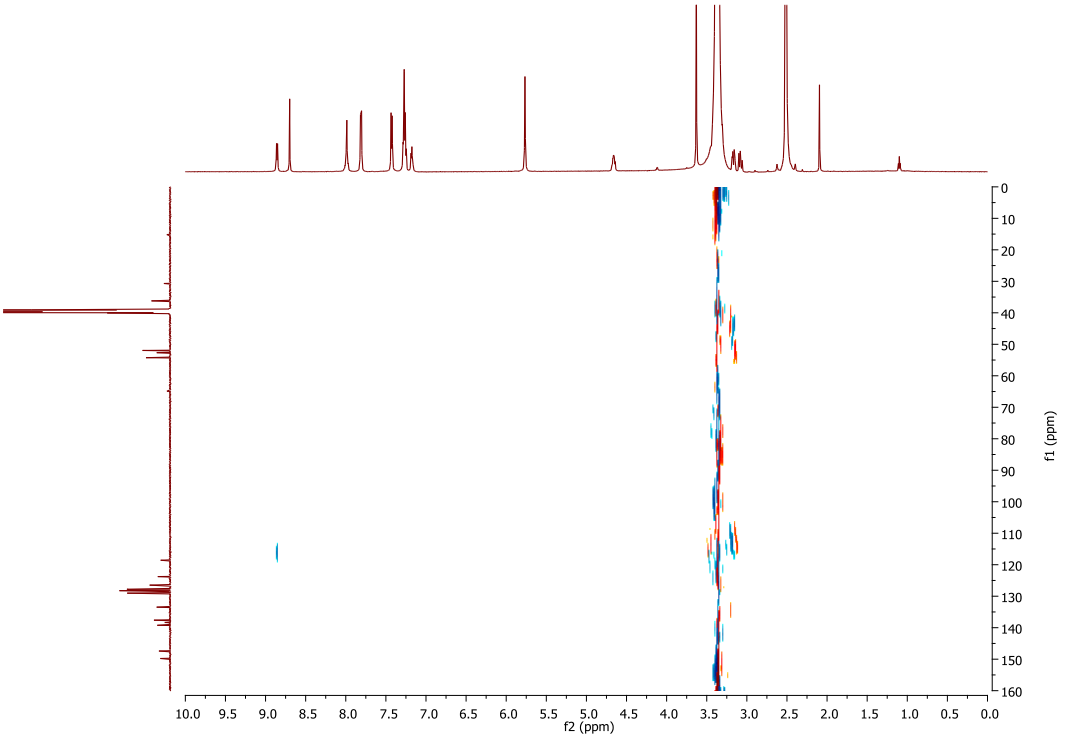

Figure B.34 NH COSY (600 MHz, DMSO-d_6) of **91-*D*-Phe**.

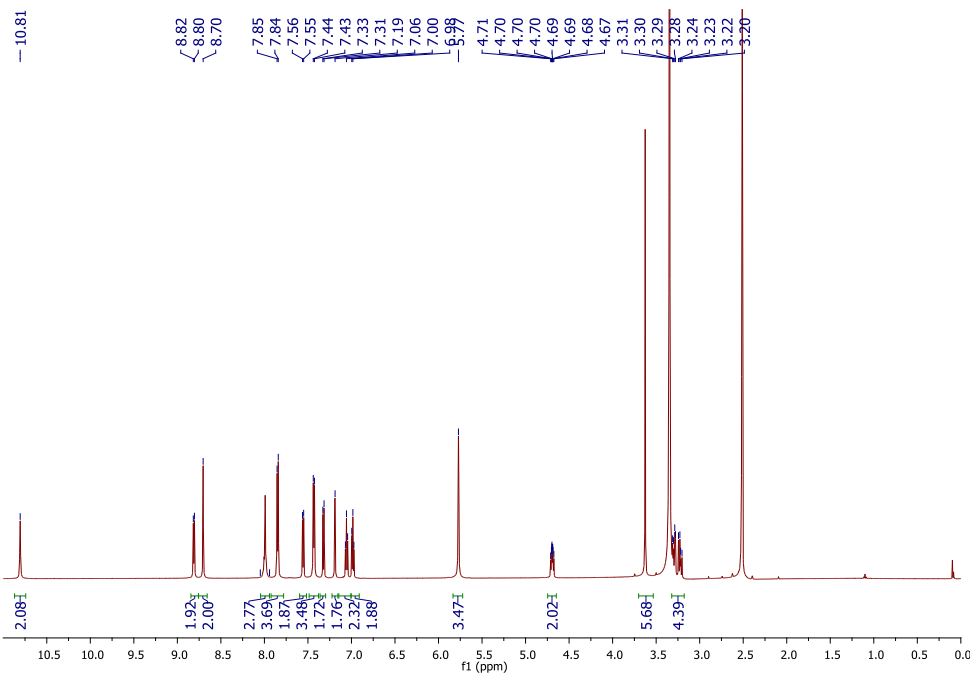

Figure B.35 ^{1}H NMR (600 MHz, DMSO-d_6) spectrum of ligand **91-*L*-Trp**.

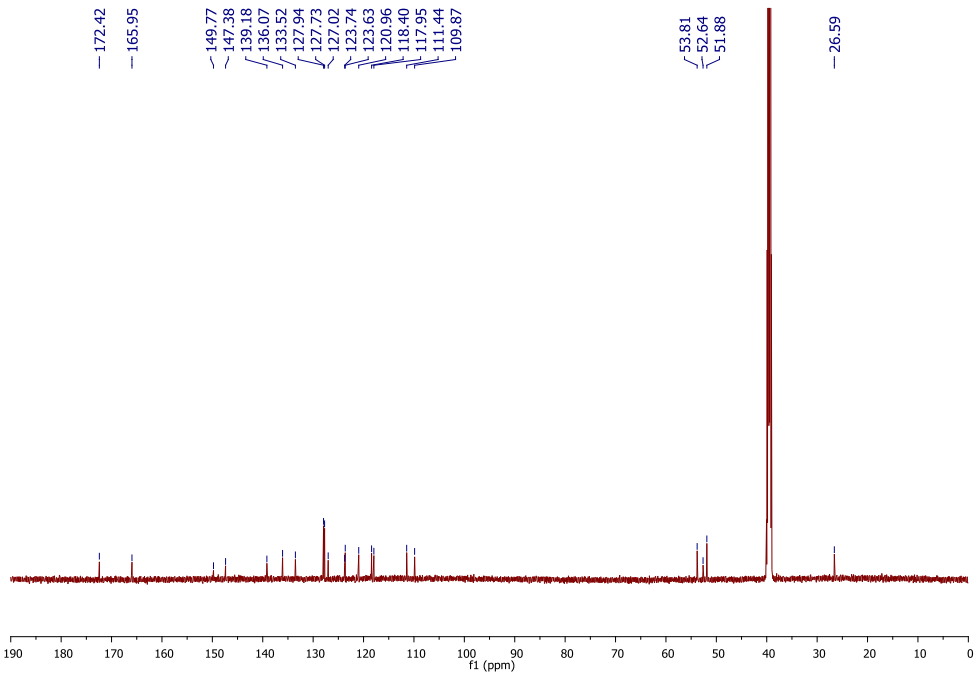

Figure B.36 ^{13}C NMR (150 MHz, DMSO-d_6) spectrum of ligand **91-*L*-Trp**.

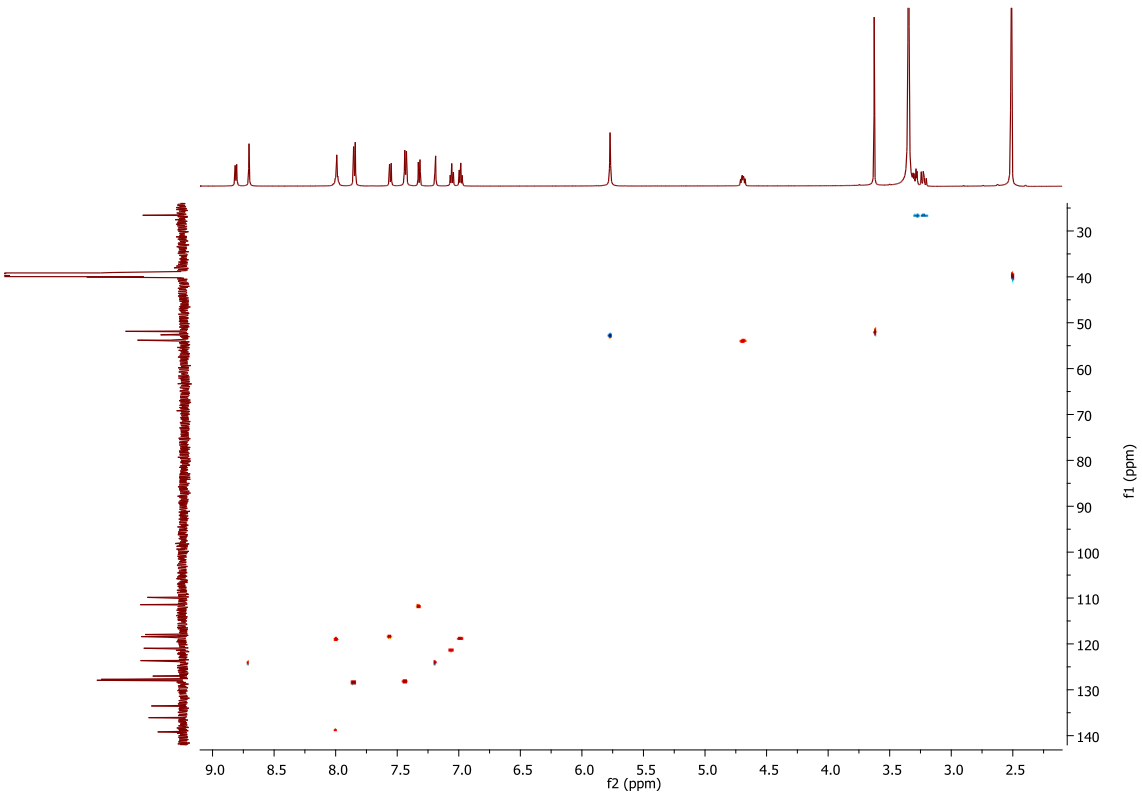

Figure B.37 HSQC (600 MHz, DMSO-d_6) of **91-*L*-Trp**.

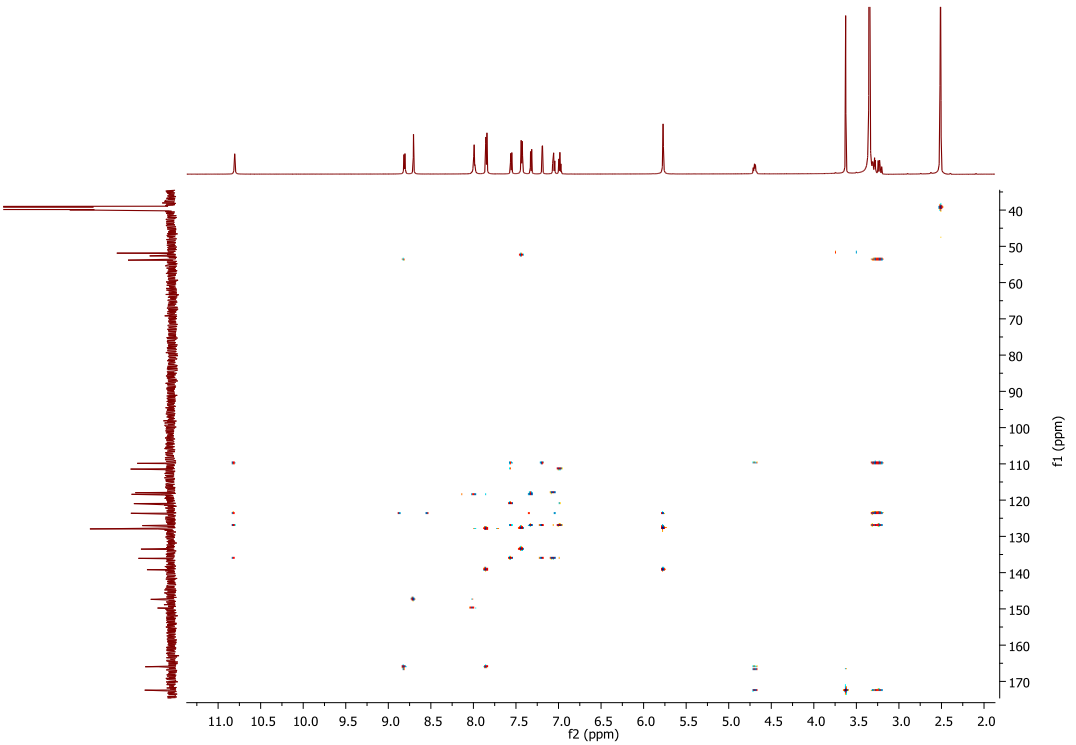

Figure B.38 HMBC (600 MHz, DMSO-d_6) of **91-*L*-Trp**.

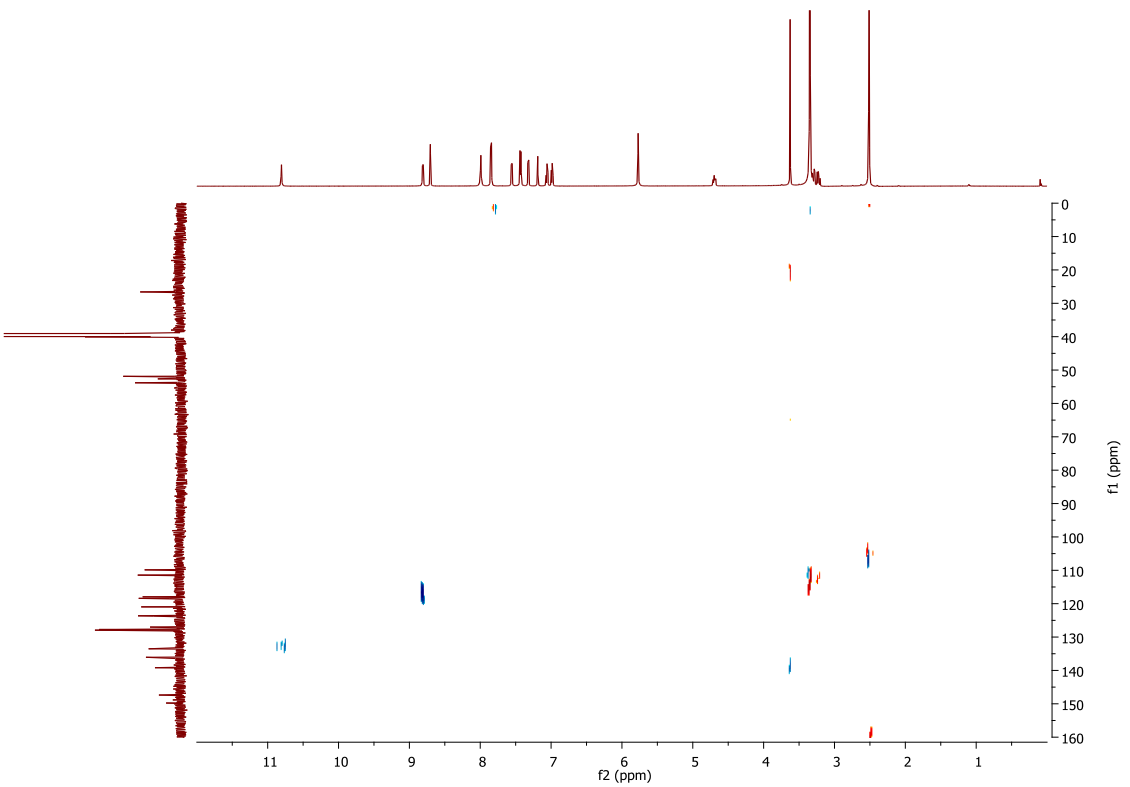

Figure B.39 NH COSY (600 MHz, DMSO-d_6) of **91-*L*-Trp**.

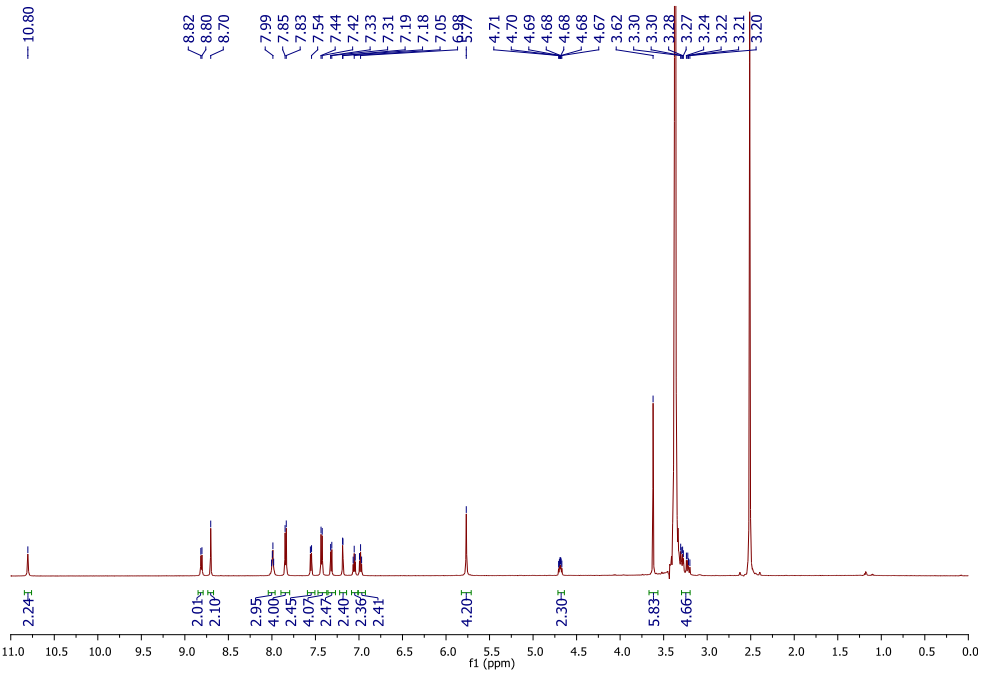

Figure B.40 ^{1}H NMR (600 MHz, DMSO-d_6) spectrum of ligand **91-*D*-Trp**.

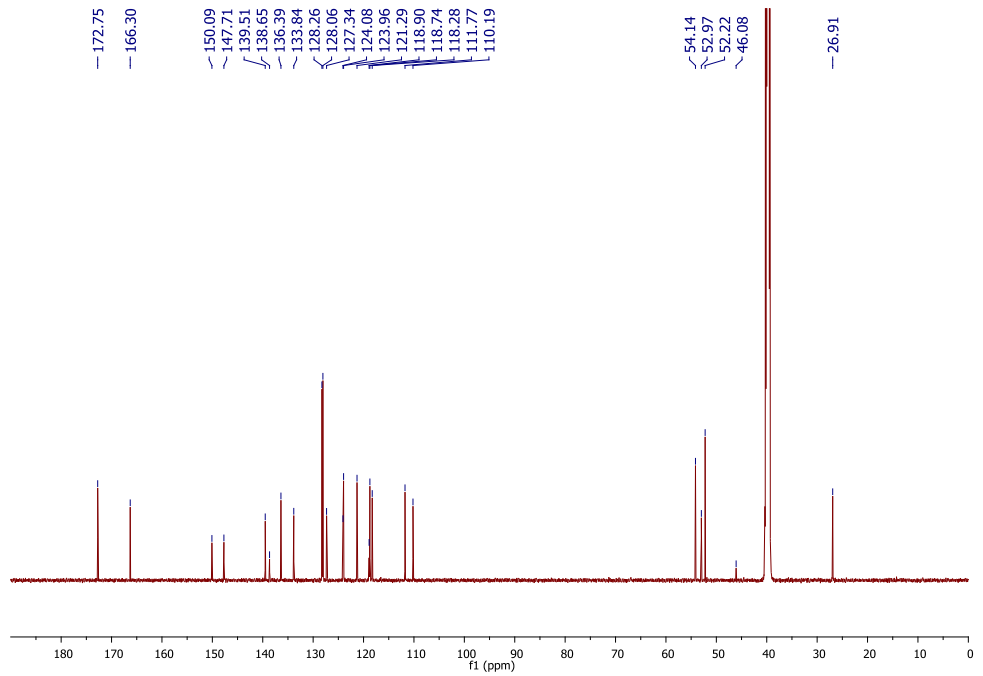

Figure B.41 ^{13}C NMR (150 MHz, DMSO-d_6) spectrum of ligand **91-*D*-Trp**

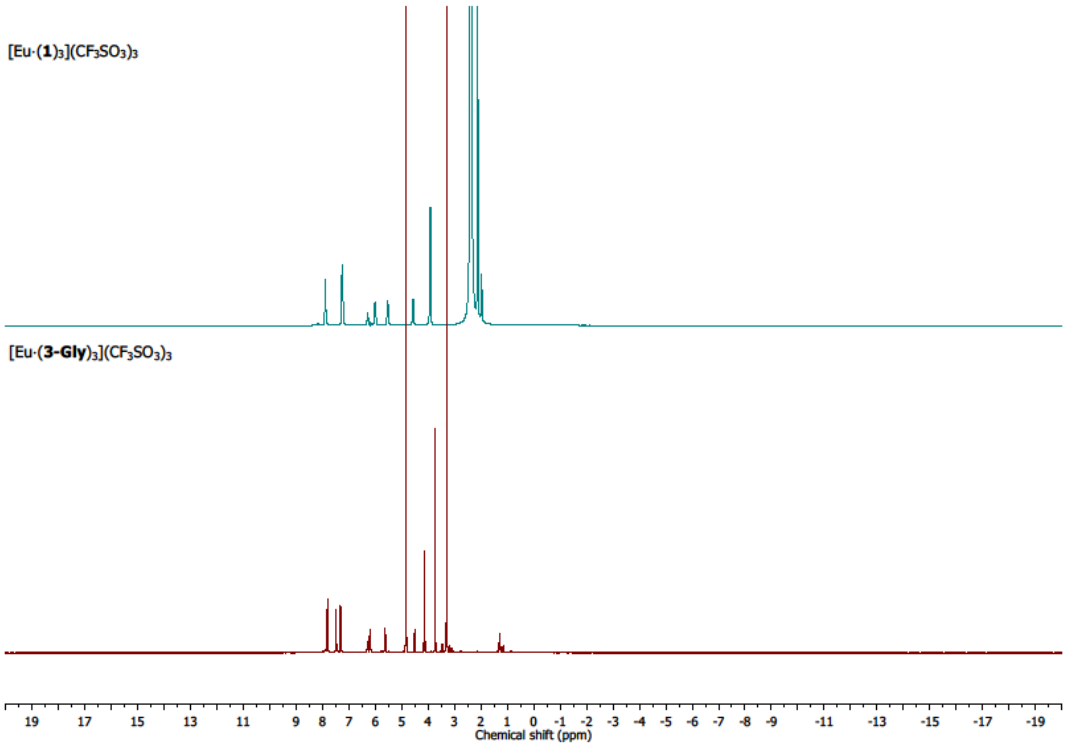

Figure B.42 ^{1}H NMR (400 MHz, CD_3CN) spectrum of $[Eu\cdot(\mathbf{88})_3](CF_3SO_3)_3$ and $[Eu\cdot(\mathbf{91\text{-}Gly})_3](CF_3SO_3)_3$

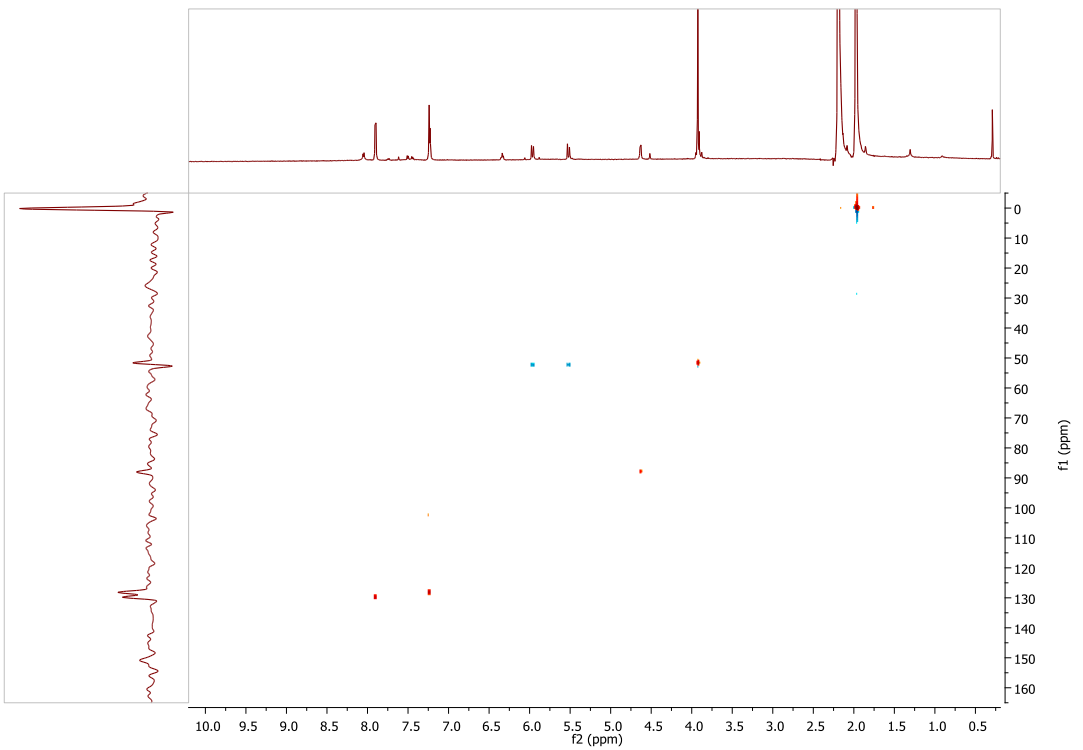

Figure B.43 HSQC (600 MHz, CD_3CN) of self-assembled $[Eu\cdot(\mathbf{88})_3](CF_3SO_3)_3$.

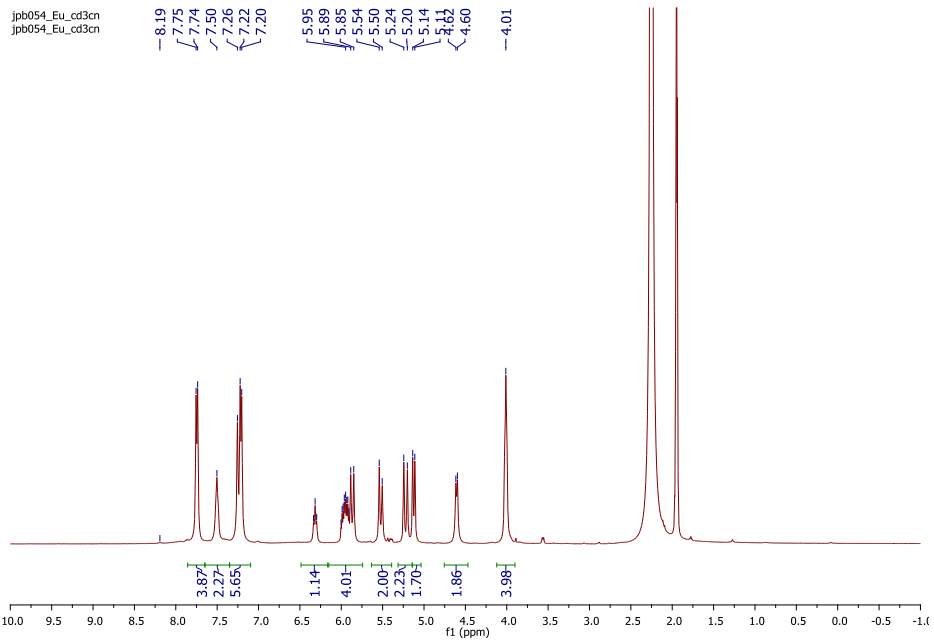

Figure B.44 ^{1}H NMR (400 MHz, CD_3CN) spectrum of [Eu·(**90**)$_3$](CF$_3$SO$_3$)$_3$.

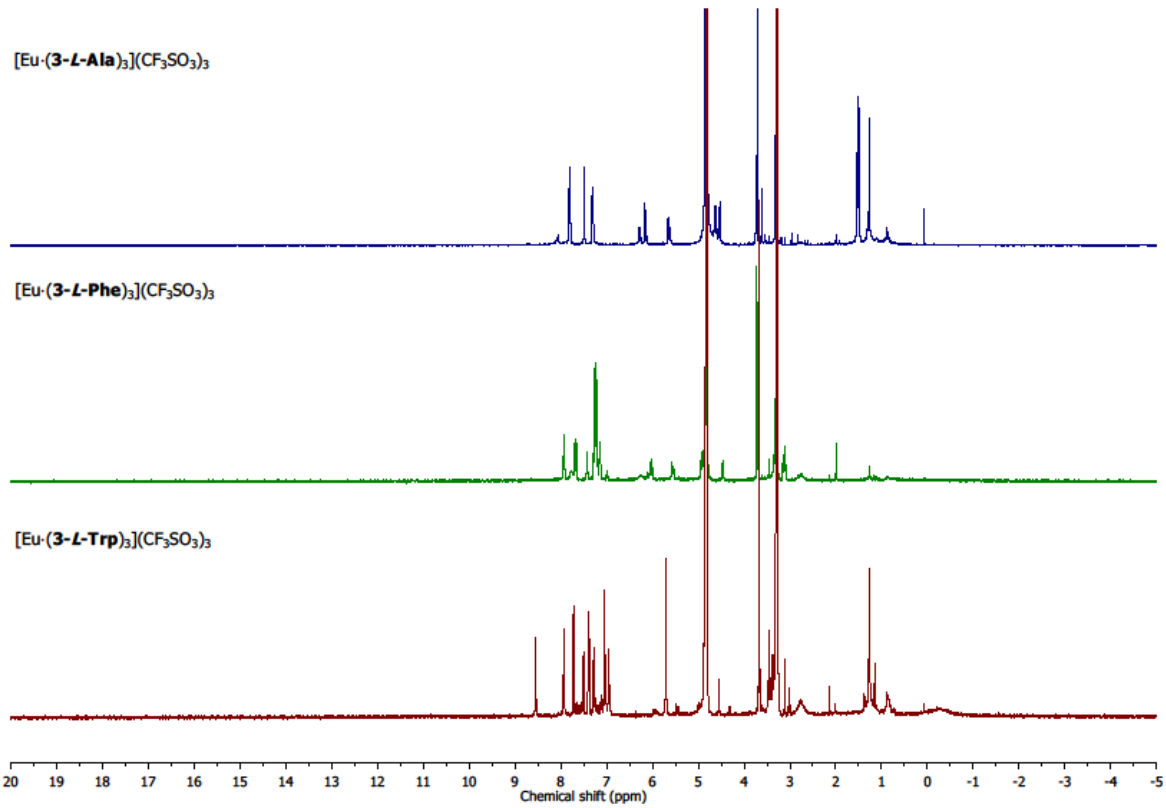

Figure B.45 ^{1}H NMR (400 MHz, CD_3CN) spectrum of [Eu·(**91-*L*-Ala**)$_3$](CF$_3$SO$_3$)$_3$, [Eu·(**91-*L*-Phe**)$_3$](CF$_3$SO$_3$)$_3$ and (CD_3OD) [Eu·(**91-*L*-Trp**)$_3$](CF$_3$SO$_3$)$_3$.

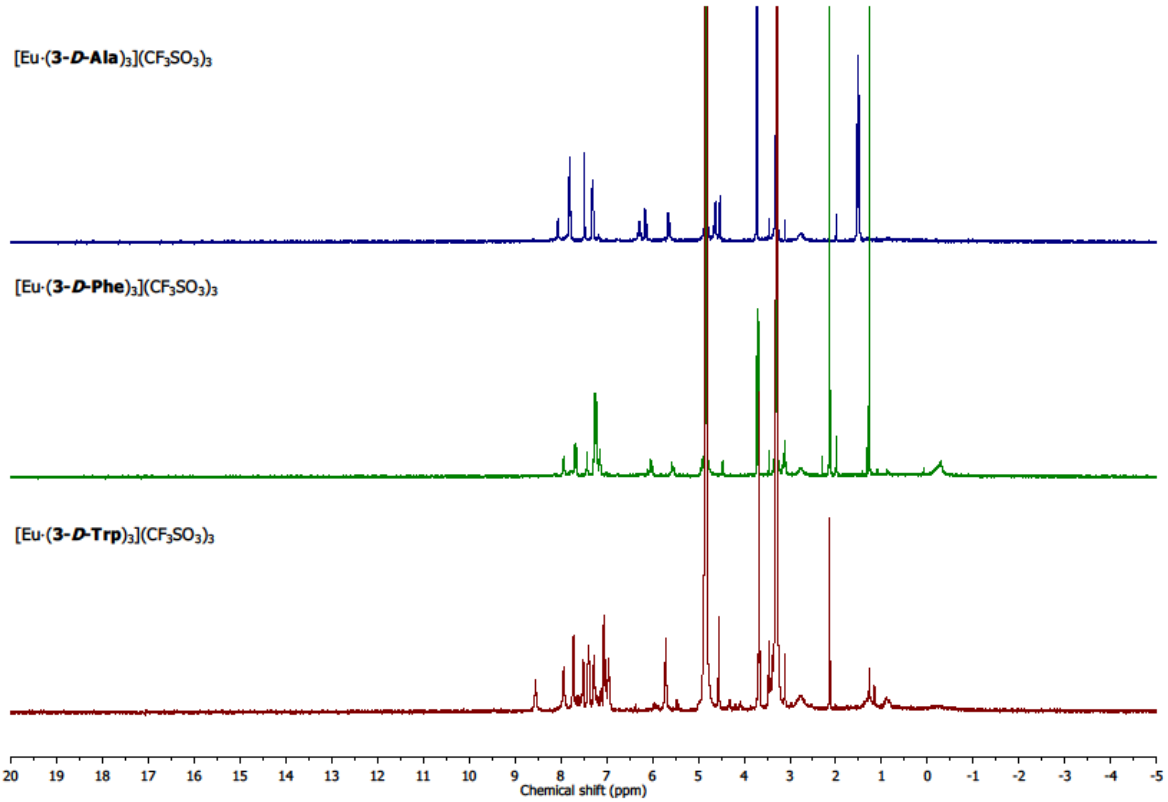

Figure B.46 ^{1}H NMR (400 MHz, CD_3CN) spectrum of [Eu·(**91-*D*-Ala**)$_3$]$(CF_3SO_3)_3$, [Eu·(**91-*D*-Phe**)$_3$]$(CF_3SO_3)_3$ and (CD_3OD) [Eu·(**91-*D*-Trp**)$_3$]$(CF_3SO_3)_3$.

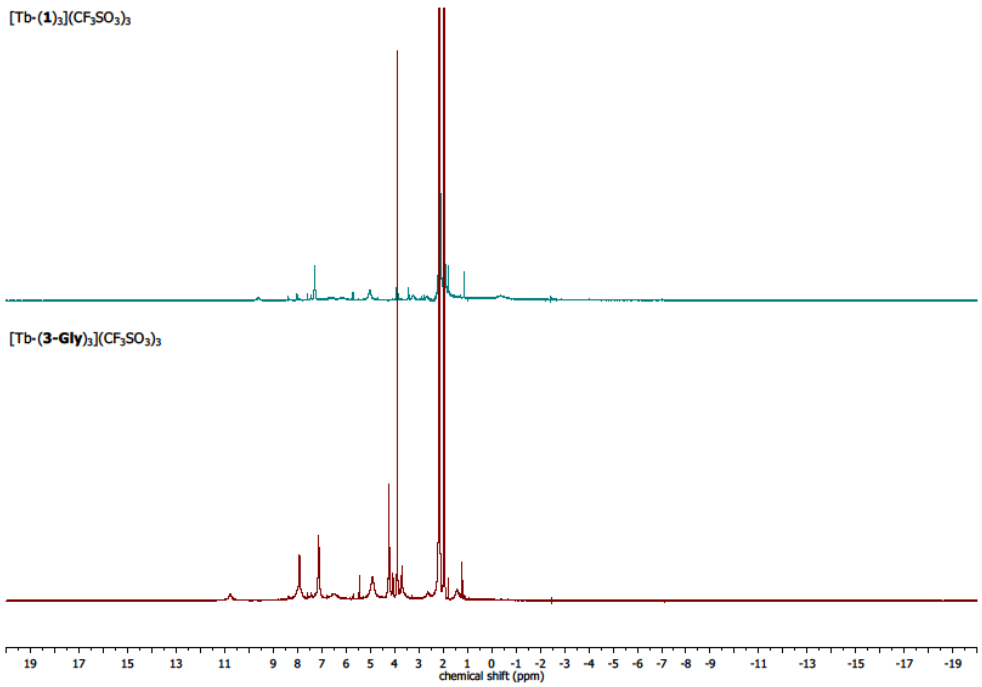

Figure B.47 ^{1}H NMR (400 MHz, CD_3CN) spectra of [Tb·(**1**)$_3$]$(CF_3SO_3)_3$ and [Tb(**91-Gly**)$_3$]$(CF_3SO_3)_3$.

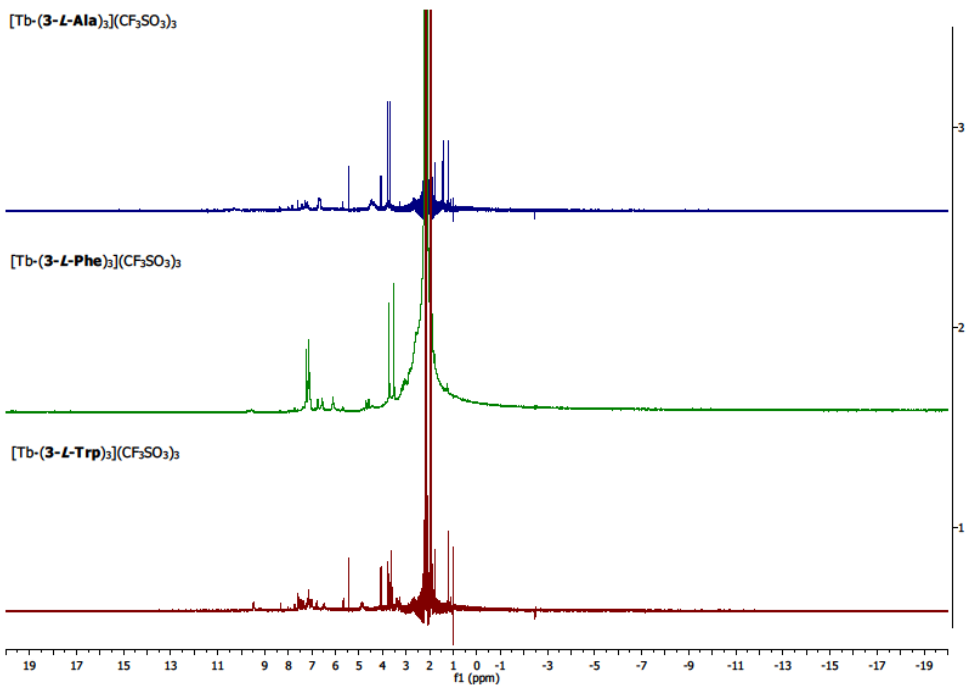

Figure B.48 ^{1}H NMR (400 MHz, CD_3CN) spectrum of [Tb·(**91-*L*-Ala**)$_3$]$(CF_3SO_3)_3$, [Tb·(**91-*L*-Phe**)$_3$]$(CF_3SO_3)_3$ and [Tb·(**91-*L*-Trp**)$_3$]$(CF_3SO_3)_3$.

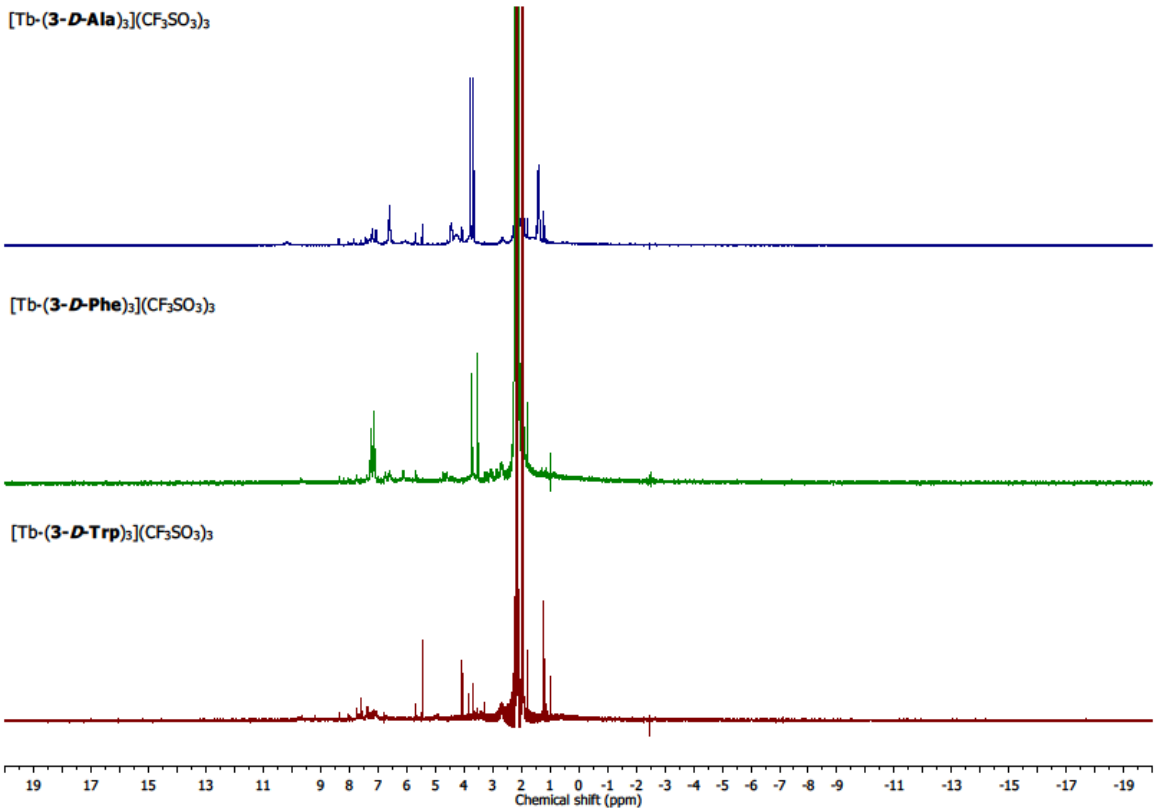

Figure B.49 ^{1}H NMR (400 MHz, CD_3CN) spectrum of [Tb·(**91-*D*-Ala**)$_3$]$(CF_3SO_3)_3$, [Tb·(**91-*D*-Phe**)$_3$]$(CF_3SO_3)_3$ and [Tb·(**91-*D*-Trp**)$_3$]$(CF_3SO_3)_3$.

B.2. Selective ROSEY and TOCSY spectra of 88, $[Eu\cdot(88)_3](CF_3SO_3)_3$ and 95

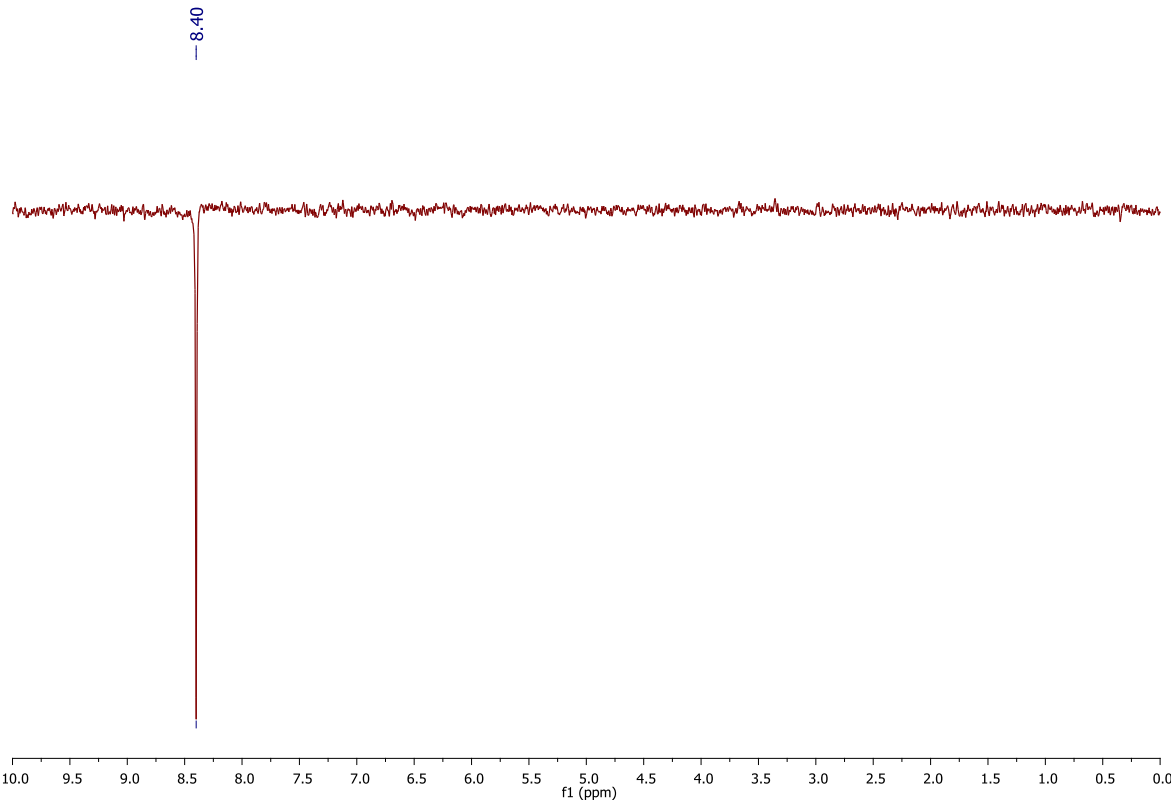

Figure B.50 Selective ROESY spectrum (400 MHz, CD_3CN) of **88**, irradiated at 8.40 ppm, showing lack of through-space interactions of ligand triazolyl resonance.

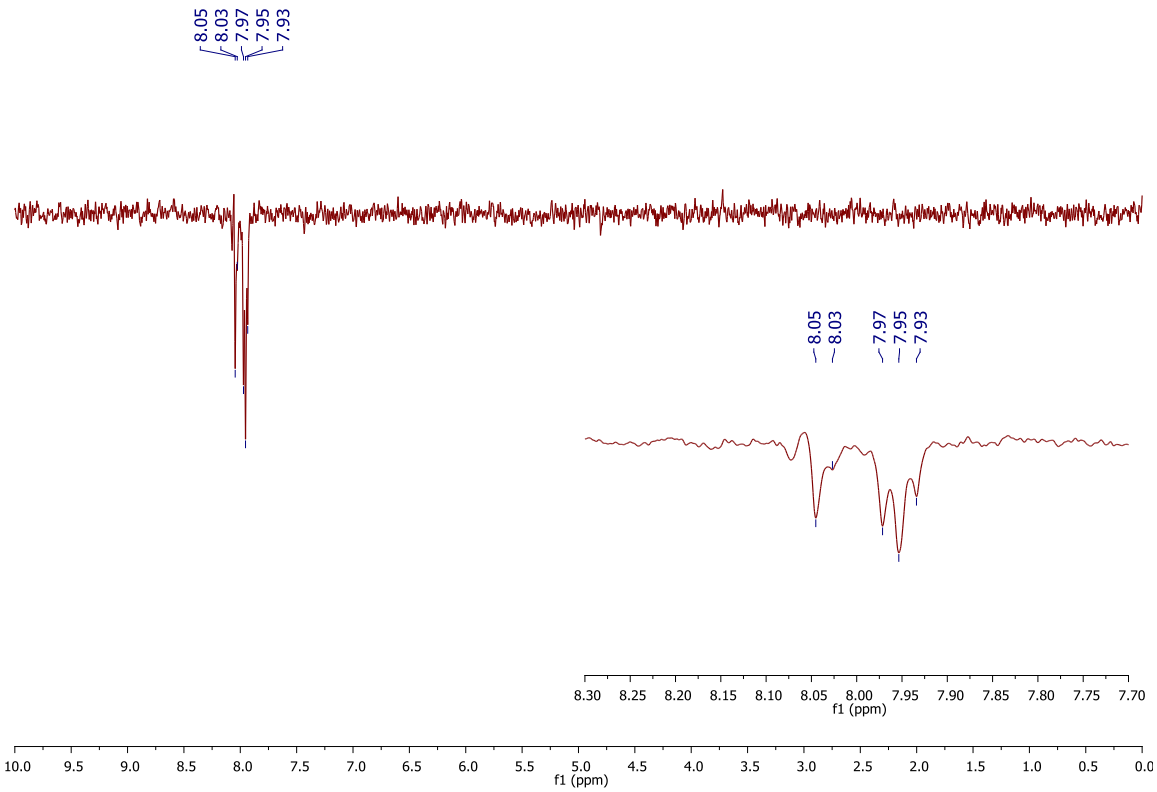

Figure B.51 ROESY spectrum (400 MHz, CD_3CN) of **88** measured upon selective irradiation of the 4-pyridyl resonance (7.95 ppm), showing through-space interactions between the 4-pyridyl CH (triplet) and **91**-- and 5-pyridyl protons (adjacent doublet). There was no through-space interaction observed with the triazolyl protons (8.40 ppm) The expanded region shows the signals in more detail.

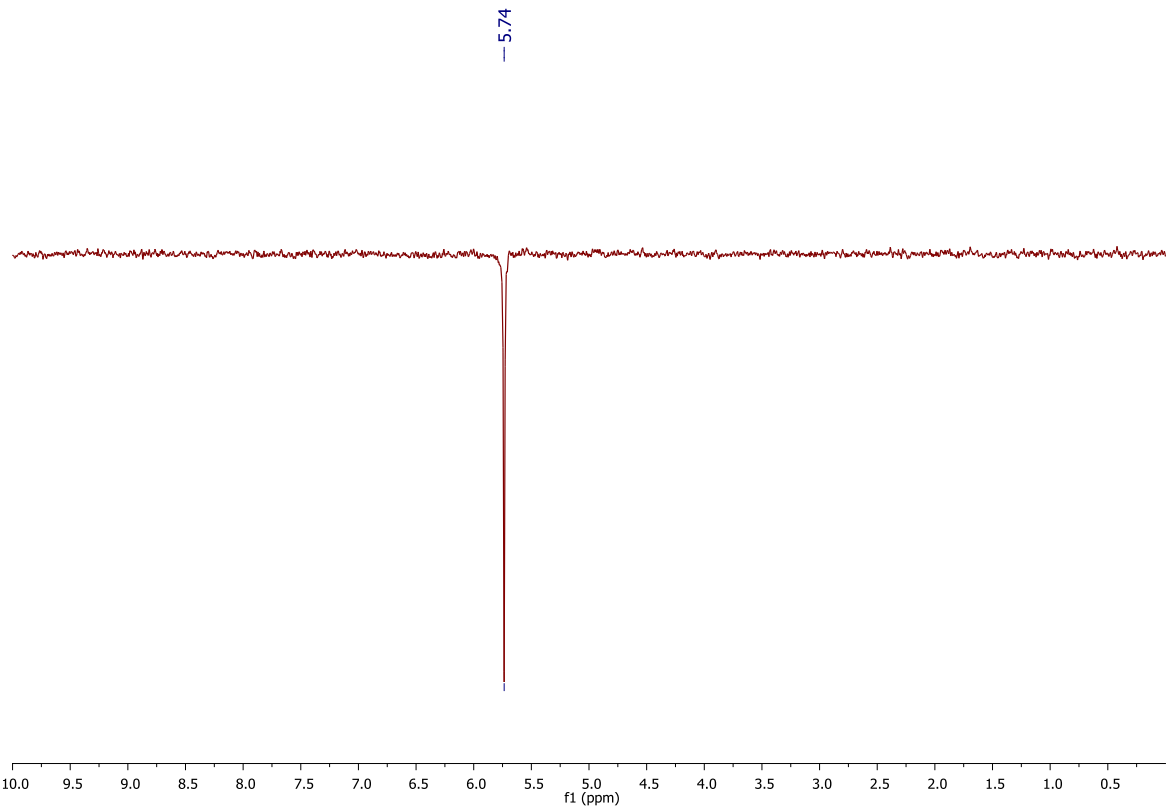

Figure B.52 Selective ROESY spectrum (400 MHz, CD_3CN) of **88**, irradiated at 5.74 ppm, showing lack of through-space interactions of CH_2 resonance.

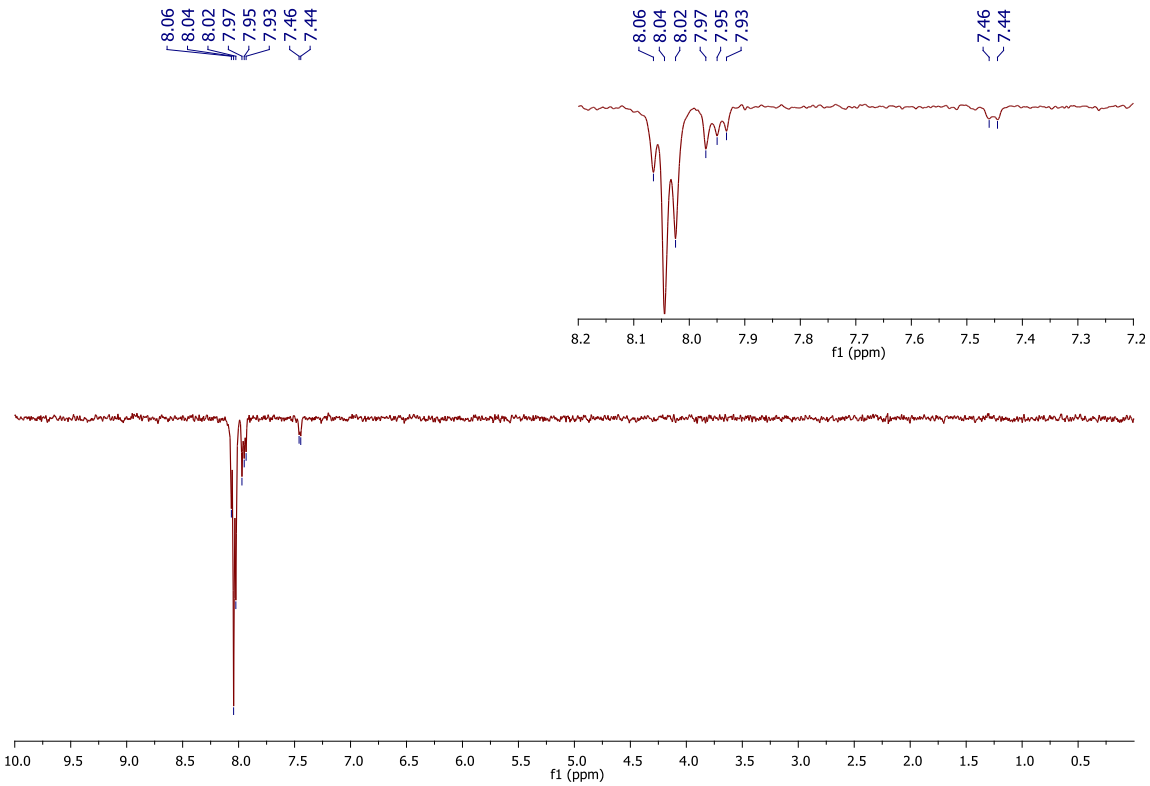

Figure B.53 ROESY spectrum (400 MHz, CD_3CN) of ligand **88**, selectively irradiated at 8.05 ppm, showing that the overlapping peaks at this chemical shift have through-space interactions with the 4-pyridyl proton (triplet at 7.95 ppm) and a phenyl CH (doublet at 7.45 ppm). The expanded region shows the signals in more detail. Particularly of note is the absence of interactions with the triazolyl resonance at 8.40 ppm, supporting an *anti-anti* ligand geometry.

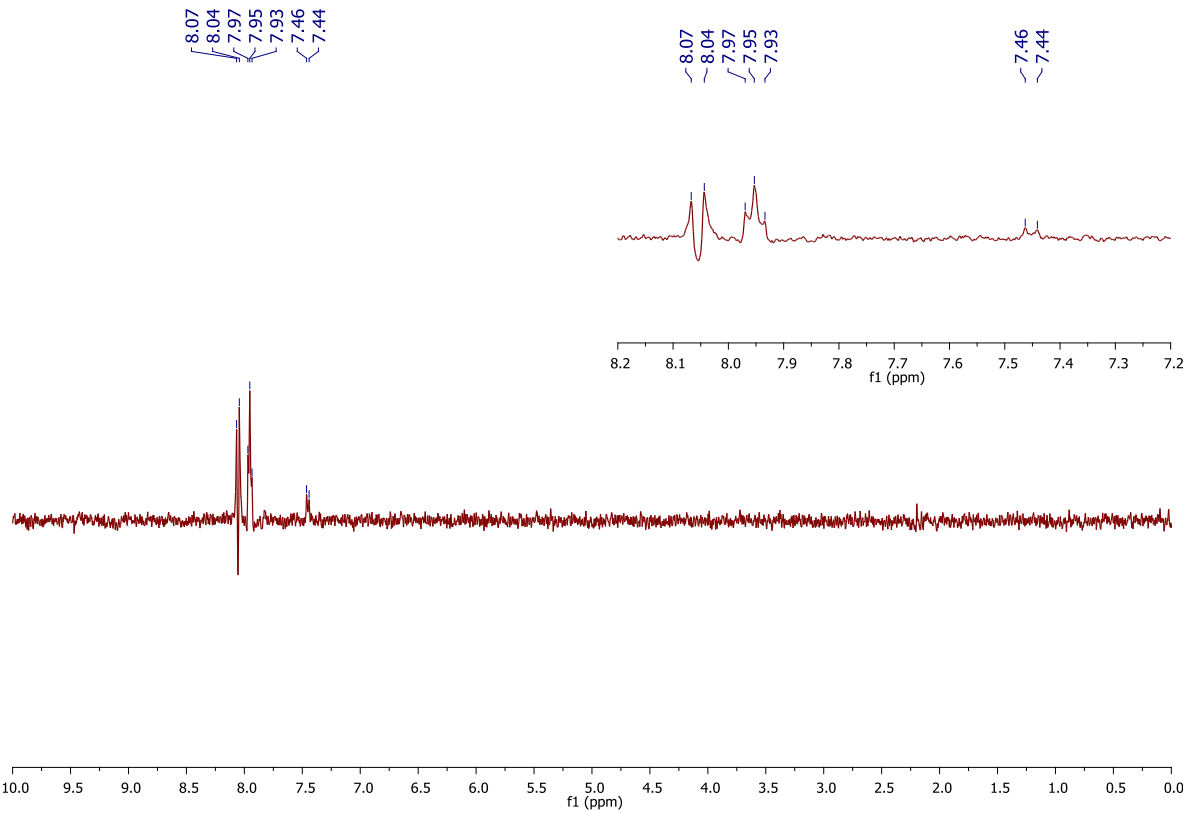

Figure B.54 TOCSY spectrum (400 MHz, CD_3CN) of ligand **88**, selectively irradiated at 8.05 ppm, showing that the overlapping peaks at this chemical shift are from two spin systems: the pyridyl system (evidenced by the interaction with the triplet at 7.95 ppm) and the phenyl ring (evidenced by the doublet at 7.45 ppm). The expanded region shows the signals in more detail.

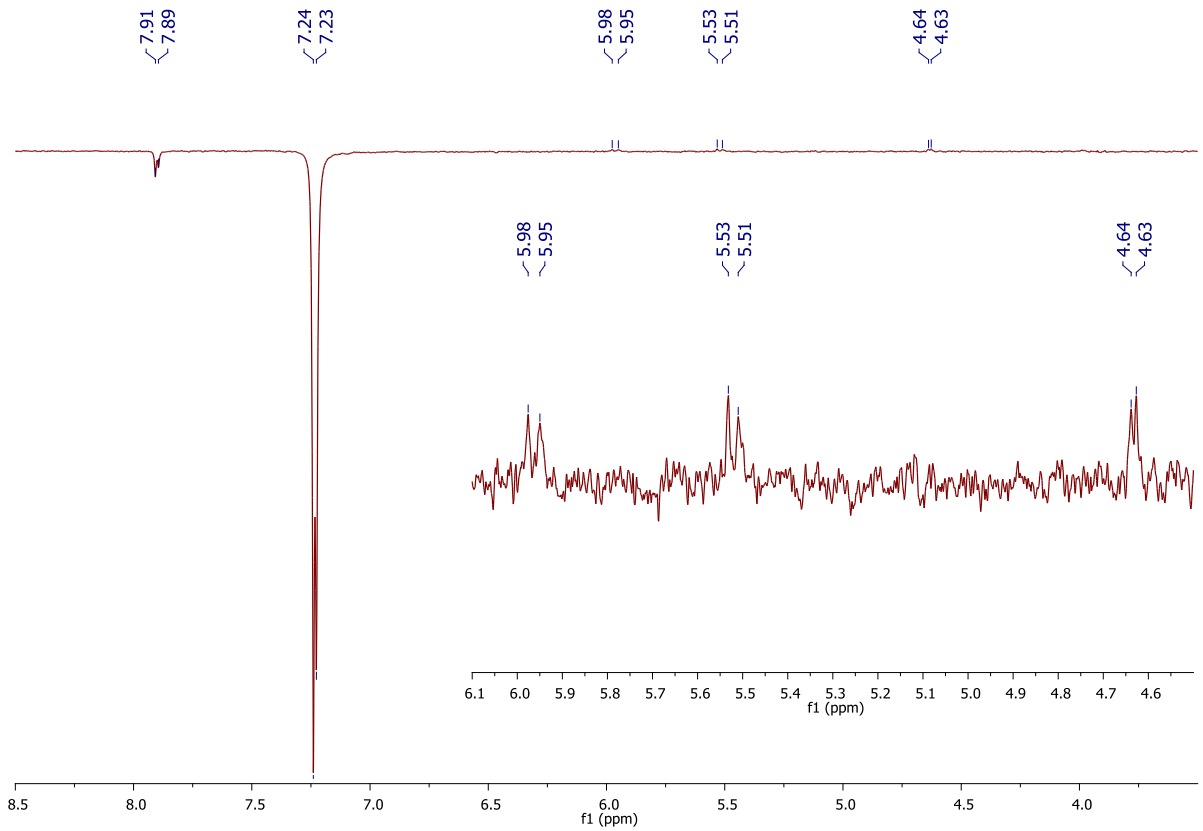

Figure B.55 ROESY spectrum (600 MHz, CD_3CN) of [Eu·(**88**)$_3$]$(CF_3SO_3)_3$ upon selective irradiation of the overlapping signals at 7.24 ppm (assigned to the triazolyl and phenyl protons by 2D spectroscopy), showing through-space interactions with the phenyl signal at 7.90 ppm, as well as with the split CH_2 signals at 5.96 and 5.52 ppm and the **91**--pyridyl signal at 4.63 ppm. This suggests the **btp** motif has adopted a *syn-syn* conformation, where the triazolyl and pyridyl protons had through-space interactions. Expanded region shows CH_2 and **91**--pyridyl resonances in more detail.

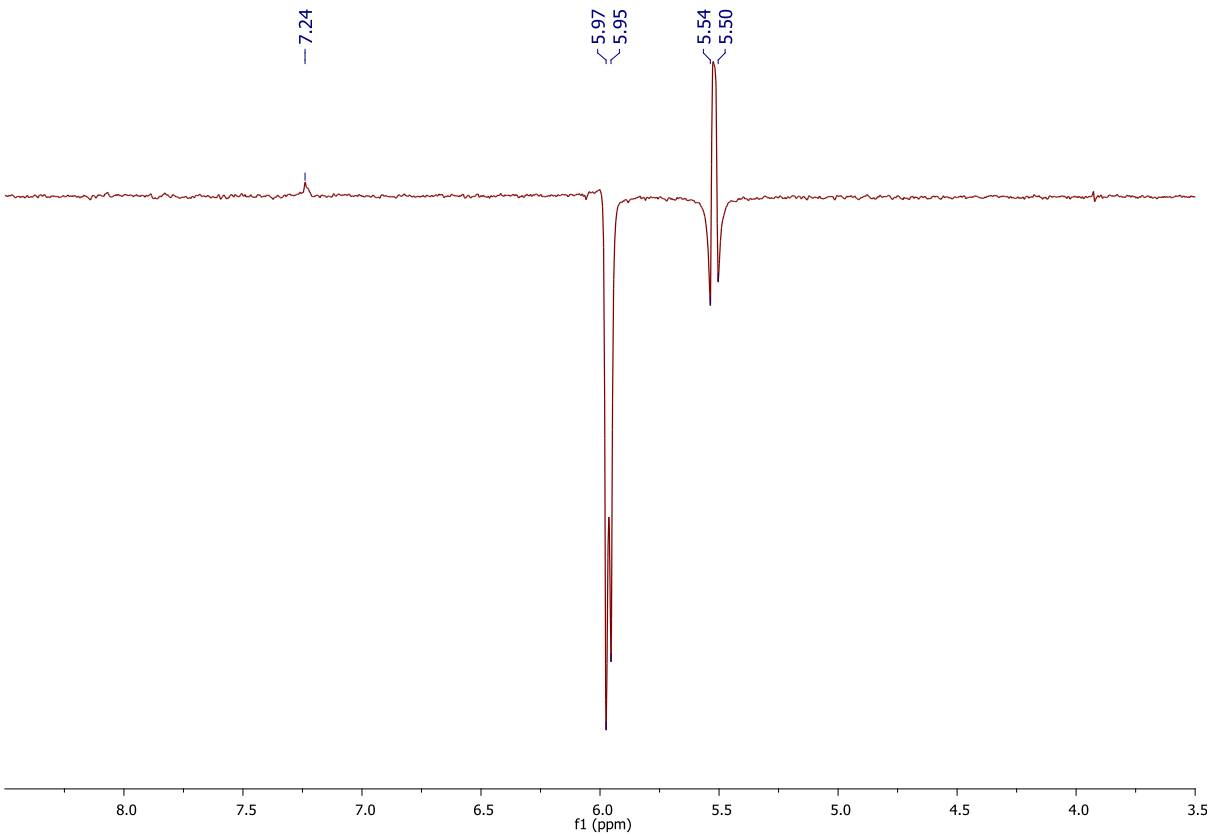

Figure B.56 ROESY spectrum (600 MHz, CD_3CN) of [Eu·(**88**)$_3$](CF_3SO_3)$_3$ upon selective irradiation at 5.52 ppm showing through-space interactions with the germinal protons (at 5.96 ppm) and a signal at 7.24 ppm.

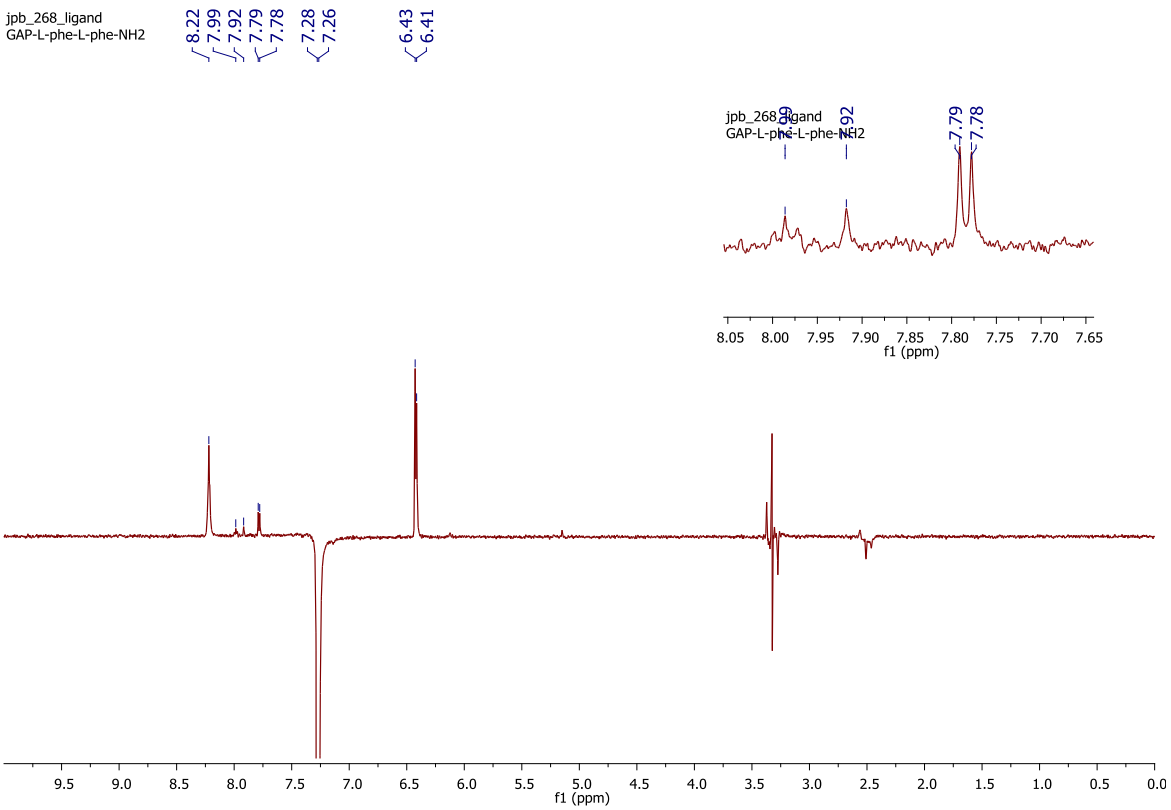

Figure B.57 ROESY spectrum (600 MHz, CD_3CN) of **95** upon selective irradiation of the phenyl resonance at 7.27 ppm showing through-space interactions the other phenyl doublet at 6.42 ppm and the amide NH at 8.22 ppm, as would be expected in a monomer. Unusually, through-space interactions were also seen with the resonances assigned to the **btp** motif (magnified in the inset). This is consistent with the through-space interactions between the phenyl rings and **btp** motif seen in the solid state structure, and is supportive of the formation of a [2]catenane structure in solution state.

B.1. Infrared spectra

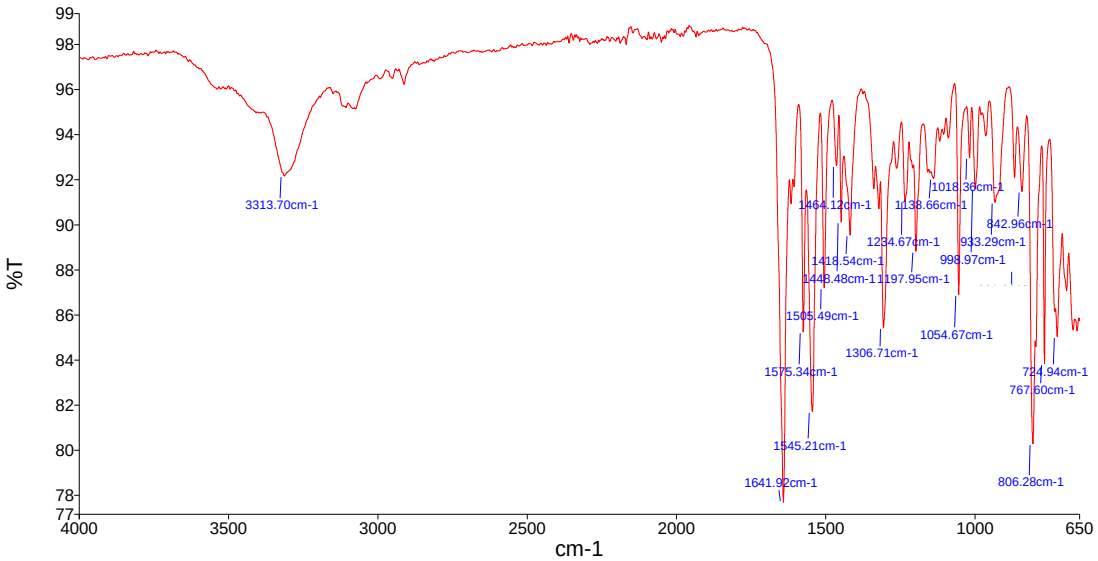

Figure B.58 IR spectrum of ligand **90**.

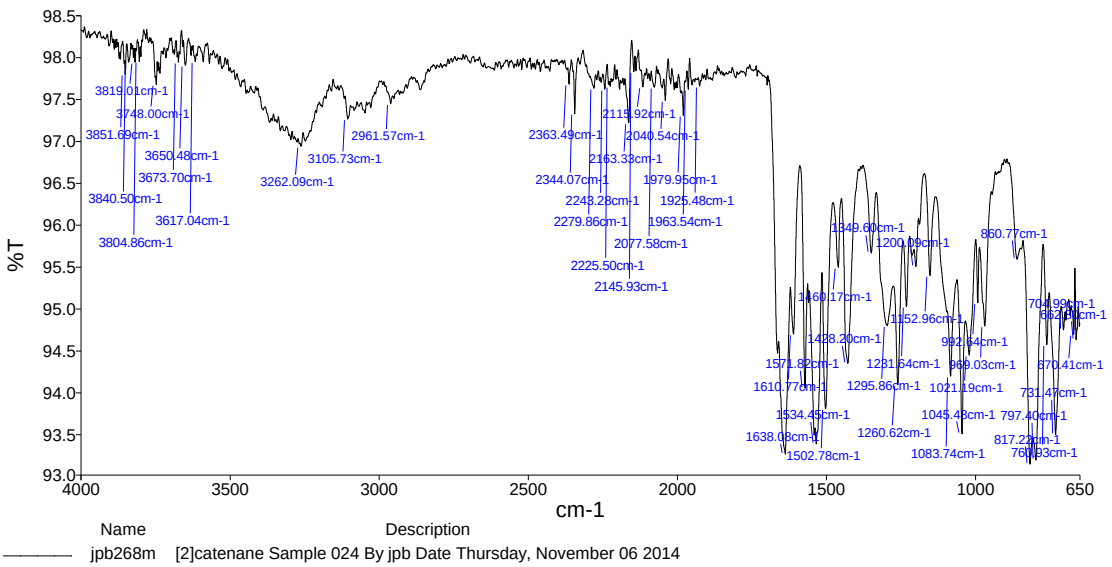

Figure B.59 IR spectrum of [2]catenane **95**.

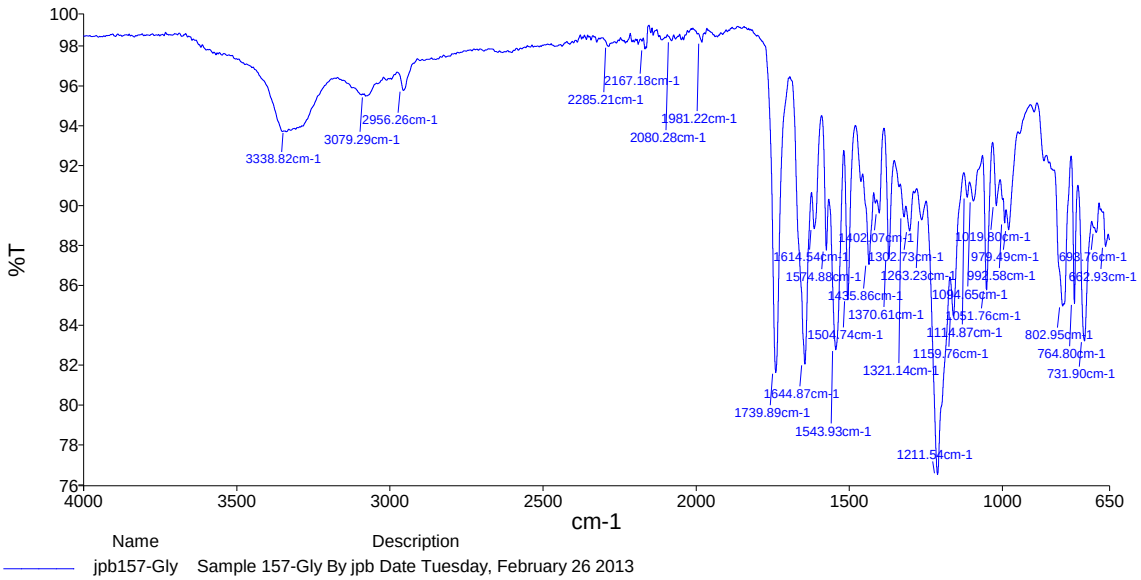

Figure B.60 IR spectrum of ligand **91-Gly**.

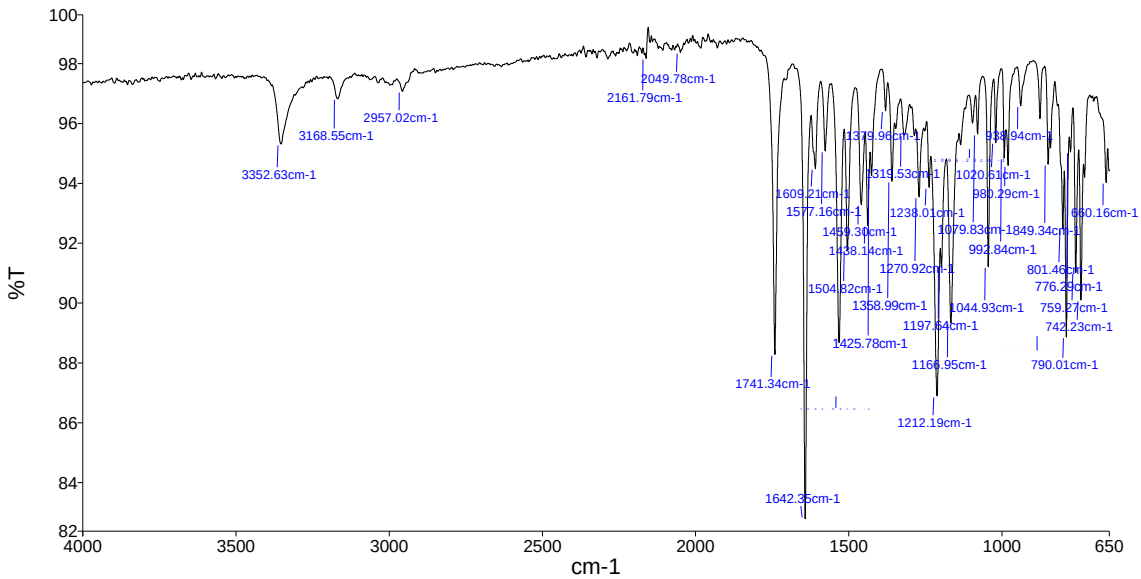

Figure B.61 IR spectrum of ligand **91-*L*-Ala**.

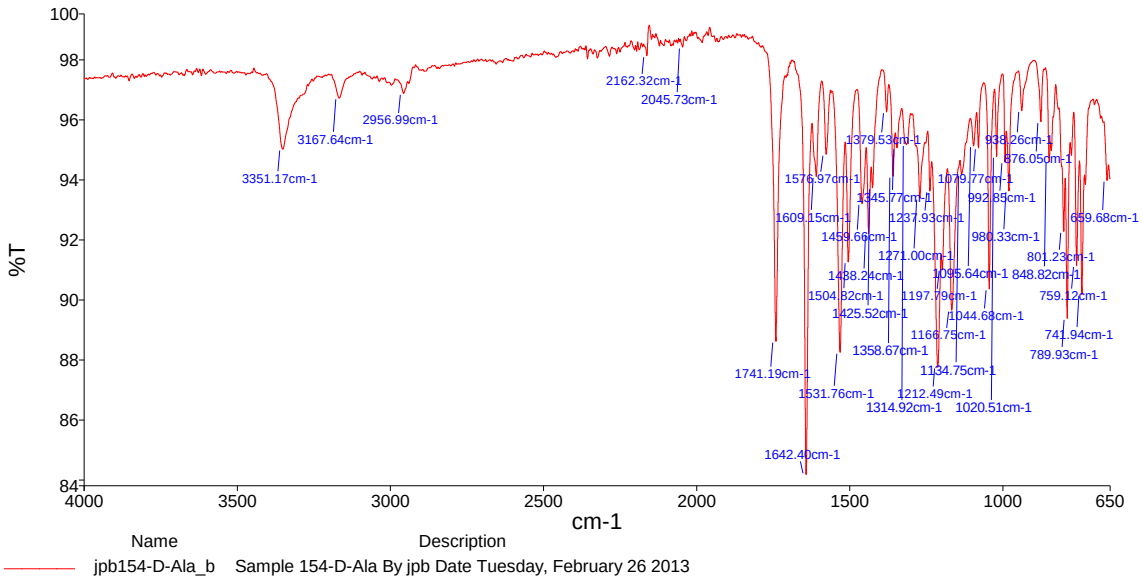

Figure B.62 IR spectrum of ligand **91-*D*-Ala**.

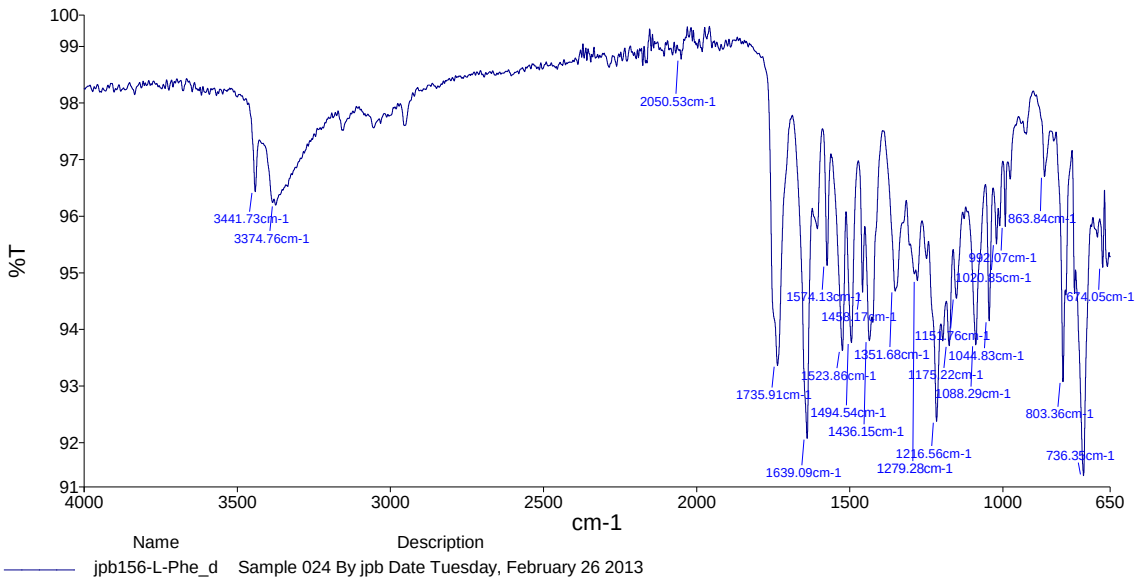

Figure B.63 IR spectrum of ligand **91-*L*-Phe**.

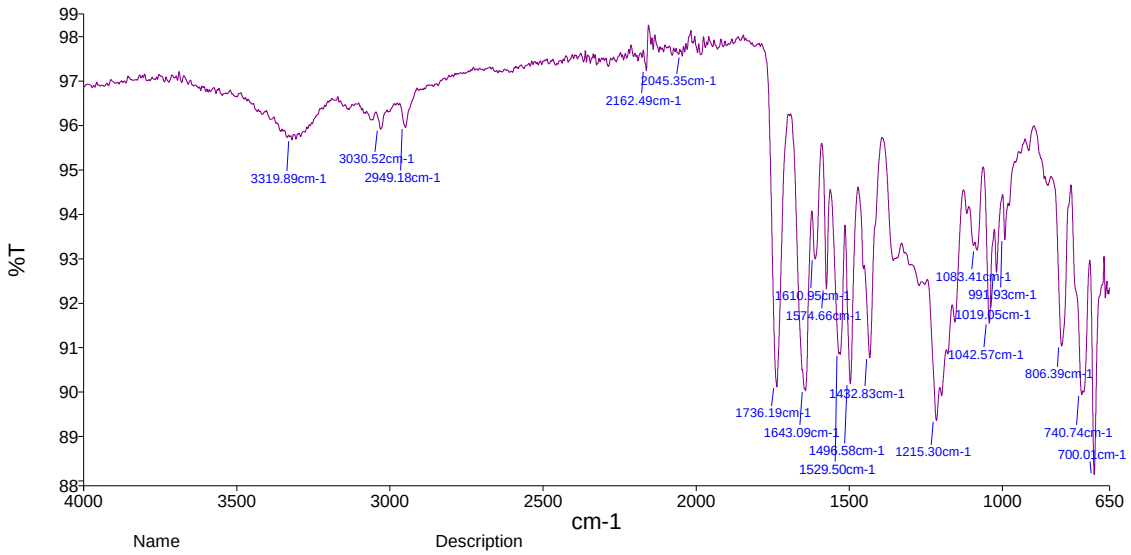

Figure B.64 IR spectrum of ligand **91-*D*-Phe**.

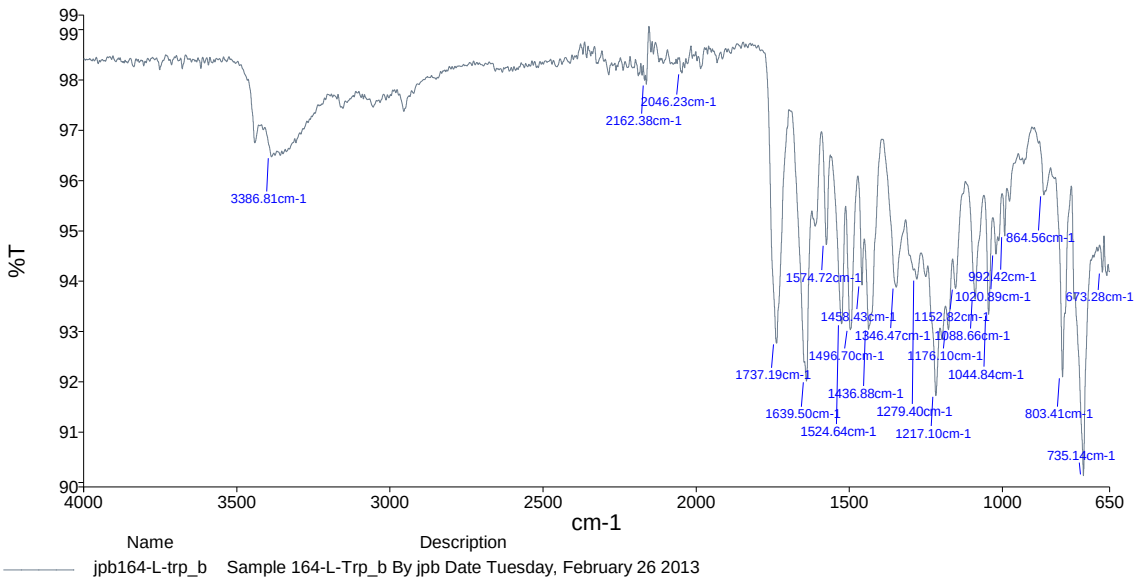

Figure B.65 IR spectrum of ligand **91-*L*-Trp**.

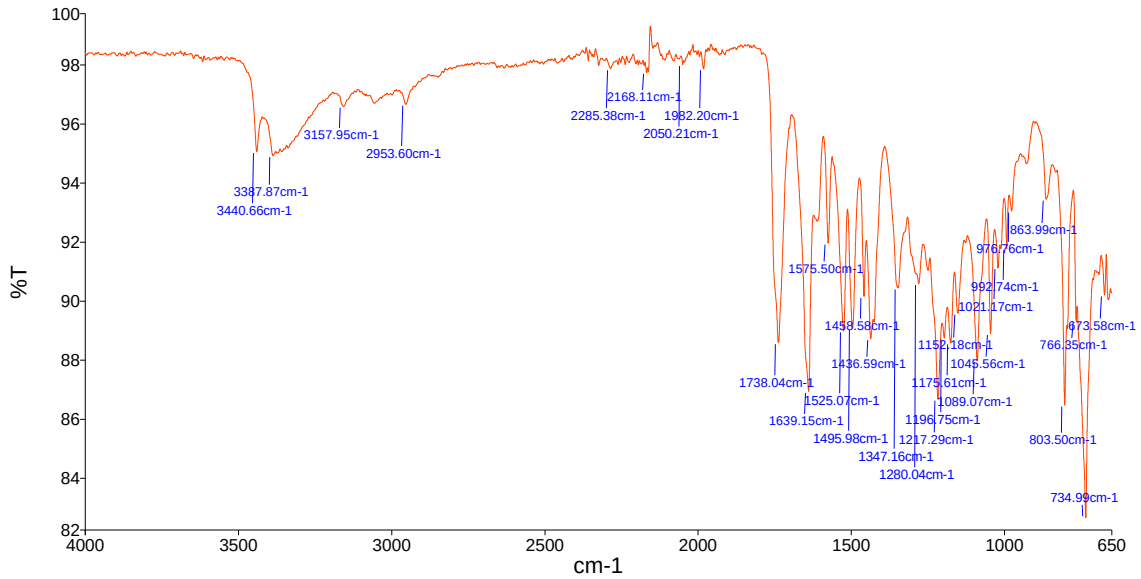

Figure B.66 IR spectrum of ligand **91-*D*-Trp**.

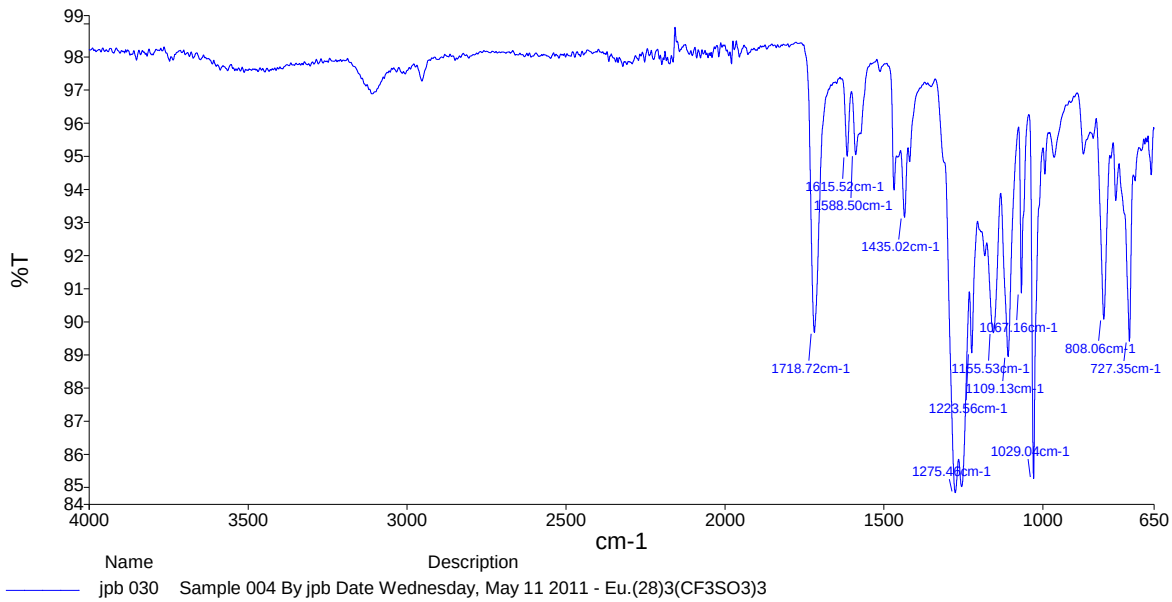

Figure B.67 IR spectrum of complex $[Eu\cdot(\mathbf{88})_3](CF_3SO_3)_3$.

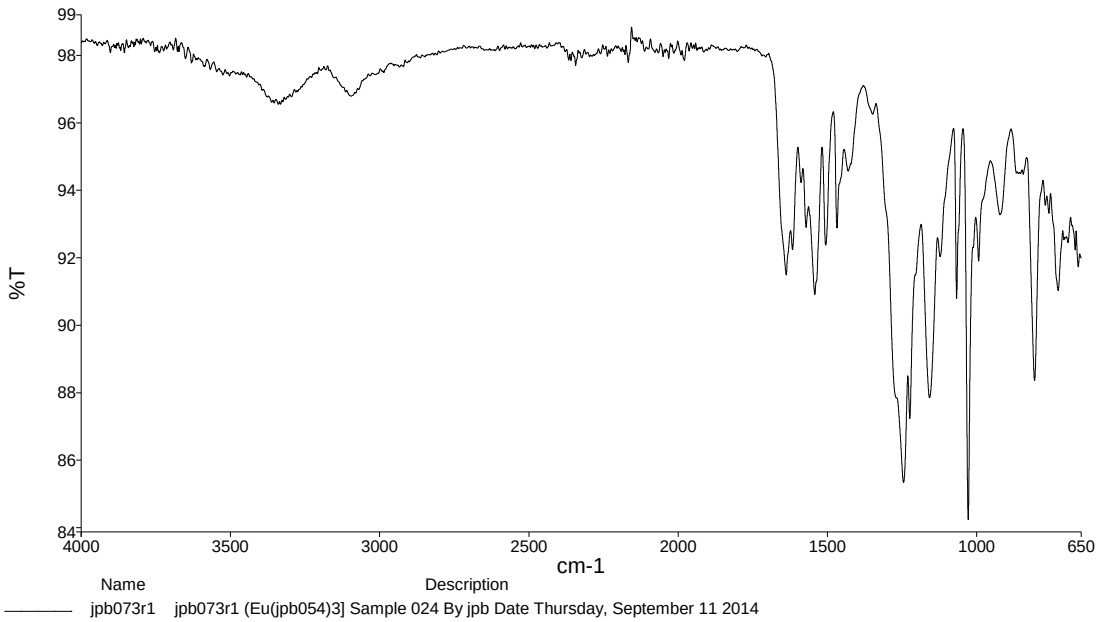

Figure B.68 IR spectrum of complex [Eu·(**90**)$_3$](CF$_3$SO$_3$)$_3$.

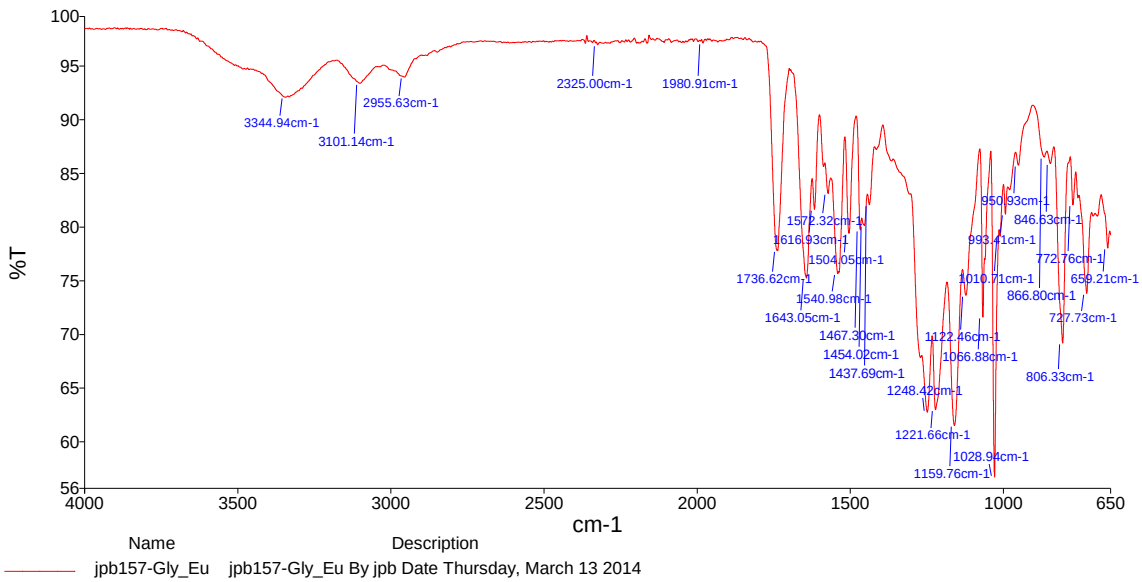

Figure B.69 IR spectrum of complex [Eu·(**91-Gly**)$_3$](CF$_3$SO$_3$)$_3$.

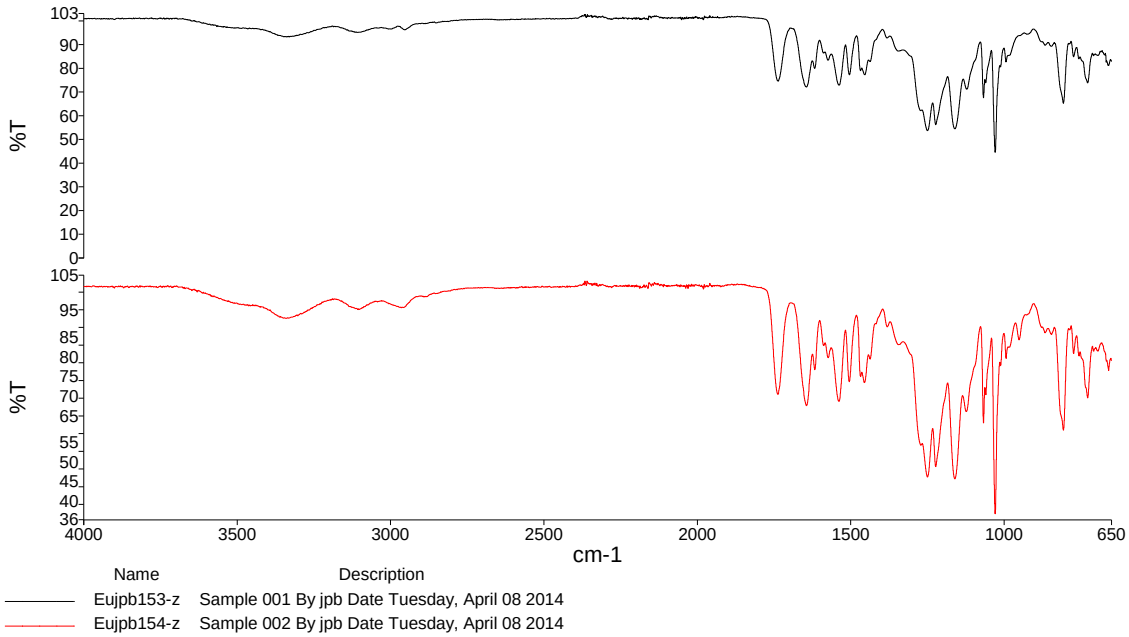

Figure B.70 IR spectra of complexes [Eu·(**91-*L*-Ala**)$_3$](CF_3SO_3)$_3$.(top) and [Eu·(**91-*D*-Ala**)$_3$](CF_3SO_3)$_3$ (bottom).

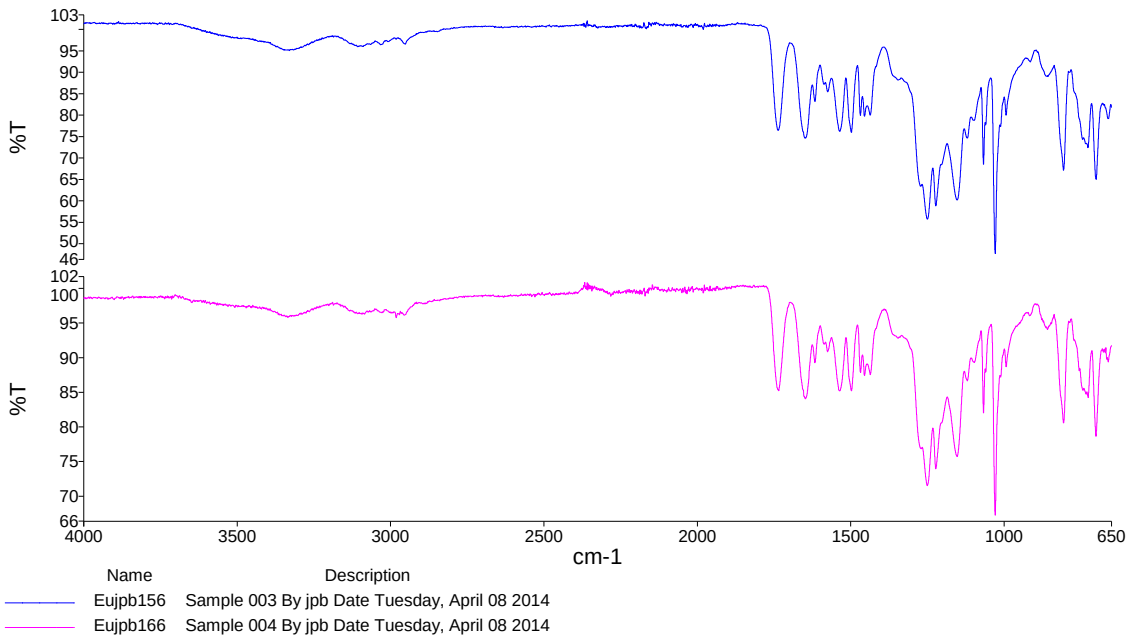

Figure B.71 IR spectra of complexes [Eu·(**91-*L*-Phe**)$_3$](CF_3SO_3)$_3$.(top) and [Eu·(**91-*D*-Phe**)$_3$](CF_3SO_3)$_3$ (bottom).

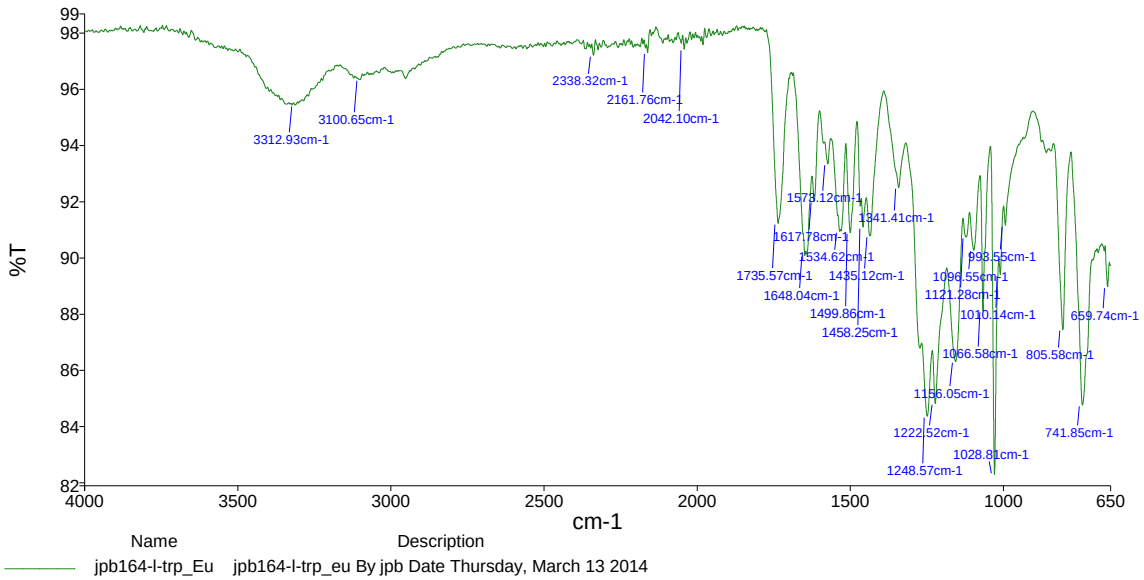

Figure B.72 IR spectrum of complex [Eu·(**91-*D*-Trp**)$_3$](CF$_3$SO$_3$)$_3$.

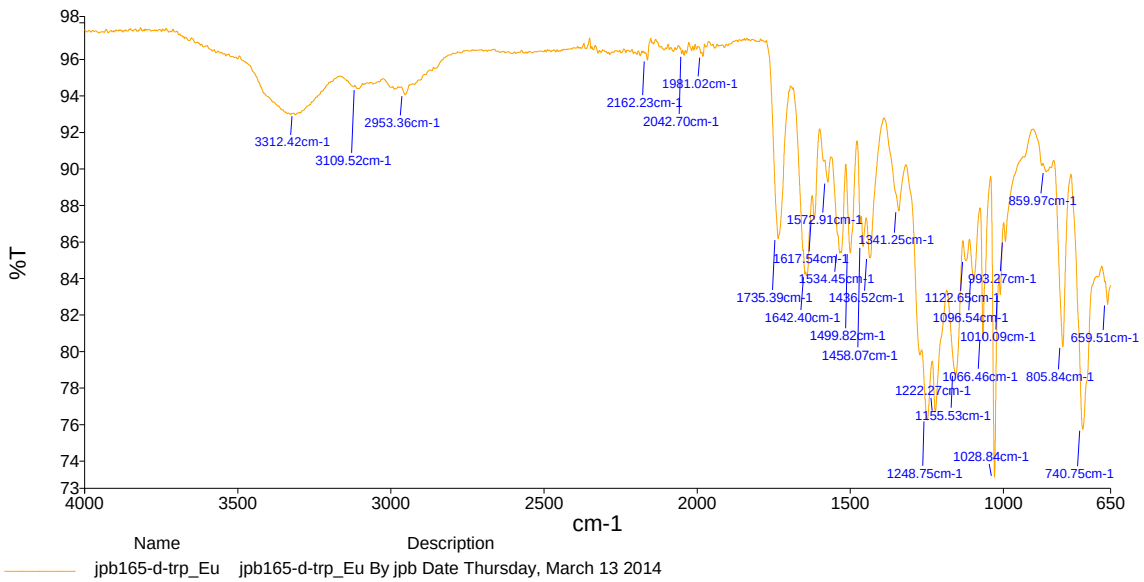

Figure B.73 IR spectrum of complex [Eu·(**91-*D*-Trp**)$_3$](CF$_3$SO$_3$)$_3$.

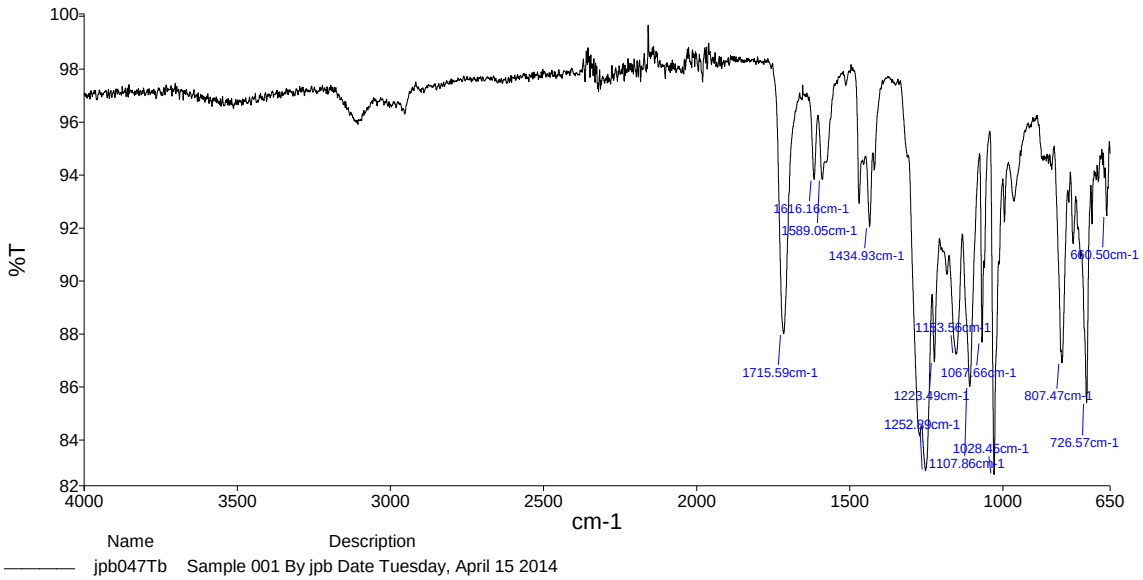

Figure B.74 IR spectrum of complex [Tb·(**88**)$_3$](CF$_3$SO$_3$)$_3$.

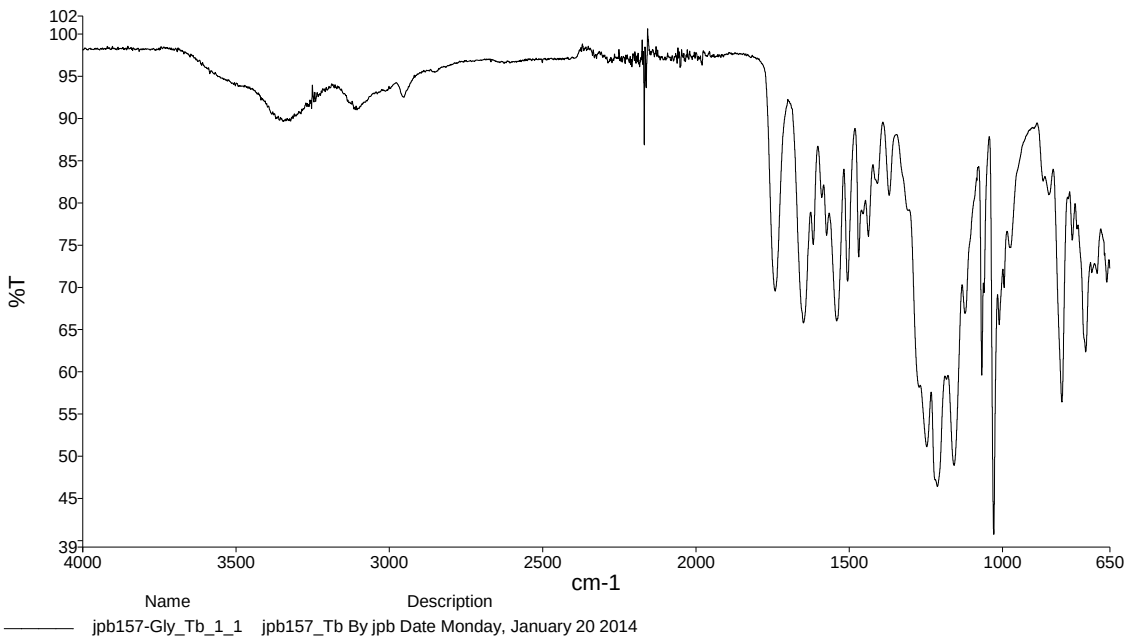

Figure B.75 IR spectrum of complex [Tb·(**91-Gly**)$_3$](CF$_3$SO$_3$)$_3$.

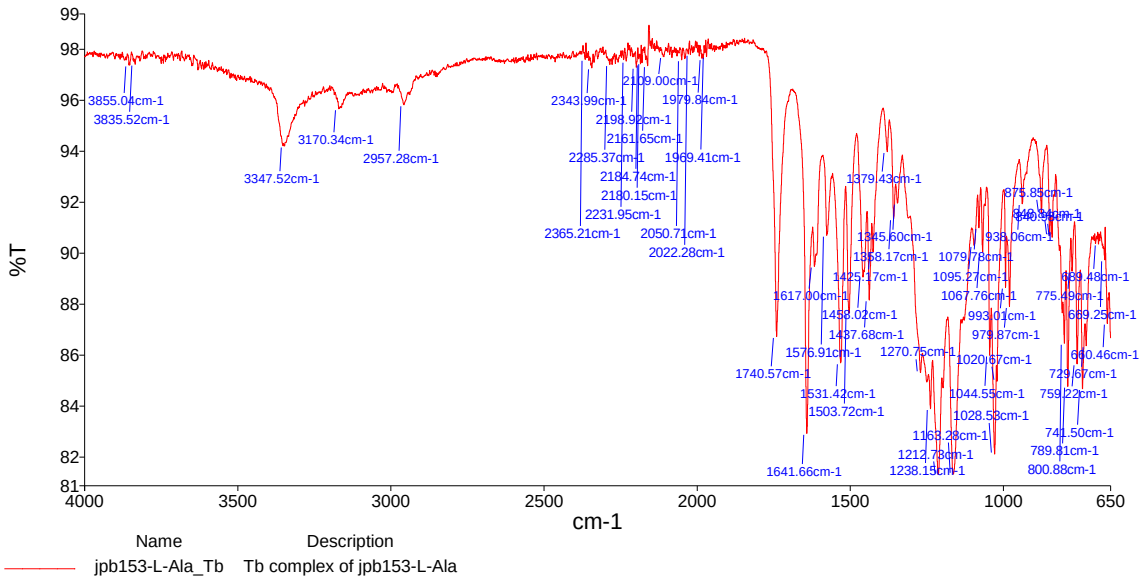

Figure B.76 IR spectrum of complex [Tb·(**91-*L*-Ala**)$_3$](CF$_3$SO$_3$)$_3$.

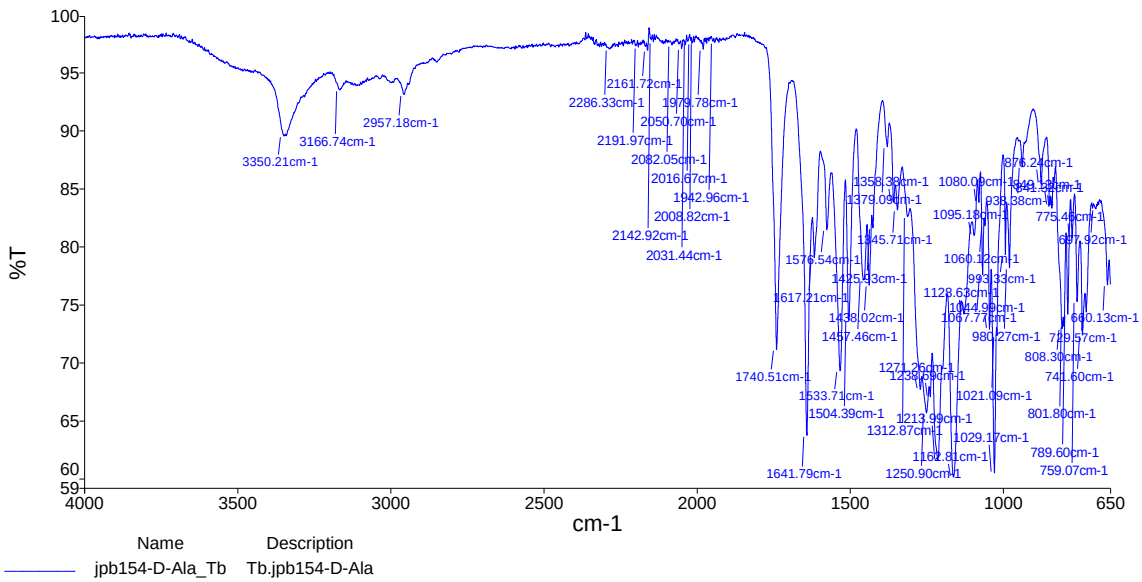

Figure B.77 IR spectrum of complex [Tb·(**91-*D*-Ala**)$_3$](CF$_3$SO$_3$)$_3$.

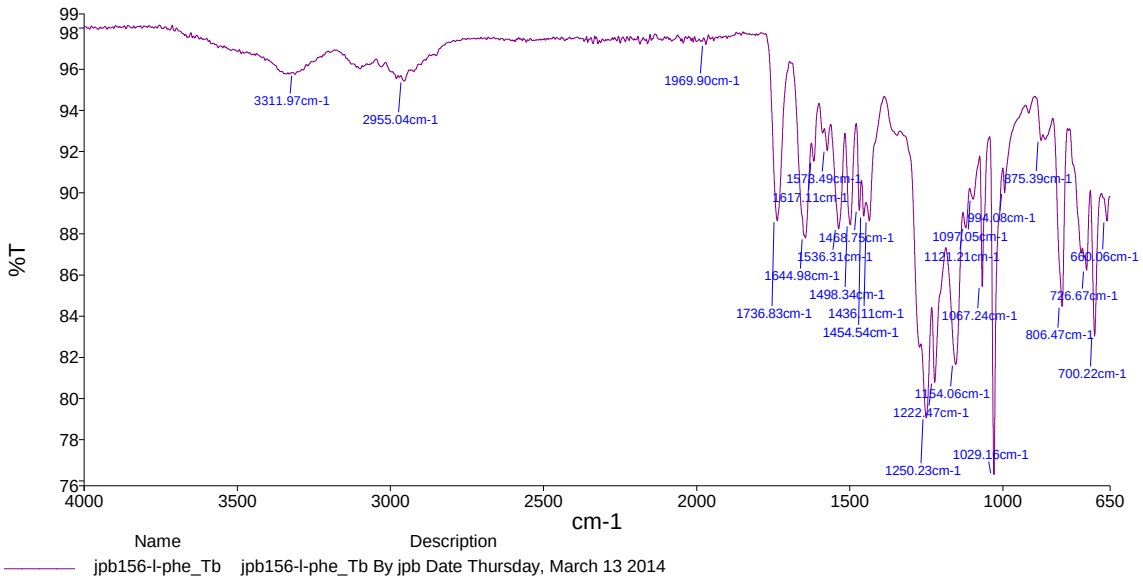

Figure B.78 IR spectrum of complex [Tb·(**91-*L*-Phe**)$_3$](CF$_3$SO$_3$)$_3$.

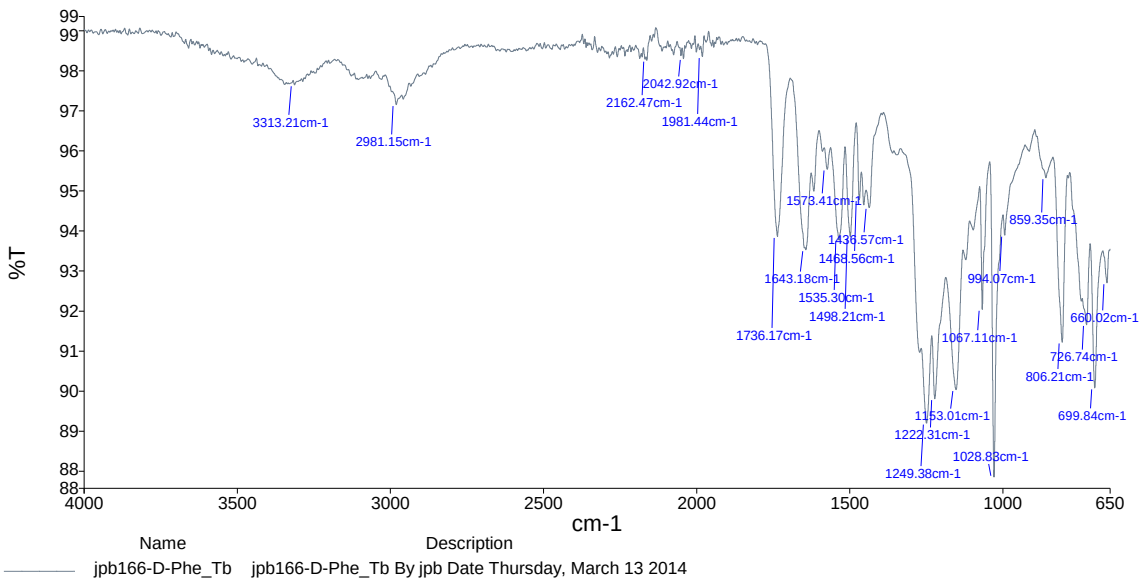

Figure B.79 IR spectrum of complex [Tb·(**91-*D*-Phe**)$_3$](CF$_3$SO$_3$)$_3$.

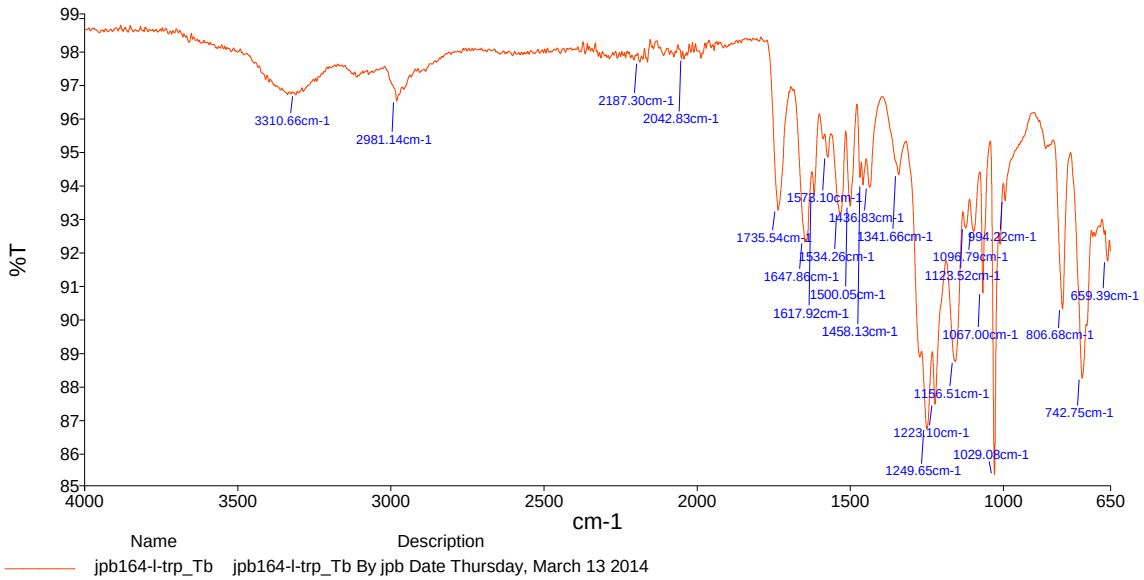

Figure B.80 IR spectrum of complex [Tb·(**91-*L*-Trp**)$_3$](CF$_3$SO$_3$)$_3$.

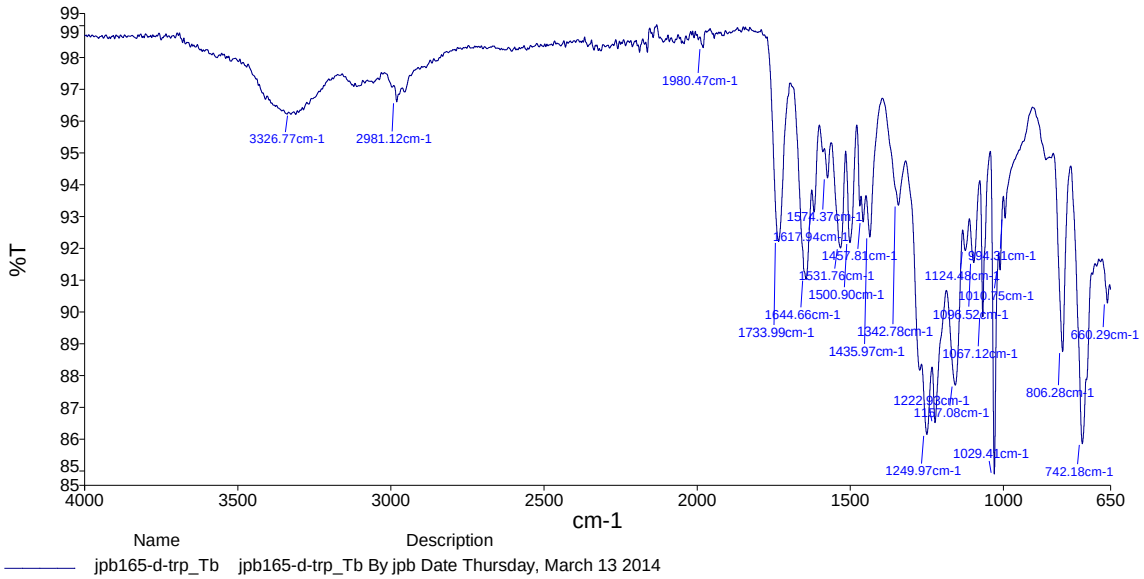

Figure B.81 IR spectrum of complex [Tb·(**91-*D*-Trp**)$_3$](CF$_3$SO$_3$)$_3$.

B.2. Mass spectrometry of complexes

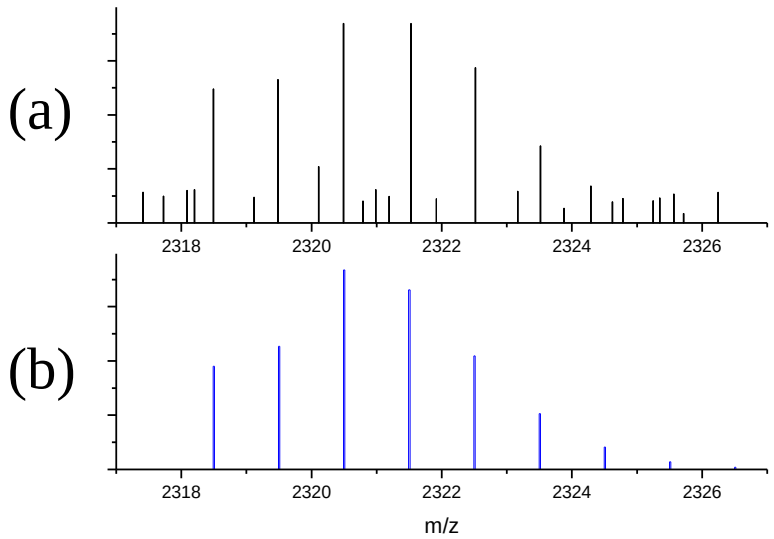

Figure B.82 (a) Experimental and **(b)** calculated HRMS isotopic pattern distribution for [Eu·(**91-Gly**)$_3$](CF$_3$SO$_3$)$_3$. Calculated for $C_{95}H_{87}N_{27}O_{24}S_2F_6Eu^+$ *m/z* = 2320.4975 $[EuL_3(CF_3SO_3)_3]^+$. Found *m/z* = 2320.4885.

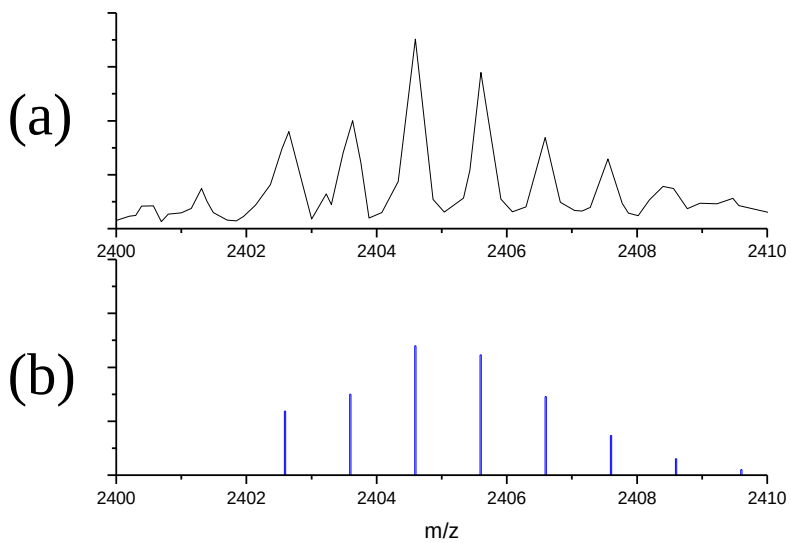

Figure B.83 (a) Experimental and **(b)** calculated HRMS isotopic pattern distribution for [Eu·(**91-*L*-Ala**)$_3$](CF$_3$SO$_3$)$_3$. Calculated for $C_{101}H_{99}N_{27}O_{24}S_2F_6Eu^+$ *m/z* = 2404.5914 $[EuL_3(CF_3SO_3)_2]^+$. Found *m/z* = 2404.5989.

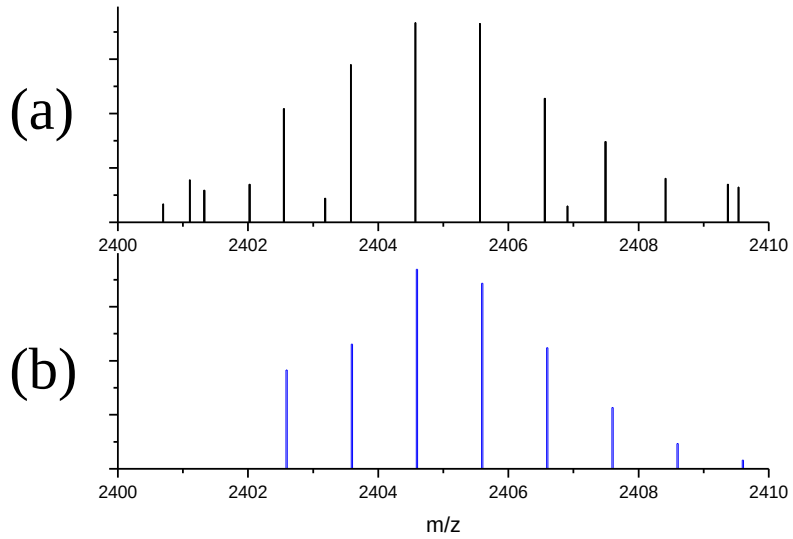

Figure B.84 (a) Experimental and **(b)** calculated HRMS isotopic pattern distribution for [Eu·(**91-*D*-Ala**)$_3$]$(CF_3SO_3)_3$. Calculated for $C_{101}H_{99}N_{27}O_{24}S_2F_6Eu^+$ *m/z* = 2404.5914 $[EuL_3(CF_3SO_3)_2]^+$. Found *m/z* = 2404.5710.

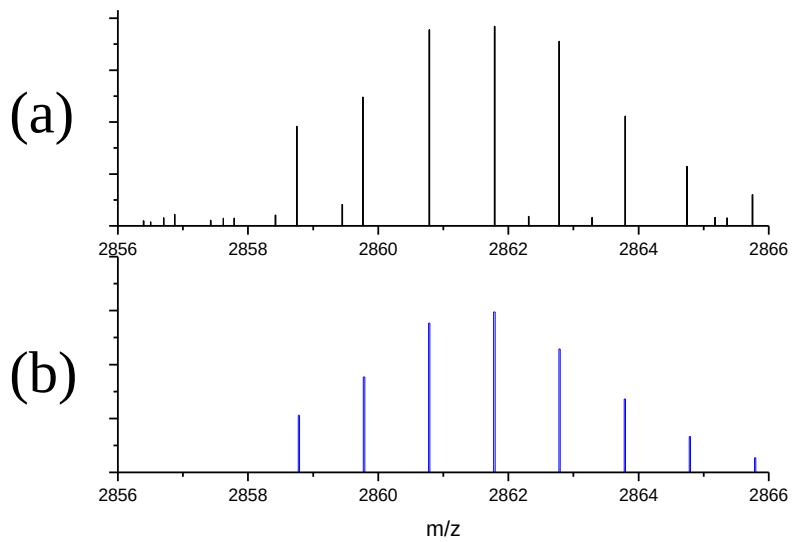

Figure B.85 (a) Experimental and **(b)** calculated HRMS isotopic pattern distribution for [Eu·(**91-*L*-Phe**)$_3$]$(CF_3SO_3)_3$. Calculated for $C_{137}H_{123}N_{27}O_{24}S_2F_6Eu^+$ *m/z* = 2860.7792 $[EuL_3(CF_3SO_3)_2]^+$. Found *m/z* = 2860.7832.

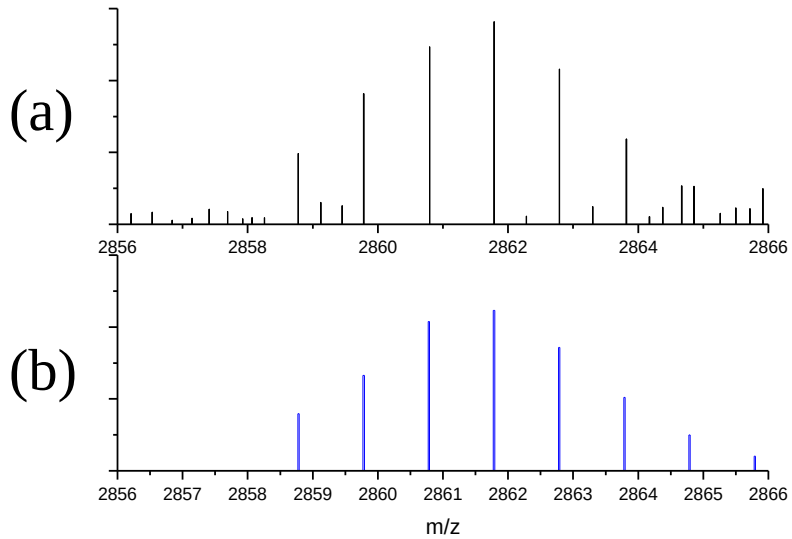

Figure B.86 (a) Experimental and **(b)** calculated HRMS isotopic pattern distribution for [Eu·(**91-*D*-Phe**)$_3$](CF$_3$SO$_3$)$_3$. Calculated for $C_{137}H_{123}N_{27}O_{24}S_2F_6Eu^+$ *m/z* = 2860.7792 $[EuL_3(CF_3SO_3)_2]^+$. Found *m/z* = 2860.7866.

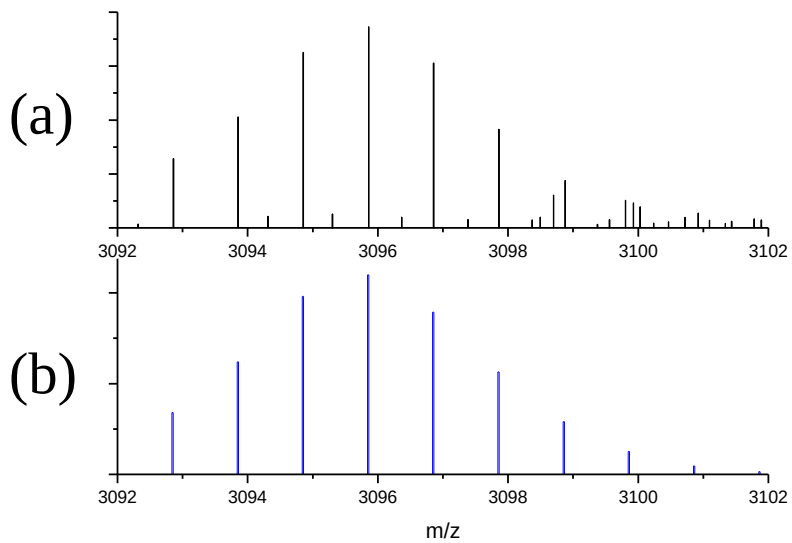

Figure B.87 (a) Experimental and **(b)** calculated HRMS isotopic pattern distribution for [Eu·(**91-*L*-Trp**)$_3$](CF$_3$SO$_3$)$_3$. Calculated for $C_{149}H_{129}N_{33}O_{24}F_6S_2Eu^+$ *m/z* = 3094.8446 $[EuL_3(CF_3SO_3)_2]^+$. Found *m/z* = 3094.8521.

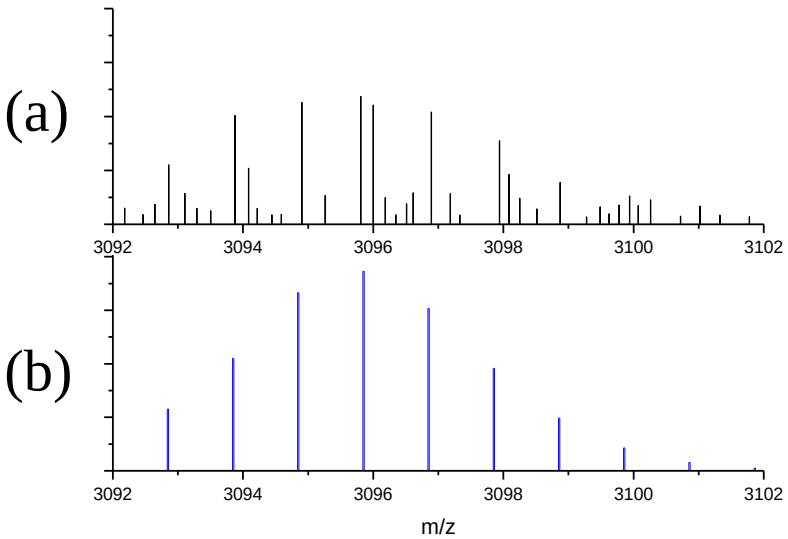

Figure B.88 (a) Experimental and **(b)** calculated HRMS isotopic pattern distribution for [Eu·(**91-*D*-Trp**)$_3$]$(CF_3SO_3)_3$. Calculated for $C_{149}H_{129}N_{33}O_{24}F_6S_2Eu^+$ *m/z* = 3094.8446 $[EuL_3(CF_3SO_3)_2]^+$. Found *m/z* = 3094.8599.

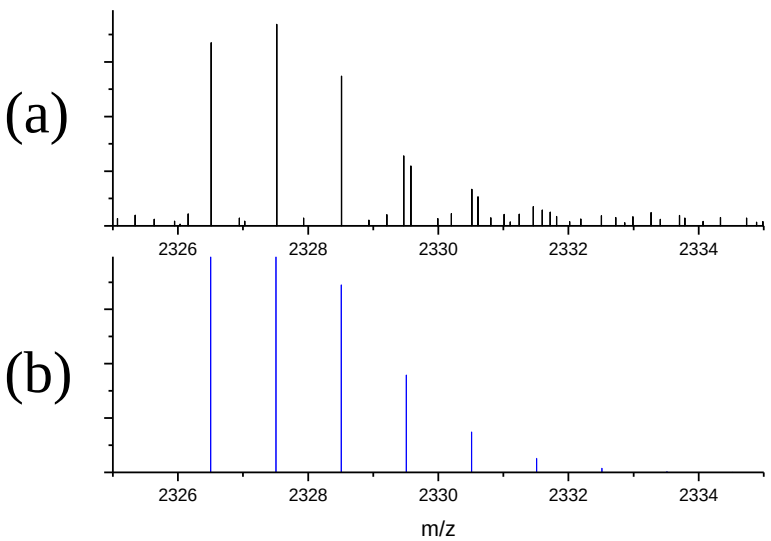

Figure B.89 (a) Experimental and **(b)** calculated HRMS isotopic pattern distribution for [Tb·(**91-Gly**)$_3$]$(CF_3SO_3)_3$. Calculated for $C_{95}H_{87}N_{27}O_{24}S_2F_6Tb^+$ *m/z* = 2326.5016 $[TbL_3(CF_3SO_3)_2]^+$. Found *m/z* = 2326.5088.

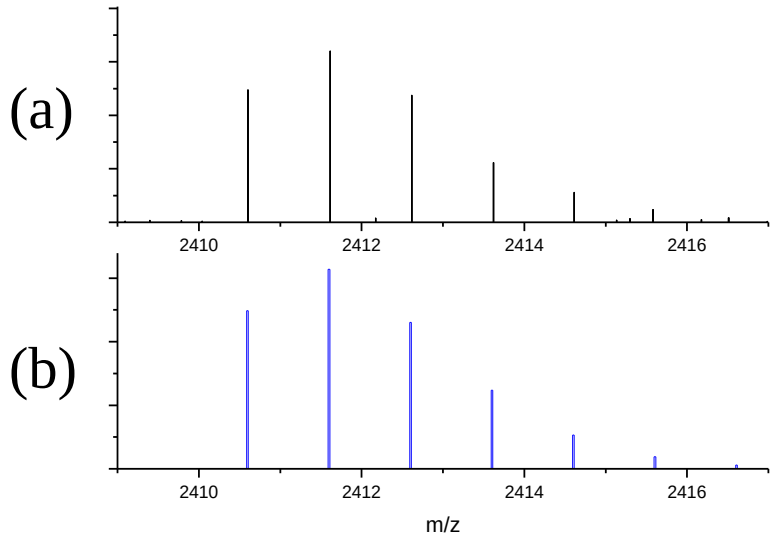

Figure B.90 (a) Experimental and **(b)** calculated HRMS isotopic pattern distribution for [Tb·(**91-*L*-Ala**)$_3$](CF$_3$SO$_3$)$_3$. Calculated for $C_{101}H_{99}N_{27}O_{24}S_2F_6Tb^+$ *m/z* = 2410.5955 $[TbL_3(CF_3SO_3)_2]^+$. Found *m/z* = 2410.6018.

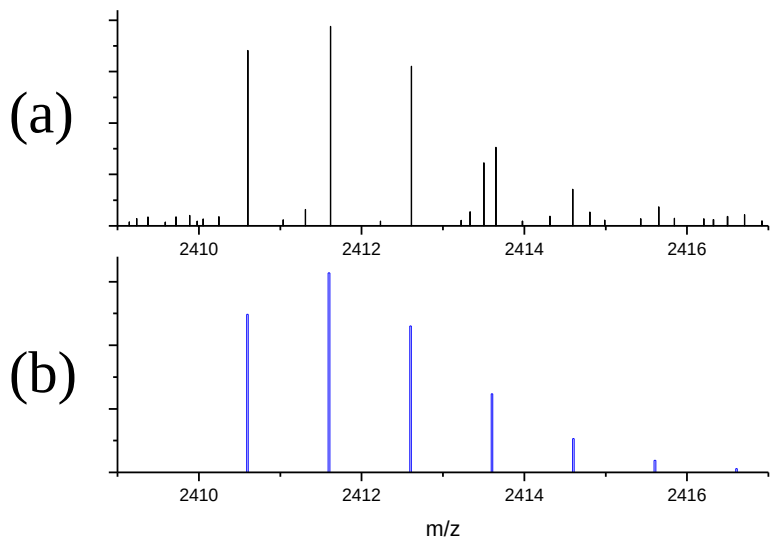

Figure B.91 (a) Experimental and **(b)** calculated HRMS isotopic pattern distribution for [Tb·(**91-*D*-Ala**)$_3$](CF$_3$SO$_3$)$_3$. Calculated for $C_{101}H_{99}N_{27}O_{24}S_2F_6Tb^+$ *m/z* = 2410.5955 $[TbL_3(CF_3SO_3)_2]^+$. Found *m/z* = 2410.6016.

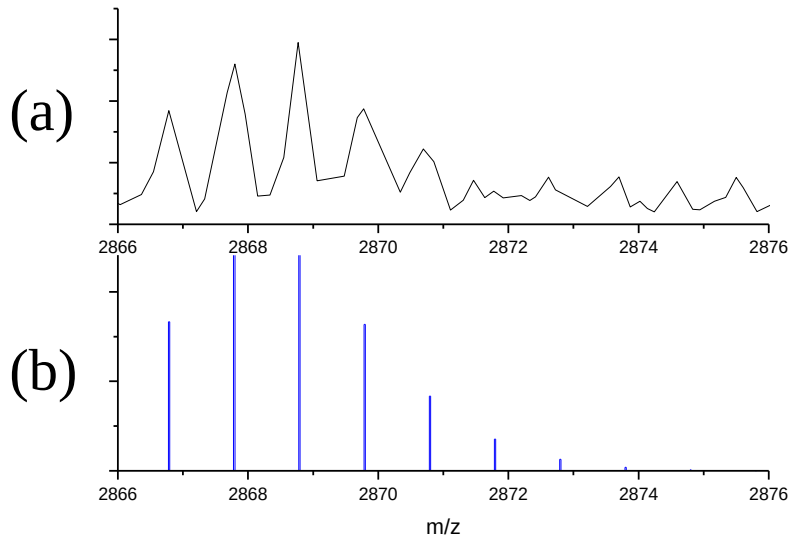

Figure B.92 (a) Experimental and **(b)** calculated HRMS isotopic pattern distribution for [Tb·(**91-*L*-Phe**)$_3$]$(CF_3SO_3)_3$. Calculated for $C_{137}H_{123}N_{27}O_{24}S_2F_6Tb^+$ *m/z* = 2866.7833 $[TbL_3(CF_3SO_3)_2]^+$. Found *m/z* = 2866.7837.

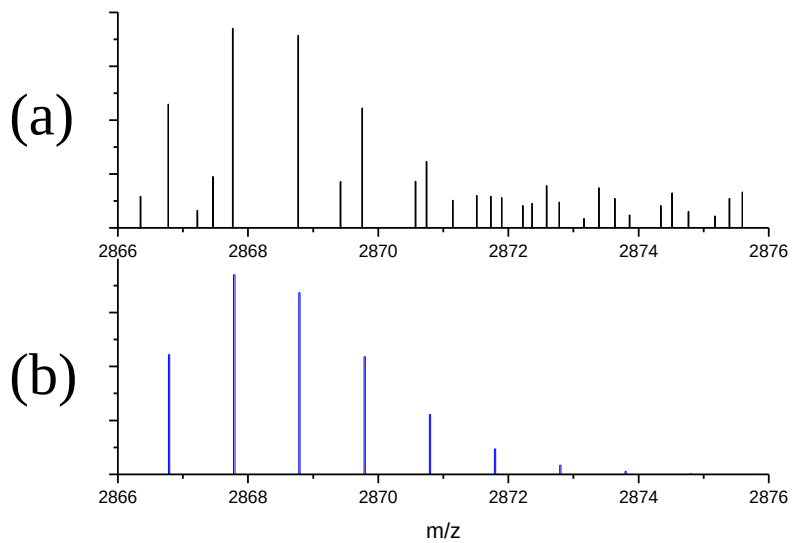

Figure B.93 (a) Experimental and **(b)** calculated HRMS isotopic pattern distribution for [Tb·(**91-*D*-Phe**)$_3$]$(CF_3SO_3)_3$. Calculated for $C_{137}H_{123}N_{27}O_{24}S_2F_6Tb^+$ *m/z* = 2866.7833 $[TbL_3(CF_3SO_3)_2]^+$. Found *m/z* = 2866.7734.

B.3. Ligand photophyscial spectra

Photophysical spectra for ligands **88**, **91--Gly**, **91-*D*-Ala**, **91-*D*-Phe** and **91-*D*-Trp** are shown in the main text. The UV-Vis absorbance, excitation and fluorescence emission spectra of the *D*-enantiomers are provided here for completeness.

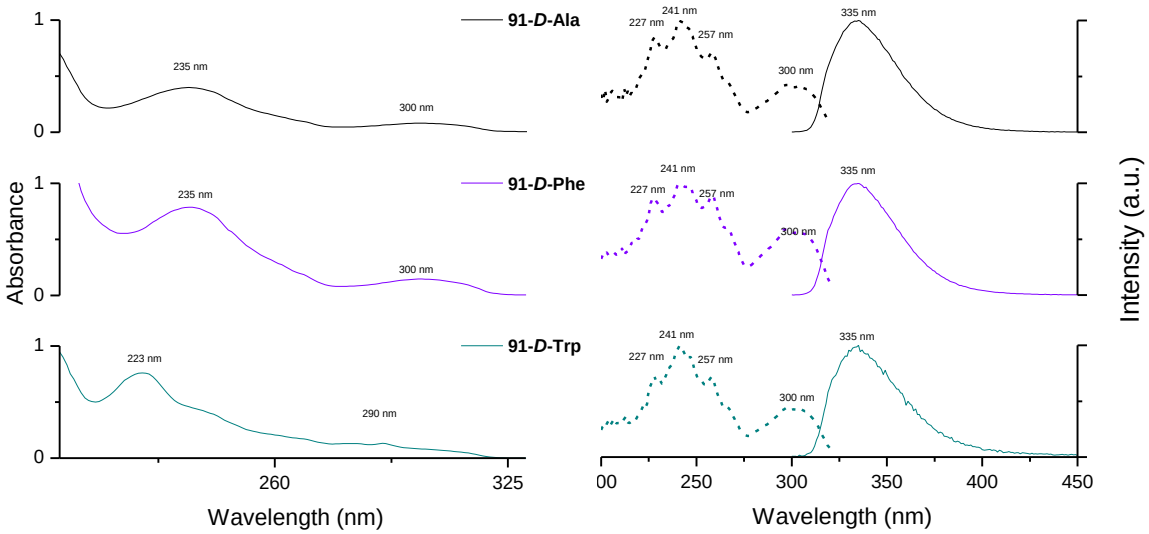

Figure B.94 UV-Vis absorbance, excitation and fluorescence spectra of ligands **91-*D*-Ala**, **91-*D*-Phe** and **91-*D*-Trp**

B.4. Ln(III) complex photophysical spectra

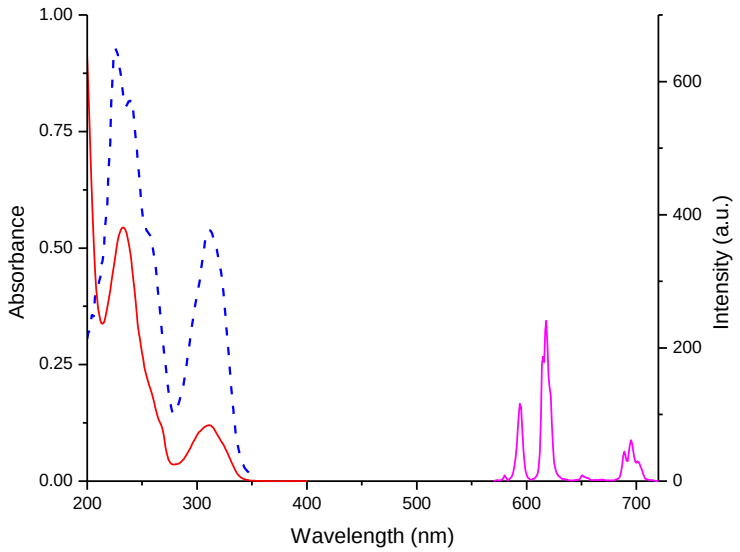

Figure B.95 UV-Vis absorbance (red), excitation (dashed blue) and Eu(III) phosphorescence (magenta) spectra of [Eu·(**91-Gly**)$_3$](CF$_3$SO$_3$)$_3$.

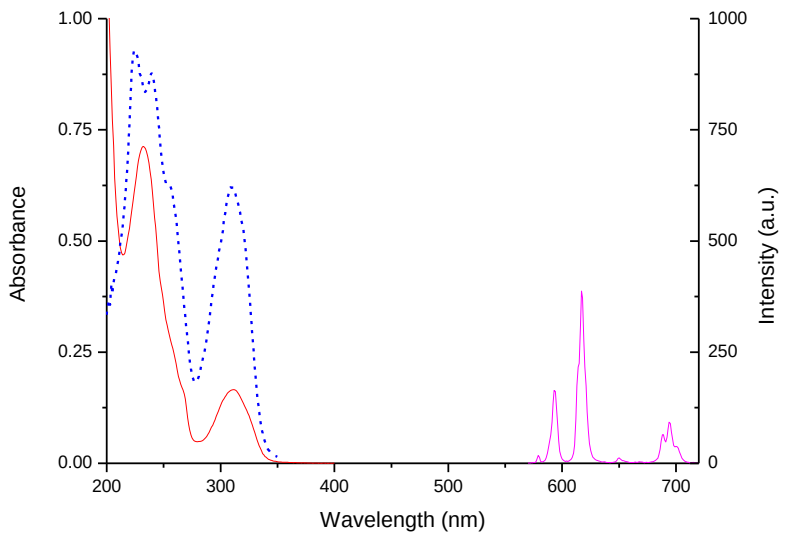

Figure B.96 UV-Vis absorbance (red), excitation (dashed blue) and Eu(III) phosphorescence (magenta) spectra of [Eu·(**91-*L*-Ala**)$_3$](CF$_3$SO$_3$)$_3$.

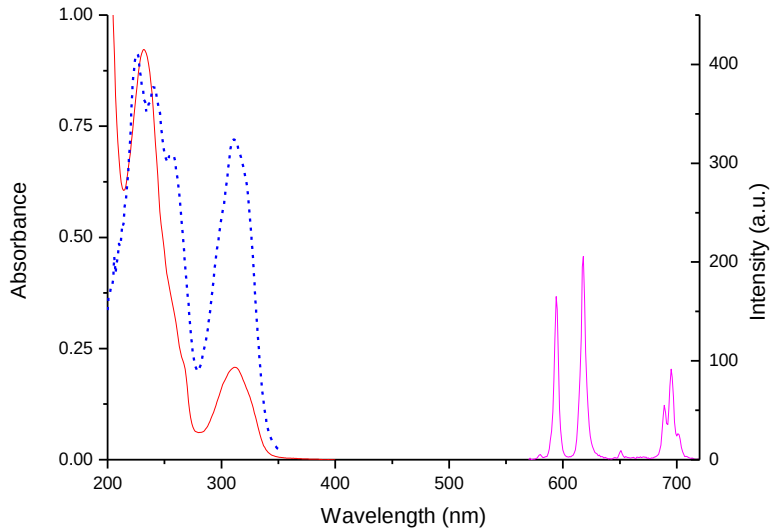

Figure B.97 UV-Vis absorbance (red), excitation (dashed blue) and Eu(III) phosphorescence (magenta) spectra of [Eu·(**91-*D*-Ala**)$_3$](CF$_3$SO$_3$)$_3$.

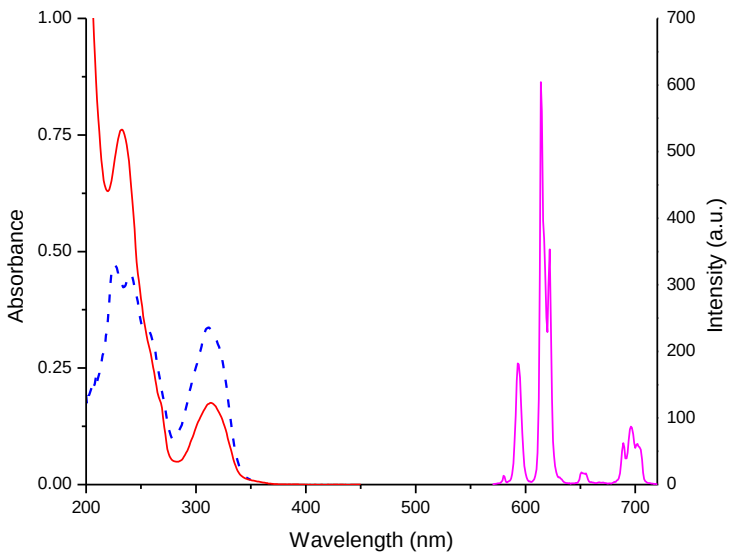

Figure B.98 UV-Vis absorbance (red), excitation (dashed blue) and Eu(III) phosphorescence (magenta) spectra of [Eu·(**91-*D*-Phe**)$_3$](CF$_3$SO$_3$)$_3$.

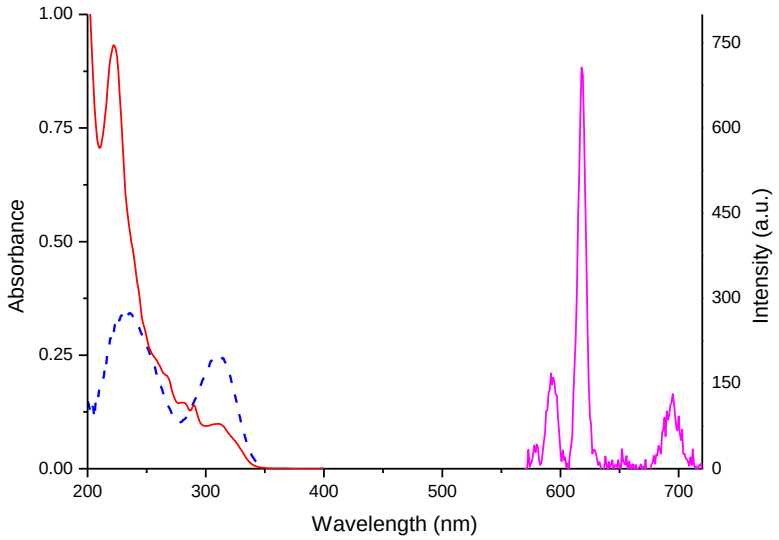

Figure B.99 UV-Vis absorbance (red), excitation (dashed blue) and Eu(III) phosphorescence (magenta) spectra of [Eu·(**91-*L*-Trp**)$_3$](CF$_3$SO$_3$)$_3$.

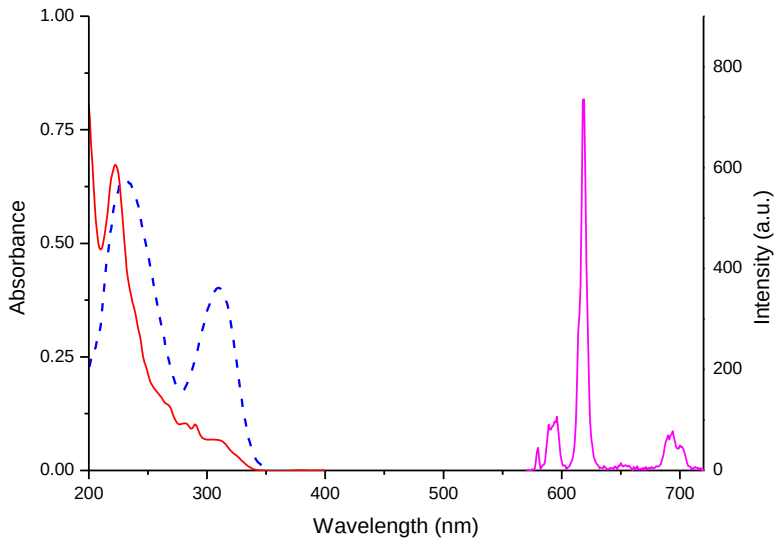

Figure B.100 UV-Vis absorbance (red), excitation (dashed blue) and Eu(III) phosphorescence (magenta) spectra of [Eu·(**91-*D*-Trp**)$_3$](CF$_3$SO$_3$)$_3$.

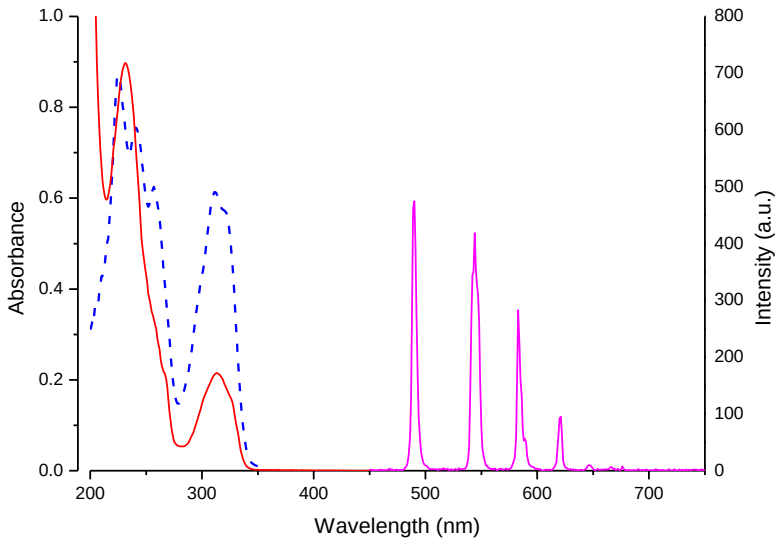

Figure B.101 UV-Vis absorbance (red), excitation (dashed blue) and Tb(III) phosphorescence (magenta) spectra of [Tb·(**91-Gly**)$_3$](CF$_3$SO$_3$)$_3$.

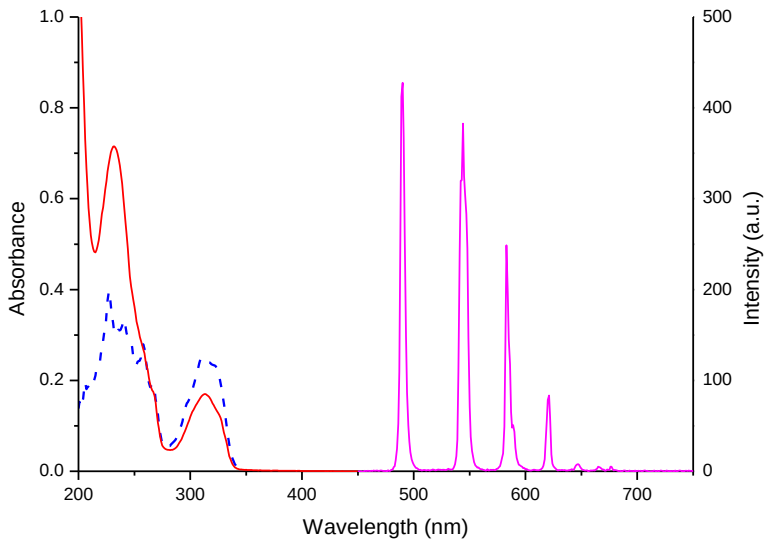

Figure B.102 UV-Vis absorbance (red), excitation (dashed blue) and Tb(III) phosphorescence (magenta) spectra of [Tb·(**91-*L*-Ala**)$_3$](CF$_3$SO$_3$)$_3$.

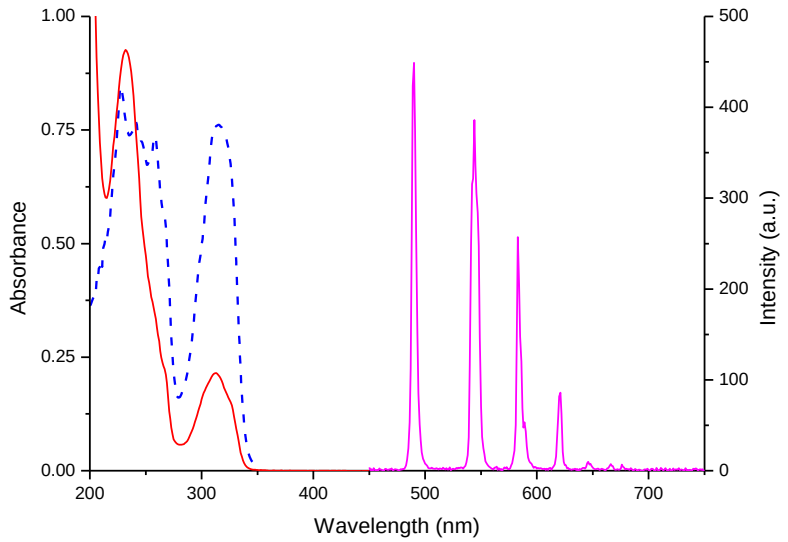

Figure B.103 UV-Vis absorbance (red), excitation (dashed blue) and Tb(III) phosphorescence (magenta) spectra of [Tb·(**91-*D*-Ala**)$_3$](CF$_3$SO$_3$)$_3$.

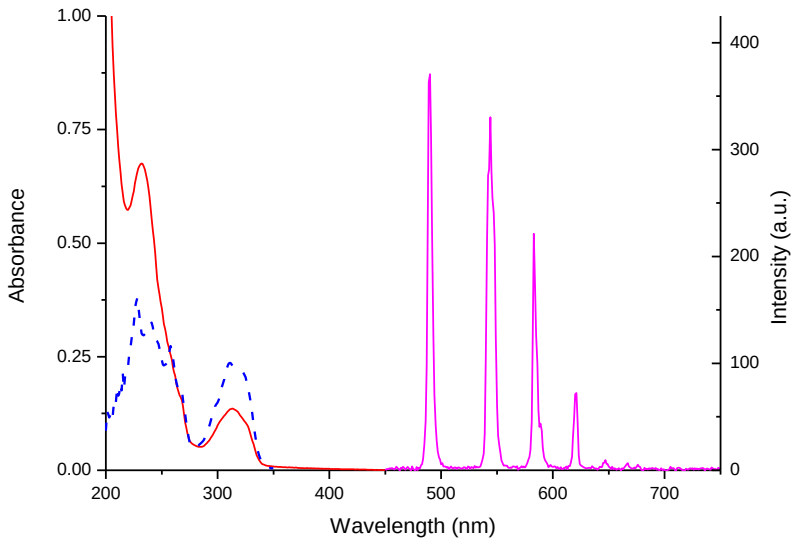

Figure B.104 UV-Vis absorbance (red), excitation (dashed blue) and Tb(III) phosphorescence (magenta) spectra of [Tb·(**91-*D*-Phe**)$_3$](CF$_3$SO$_3$)$_3$.

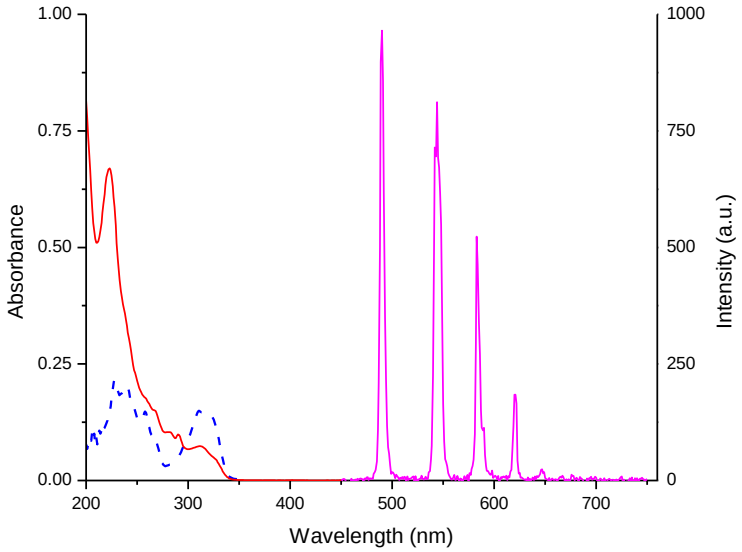

Figure B.105 UV-Vis absorbance (red), excitation (dashed blue) and Tb(III) phosphorescence (magenta) spectra of [Tb·(**91-*L*-Trp**)$_3$](CF$_3$SO$_3$)$_3$.

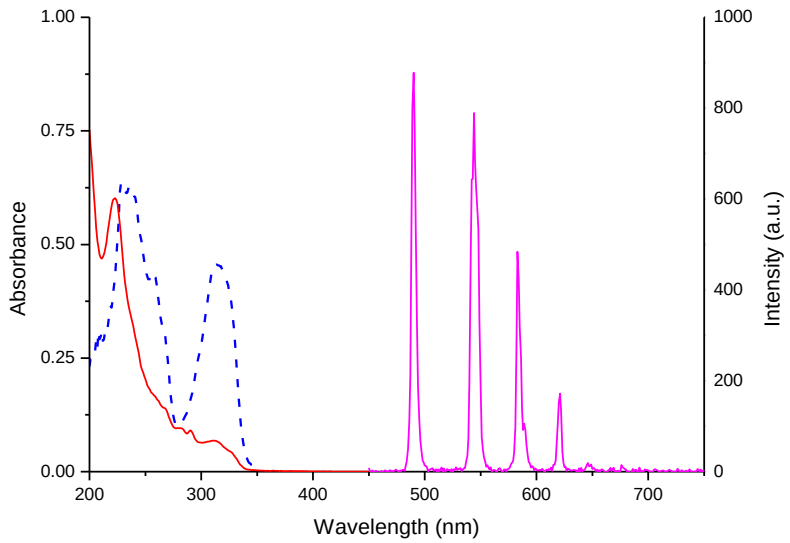

Figure B.106 UV-Vis absorbance (red), excitation (dashed blue) and Tb(III) phosphorescence (magenta) spectra of [Tb·(**91-*D*-Trp**)$_3$](CF$_3$SO$_3$)$_3$.

B.5. Low temperature spectroscopy

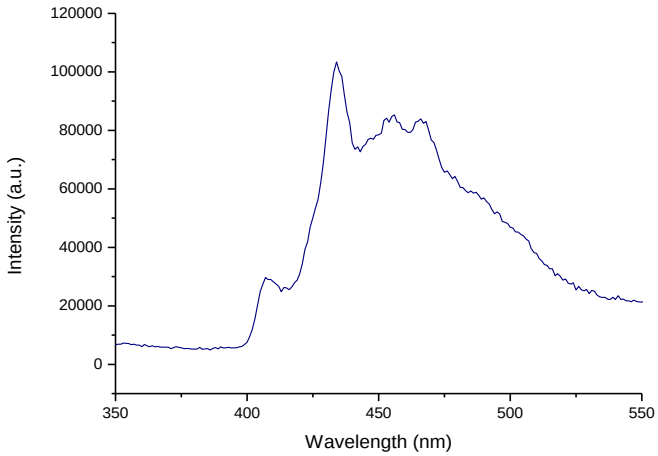

Figure B.107 Emission spectrum of $[Gd\cdot(\mathbf{88})_3](CF_3SO_3)_3$ in CH_2CN measured at 77 K, showing phosphorescence emission from the ligand triplet state

B.6. Eu(III)Spectroscopic titrations and fitting

On the following pages, the set of titrations for each ligand is presented below. Each panel of 9 plots shows: (Top row): UV-Vis absorbance spectral changes; fluorescence emission spectral changes; phosphorescence emission changes; (Middle row): Experimental (×) and calculated (solid line, if applicable) binding isotherms for the titration data directly above at various wavelengths; (Bottom row): Calculated speciation distribution diagrams for the relevant titration data, where these data have been successfully fit, as a function of [Ln(III)]; the various traces show the percentage formation of the ligand (black), 1:3 stoichiometry (blue), 1:2 stoichiometry (green) and 1:1 stoichiometry (red).

88 v. Eu(III)

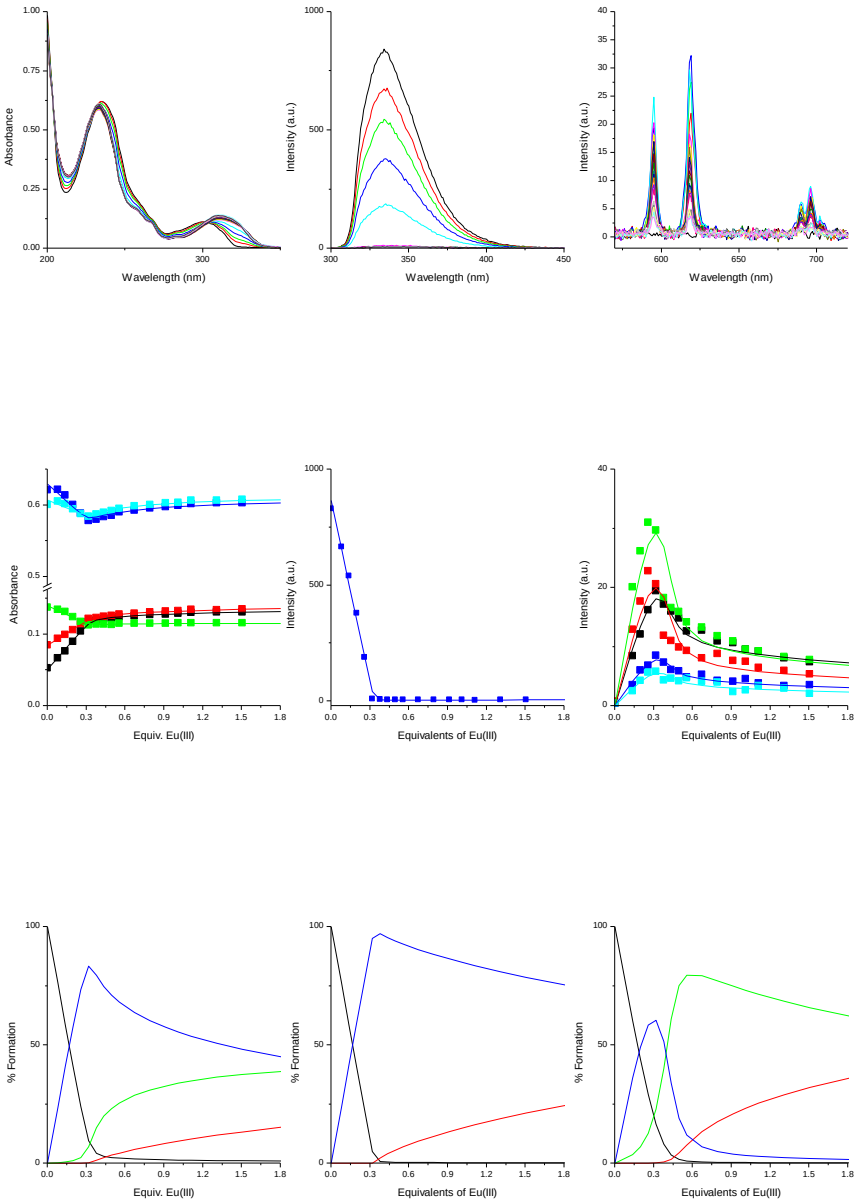
Absorbance
Wavelength (nm)
Intensity (a.u.)
Wavelength (nm)
Intensity (a.u.)
Wavelength (nm)
Absorbance
Equiv. Eu(III)
Intensity (a.u.)
Equivalents of Eu(III)
Intensity (a.u.)
Equivalents of Eu(III)
% Formation
Equiv. Eu(III)
% Formation
Equivalents of Eu(III)
% Formation
Equivalents of Eu(III)

90 v. Eu(III)

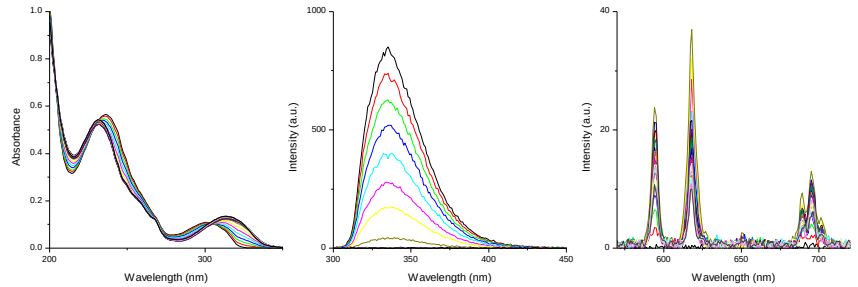
Absorbance
Wavelength (nm)
Intensity (a.u.)
Wavelength (nm)
Intensity (a.u.)
Wavelength (nm)

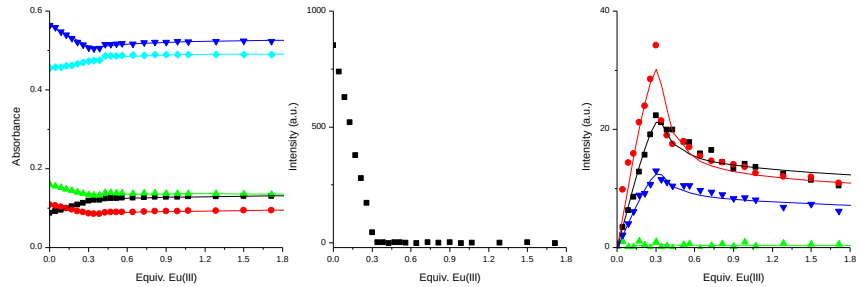
Absorbance
Equiv. Eu(III)
Intensity (a.u.)
Equiv. Eu(III)
Intensity (a.u.)
Equiv. Eu(III)

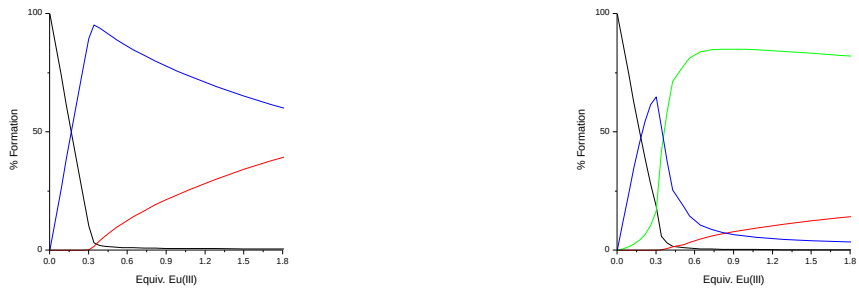
% Formation
Equiv. Eu(III)
% Formation
Equiv. Eu(III)

91-Gly v. Eu(III)

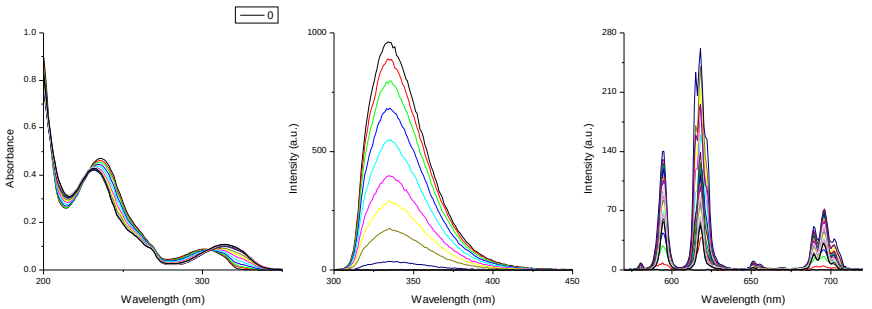

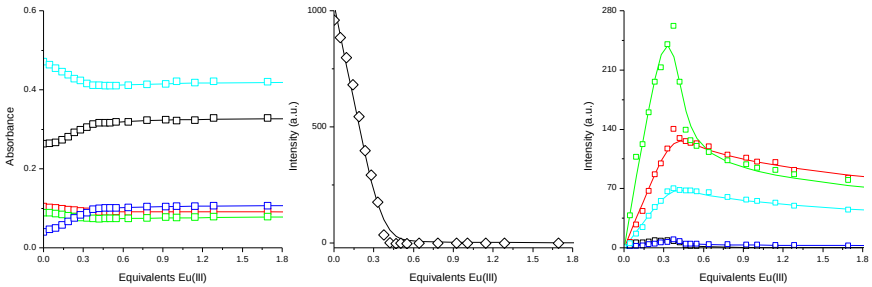

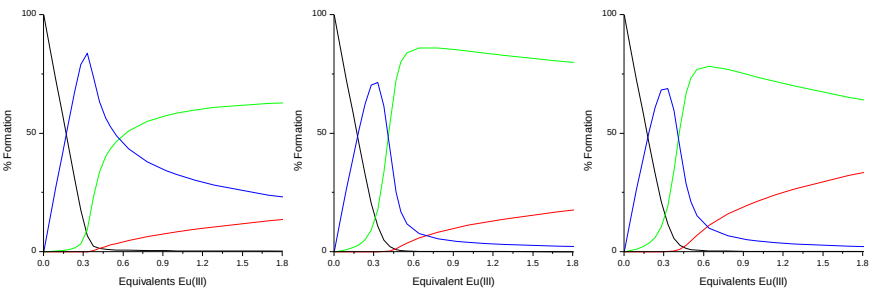

91-*L*-Ala v. Eu(III)

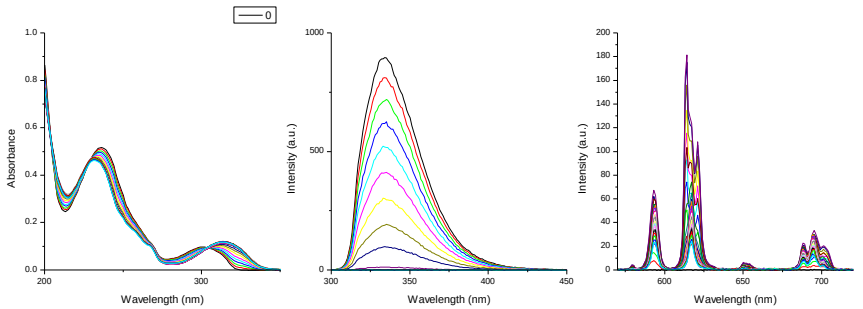

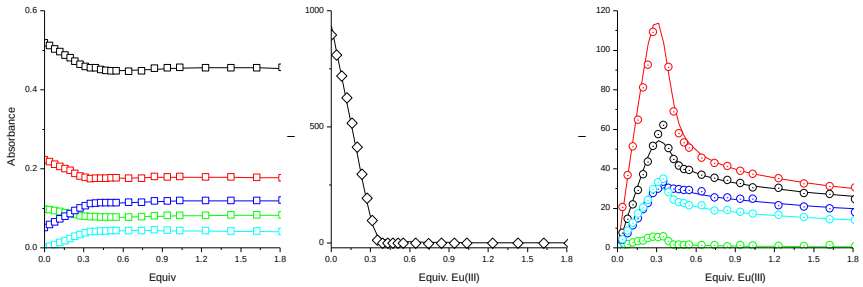

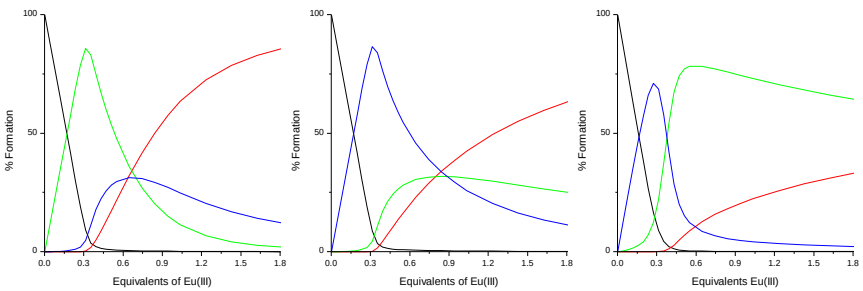

91-*D*-Ala v. Eu(III)

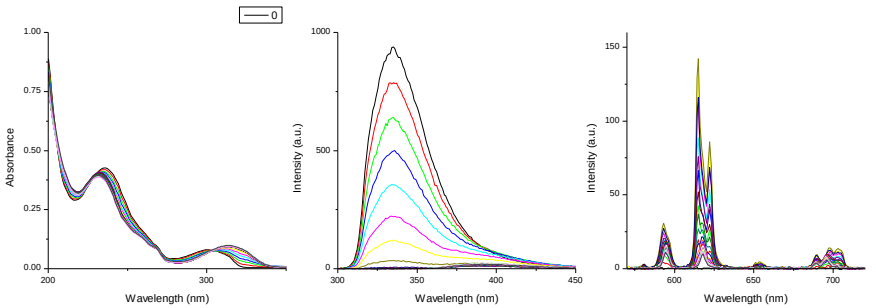

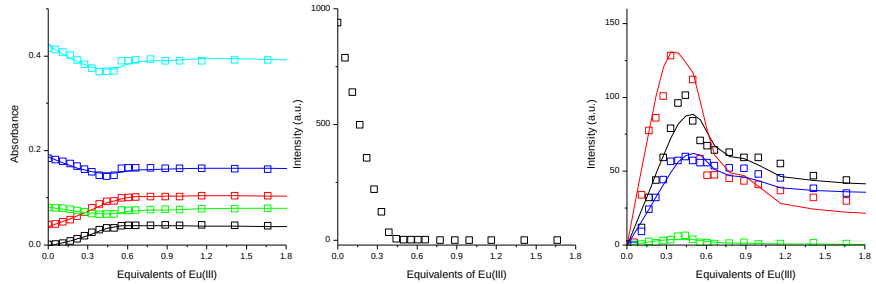

91-*L*-Phe v. Eu(III)

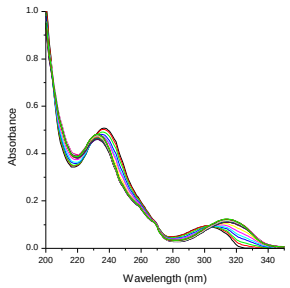

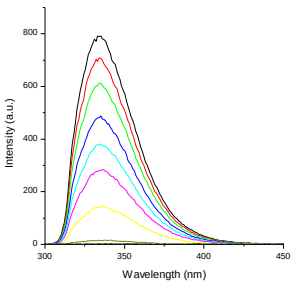

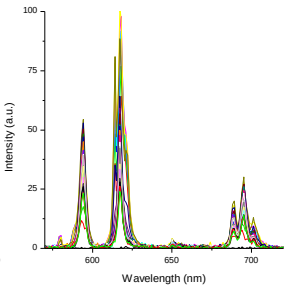

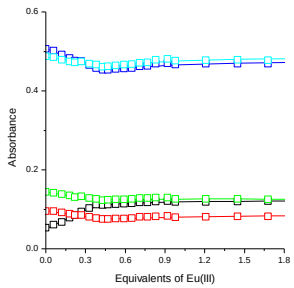

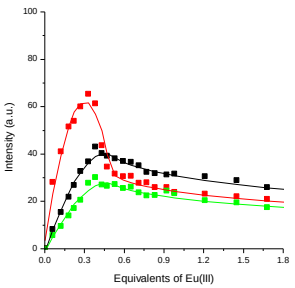

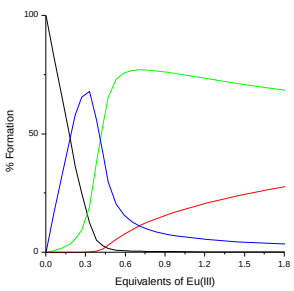

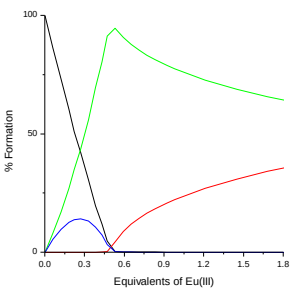

91-*D*-Phe v. Eu(III)

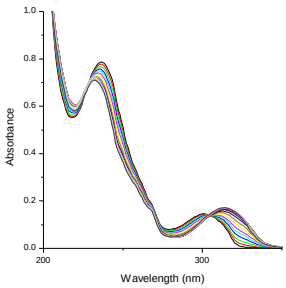

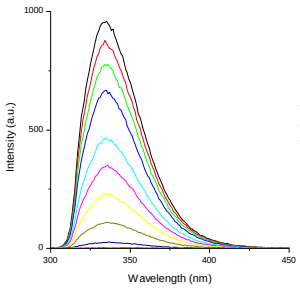

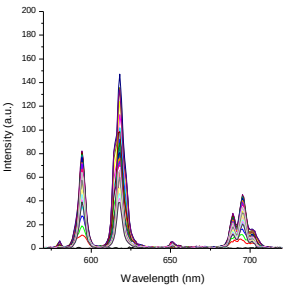

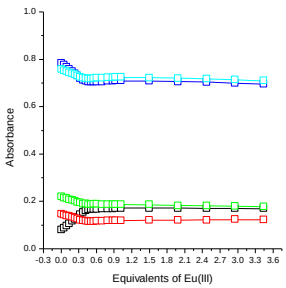

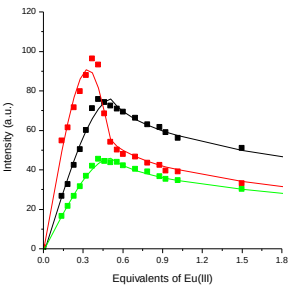

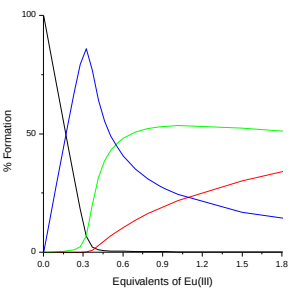

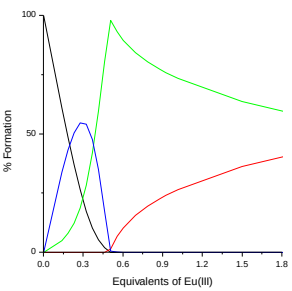

91-*L*-Trp v. Eu(III)

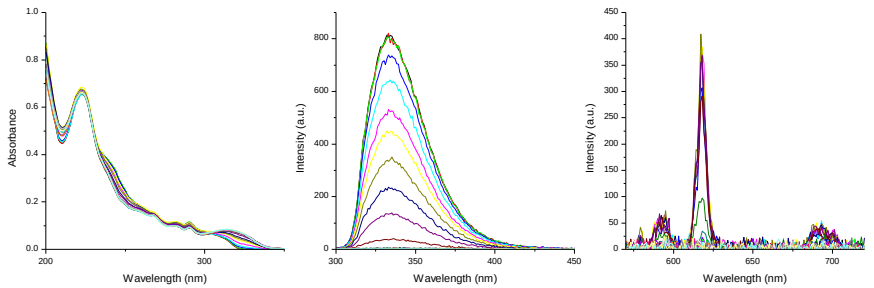

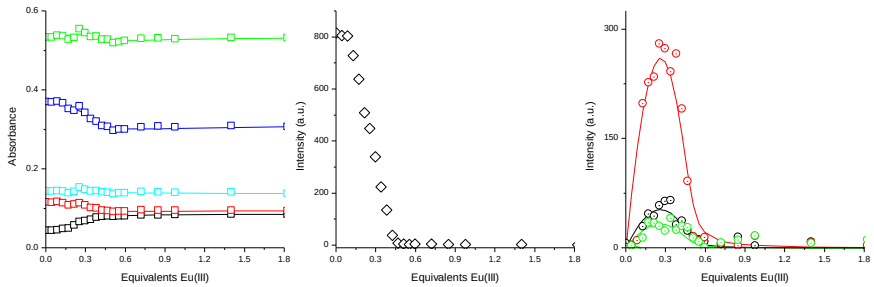

91-*D*-Trp v. Eu(III)

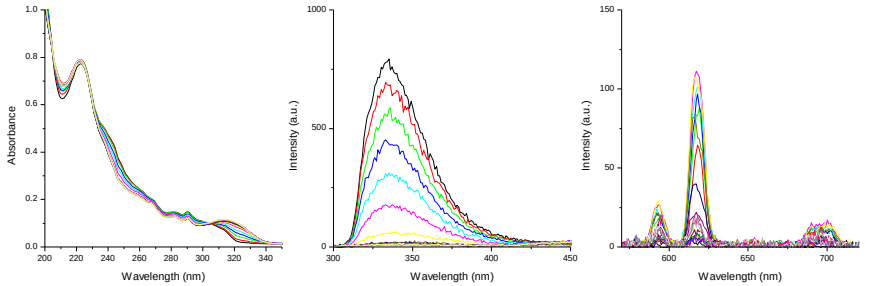

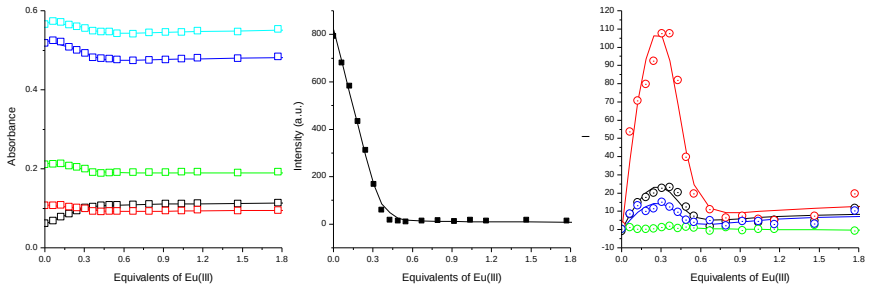

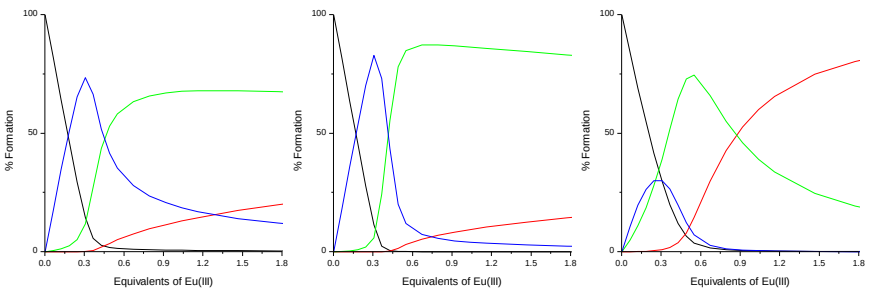

B.7. Tb(III) spectroscopic titrations and fitting

88 v. Tb(III)

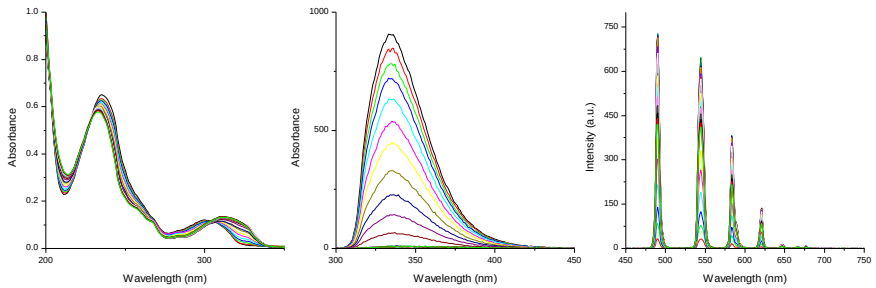

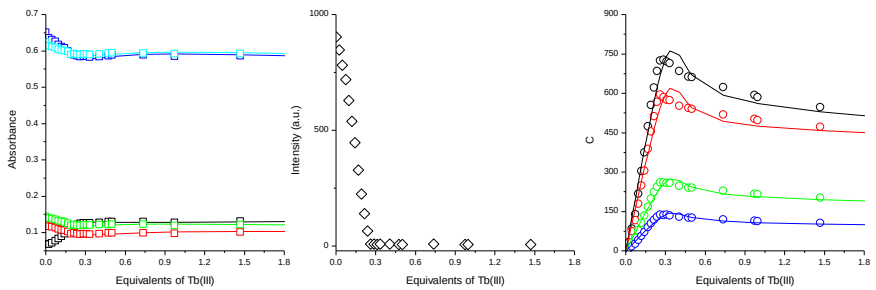

91-Gly v. Tb(III)

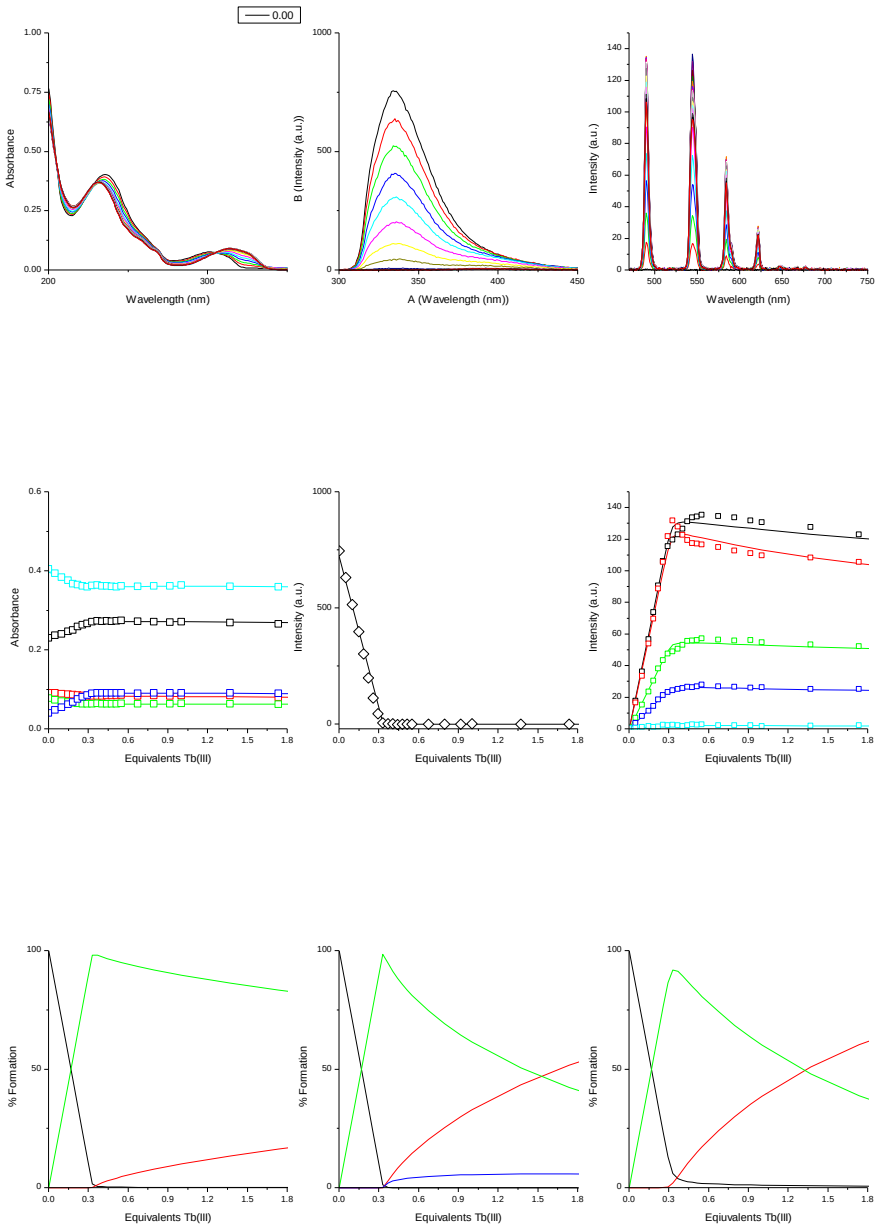

91-*L*-Ala v. Tb(III)

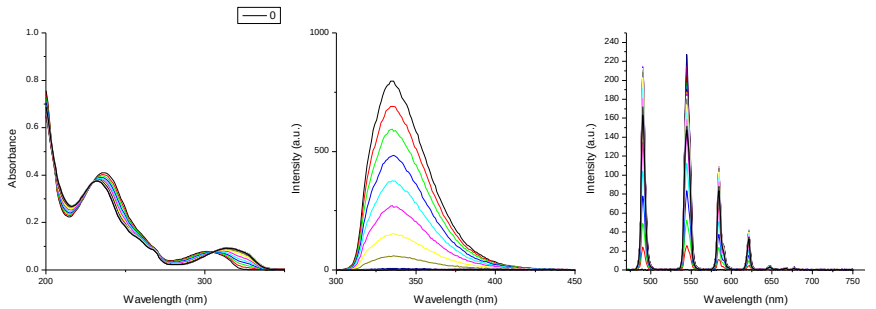

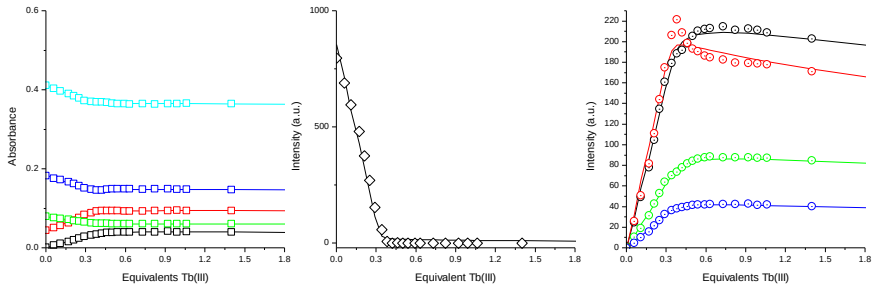

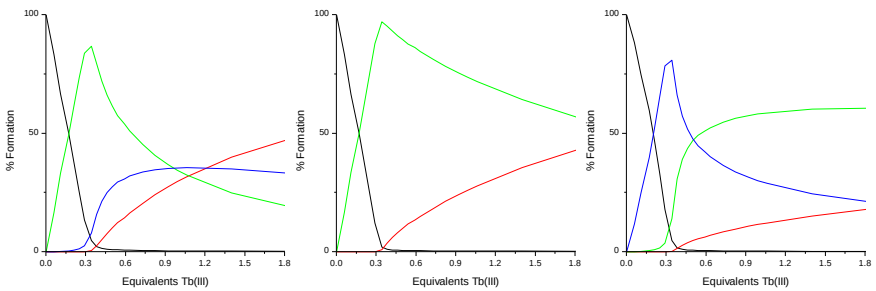

91-*D*-Ala v. Tb(III)

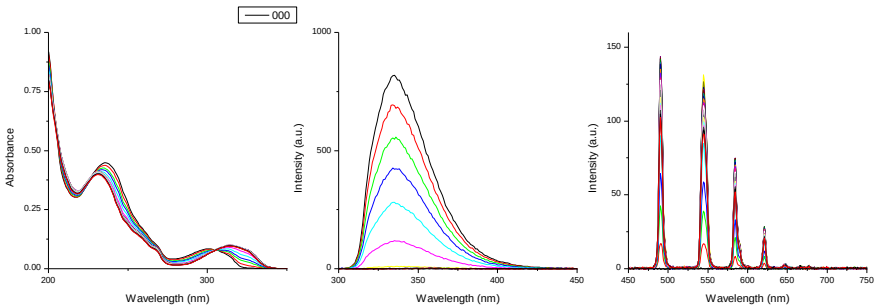

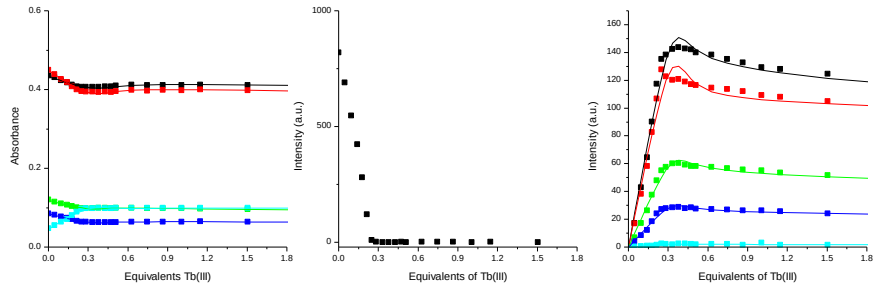

91-*L*-Phe v. Tb(III)

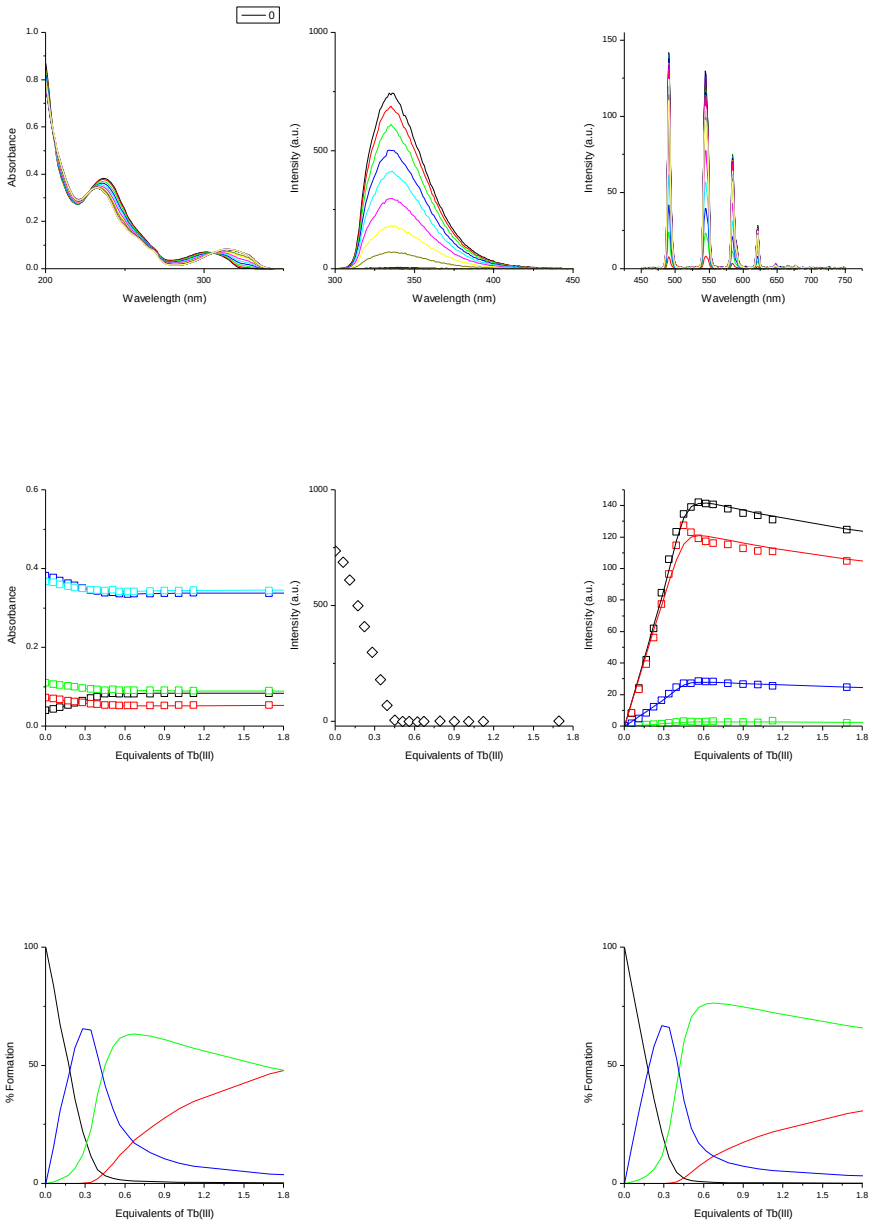

91-*D*-Phe v. Tb(III)

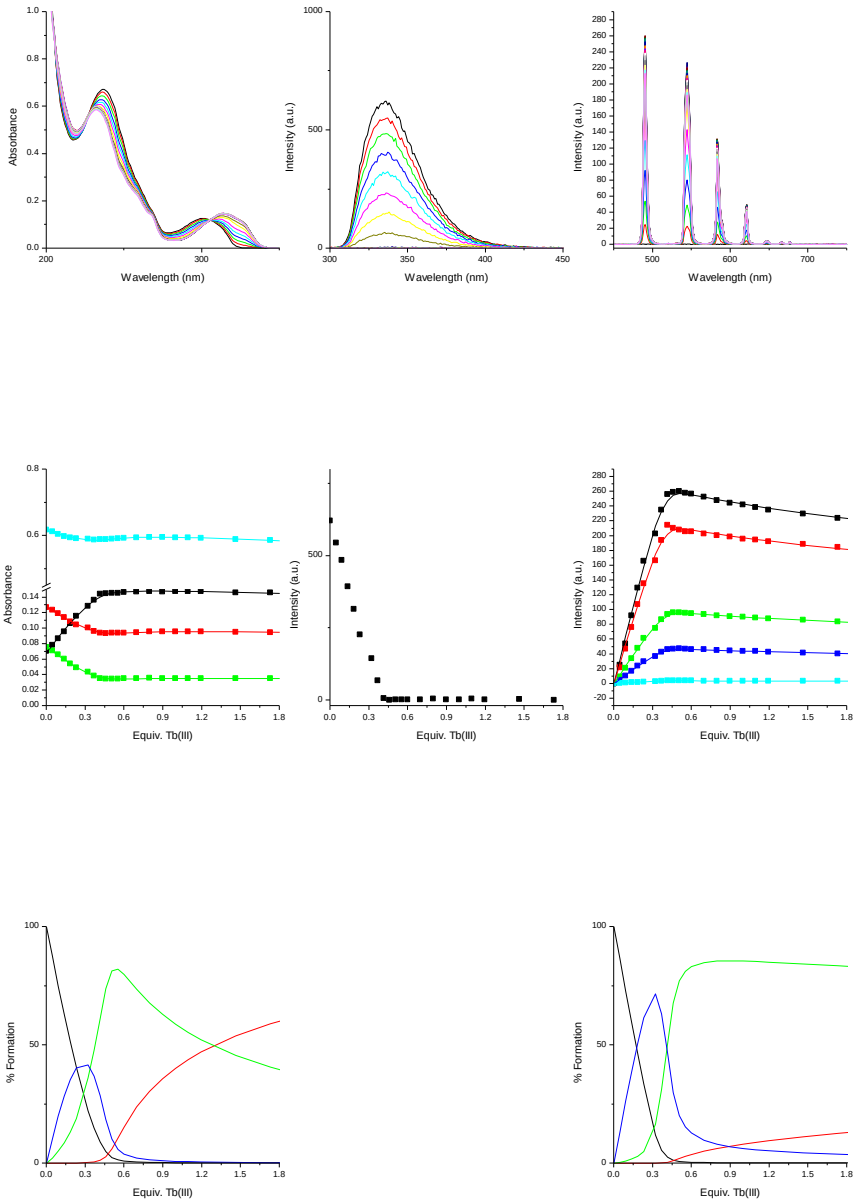

91-*L*-Trp v. Tb(III)

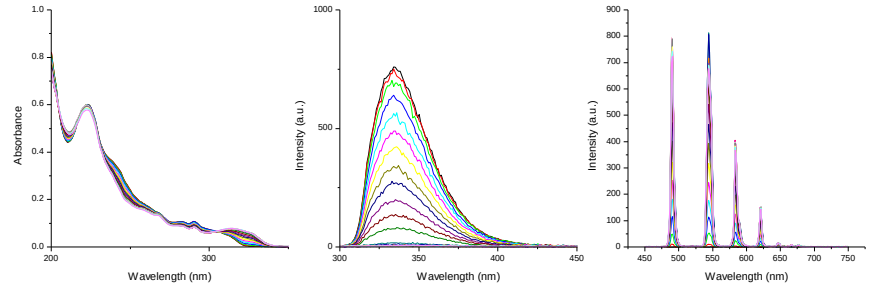

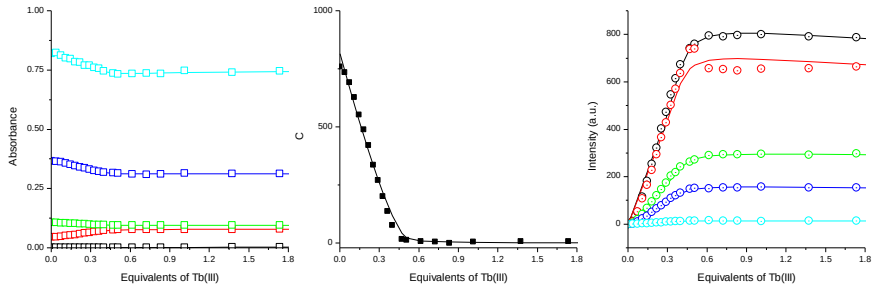

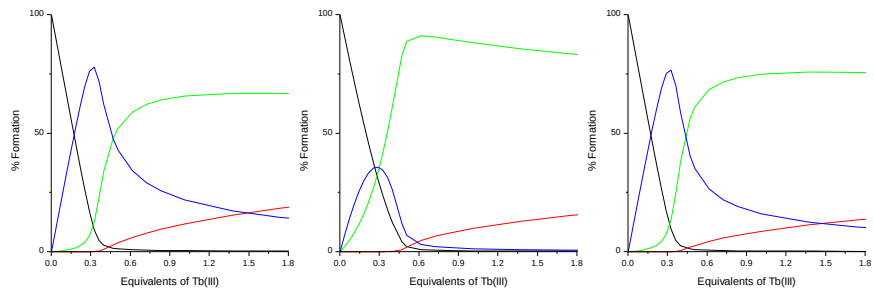

91-*D*-Trp v. Tb(III)

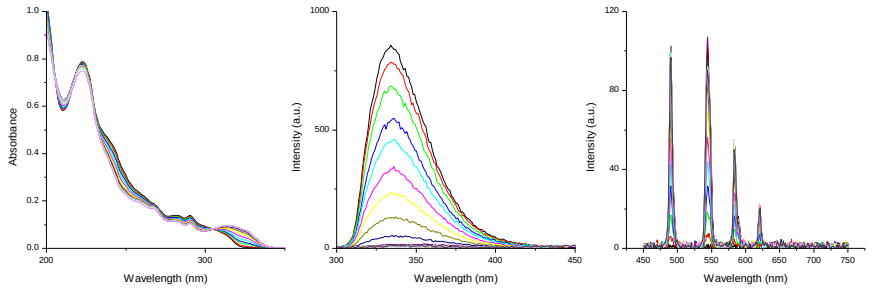

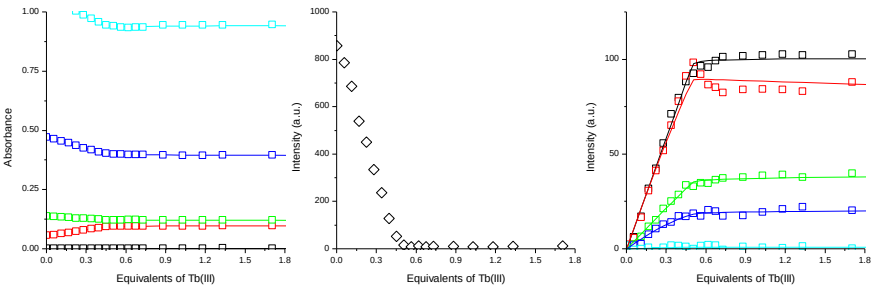

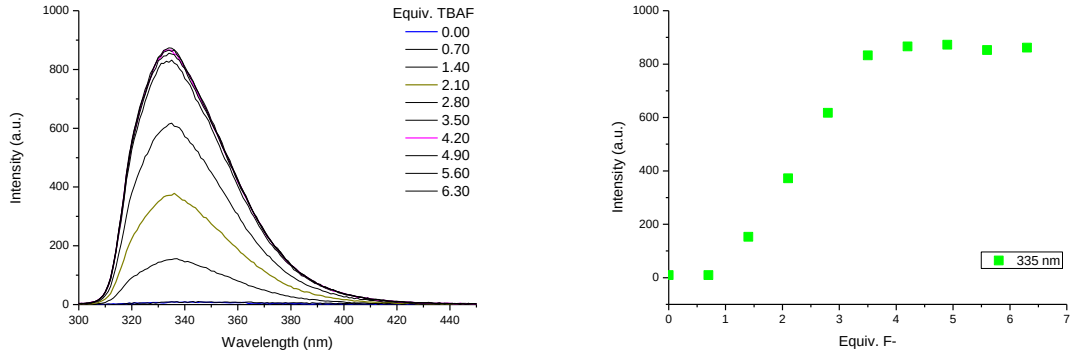

Figure B.108 Fluorescence spectral changes (*left*) and binding isotherms (*right*) of a CH_3CN solution of $[Tb\cdot(\mathbf{88})_3](CF_3SO_3)_3$ upon addition of TBAF solution.

B.8. X-ray crystallography

Table B.1 Hydrogen bond distances [Å] and angles [°] for the X-ray crystal structure of [2]catenane **95**.

D–H···A	D–H [Å]	H···A [Å]	D···A [Å]	D– H···A [°]
N5—H5···N36	0.88	2.25	2.980(10)	140.8
N6—H6···O5	0.88	1.92	2.792(10)	171.5
N14—H14A···N20	0.88	2.36	3.074(13)	138.3
N15—H15···O10	0.88	2.13	2.907(16)	146.5
N23—H23···O9	0.88	1.97	2.810(10)	158.8
N24—H24···N18	0.88	2.29	3.054(11)	144.8
N32—H32···N9	0.88	2.22	3.080(11)	166
N33—H33···O4	0.88	2.2	2.952(17)	143.3
O9—H9A···O2	0.83	1.88(3)	2.698(10)	174(10)
O9—H9B···O6	0.82	1.91(3)	2.721(10)	171(11)
O10—H10F···N21	0.83	2.91(12)	3.094(14)	95(9)
O10—H10E···O8	0.83	1.99(5)	2.800(15)	166(15)
C94—H94···N1	0.95	2.67	3.587(10)	162.5
C115—H115···N1	0.95	2.69	3.631(11)	173.5
C7—H7···N28	0.95	2.65	3.584(10)	166.4
C28—H28···N28	0.95	2.51	3.457(10)	172.8
C65—H65···N10	0.95	2.65	3.600(11)	175.5
C86—H86···N10	0.95	2.62	3.526(10)	158.8
C57—H57···N19	0.95	2.47	3.415(10)	173
C36—H36···N19	0.95	2.77	3.700(12)	168